Solubility of H_2O and CO_2 and diffusion of CO_2 in rhyolitic melts: an experimental study

Löslichkeit von H_2O und CO_2 und Diffusion von CO_2 in rhyolitischen Schmelzen: eine experimentelle Untersuchung

Von dem Fachbereich Geowissenschaften und Geographie

der Universität Hannover

zur Erlangung des Grades eines

DOKTORS DER NATURWISSENSCHAFTEN

Dr. rer. nat.

genehmigte Dissertation

von

Dipl.-Geol. Nathalie Tamic

geboren am 16.05.1972 in Nogent-sur-Marne, Frankreich

2002

Referent:	Prof. Dr. F. Holtz
Korreferenten:	Dr. H. Behrens Prof. Dr. Youxue Zhang
Tag der Promotion:	21.05.2002

Schlagworte: Rhyolitische Schmelze, Löslichkeit, Diffusion,

Keywords: rhyolitic melts, solubility, diffusion

Il ramona soigneusement ses volcans en activité.

A. de Saint Exupéry

Inhaltsverzeichnis

Danksagung **7**

Abstract **8**

Zusammenfassung **10**

Introduction **13**

CH. 1: QUANTITATIVE ANALYSIS OF CO_2 CONTENTS IN RHYOLITIC GLASSES USING IR ABSORPTION SPECTROSCOPY 15

1. Introduction **15**

2. Synthesis of standards **16**
2 1. Starting material 16
2.2. Experimental procedure 16
2.3. Run conditions 17

3. Analytical techniques **17**
3.1. Sample preparation 17
3.2. IR spectroscopy 17
3.2.1. Analysis conditions 17
3.2.2. Spectroscopic determination of CO_2 contents 18
3.3. Bulk extraction 19

4. Results and discussion **22**
4.1. Quenched products 22
4.2. Calibration 22

CH. 2: THE SOLUBILITY OF H_2O AND CO_2 IN RHYOLITIC MELTS IN EQUILIBRIUM WITH A MIXED CO_2-H_2O FLUID PHASE 25

1. Introduction **25**

2. Sample preparation **25**
2.1. Starting material and experimental procedure 25
2.2. Run conditions 26

3. Analytical techniques **27**
3.1. Determination of the fluid composition after experiment 27
3.2. Density determination 28
3.3. Karl-Fischer titration 30
3.4. IR spectroscopy 30
3.4.1. Sample preparation and analysis conditions 30
3.4.2. NIR spectroscopic determination of water contents 33
3.4.3. MIR spectroscopic determination of CO_2 contents 34

4. Results and discussion **34**
4.1. Quenched products 34
4.2. H_2O solubility 35
4.3. CO_2 solubility 37

4.4. Comparison with calculations 39
4.5. Empirical model for water solubility between 75 and 500 MPa 40

CH. 3: DIFFUSIVITY OF CO_2 IN RHYOLITIC MELTS 43

1. Introduction 43

2. Starting materials 43
2.1. Natural CO_2-free and water poor glasses 43
2.2. Synthesis of hydrous glasses 43
2.3. Hydrous CO_2-bearing glasses 44

3. Experimental and analytical procedures 45
3.1. Desorption experiments 45
3.2. Sorption experiments 45
3.2.1. Sorption in dry glasses 46
3.2.2. Sorption in hydrous glasses 46
3.3. IR spectroscopy 46

4. Results 47
4.1. Quenched products 47
4.1.1. Desorption experiments 47
4.1.2. Sorption experiments 48
4.2. Effective duration at the experimental temperature 49
4.3. Determination of diffusion coefficients 50
4.3.1. Sorption in dry glasses 50
4.3.2. Diffusion in hydrous material 53
4.3.3. Uncertainty in diffusion coefficient 55

5. Discussion 56
5.1. Validity of CO_2 solubilities derived from diffusion data fits 56
5.2. CO_2 diffusion in nominally anhydrous and water-bearing rhyolite 57
5.3. Modelling CO_2 diffusion as a function of T, P and X^m_{water} 61

Conclusions 64

Appendix 1: Tables 67

Appendix 2: Diffusion profiles and fits 77

References 95

Lebenslauf 102

Danksagung

Die vorliegende Arbeit habe ich am Institut für Mineralogie der Universität Hannover unter der Leitung von Herrn Prof. Dr. François Holtz und Herrn PD Dr. Harald Behrens angefertigt. Beiden sei für die zahlreichen Anregungen, die intensiven Diskussionen, und ihre große Geduld gedankt. Herrn Prof. Dr. Youxue Zhang danke ich für die Übernahme des Koreferats.
Willi Hurkuck und Bettina Aichinger danke ich für die technische Unterstützung bei der Durchführung der Hochdruckexperimenten. Bei Otto Diedrich bedanke ich mich für die hervorragende Anfertigung der zahlreichen, kleinen, unglaublich dünnen und zerbrechlichen doppeltpolierten Schliffen.
Bei Herrn Dr. Dieter Ziegenbein möchte ich mich für seine immerwährende Verfügbarkeit und Freundlichkeit besonders bedanken.
Herrn Dr. Jürgen Koepke und Matthi danke ich für die Unterstützung bei der Mikrosonde. Herrn Dr. Claus Rüscher danke ich für die Unterstützung bei der IR Spektroskopie.
Ferner danke ich allen Mitarbeitern des Institutes für die Unterstützung bei der Durchführung dieser Arbeit.

Meinen langjährigen Zimmernachbarn (-nachbarinnen) Susi (besonders), Tony, Bea und Jasper danke ich für ihre Geduld bei meinen lauten Selbstgesprächen und für ihre zahlreichen Anregungen und kluge Hinweise.
Meinen **lieben** Mitbewohnern (Christian, Brian, Mareile, sowie zeitweise Steffi, Ivo, und Alan) danke ich besonders für ihren Musik- und Kunstgeschmack, ihrem Mitlachen und zahlreichen Anregungen.
Dem Badminton-team, mit dem die Biere und Pizzas jede Woche "*wunderlecker"* waren, danke ich ebenfalls besonders.
Riwan sei für seine Geduld und liebevollen Beistand während der gesamten Arbeit gedankt. Enora danke ich für ihre Lebenslust.

Mein Dank geht auch an: Sébastien, Antje (deiner Name war noch nicht deutlich gedruckt), Darja, Canto Cantabile, Britta, Mellie, Astrid und Astrid, Jens, Charles, David, Marcus und Marcus, Kevin, Max, Frank, Heidi, Regina, Thorsten, Michael.
Ich hoffe, dass ich keinen vergessen habe. Wenn doch, *bitte nicht schlagen*!

Abstract

CO_2 is dissolved in rhyolitic glasses/melts only as CO_2 molecule species. A series of experiments were carried out in order to determine a new linear molar absorption coefficient for the molecular CO_2 band in IR absorption spectra of rhyolitic glasses to enable an reliable quantification of CO_2 contents. Samples with varying amounts of CO_2 and water (water is facilitating sample synthesis) have been synthesised at pressures ranging from 200 to 800 MPa and temperatures of 1100 and 1200°C by loading in a Pt-capsule a piece of natural obsidian (EDF, Erevan Dry Fountain, Armenia) together with water and silver oxalate as the CO_2-source, so that an exceeding mixed fluid phase remained after the experiment. Several pieces from different locations in the bubble-free and crystal-free quenched products have been cut off and prepared for IR-spectroscopy. CO_2-contents of the rest of the glass was measured coulometrically by CO_2-titration. The linear molar absorption coefficient of 1232 ±36 $l.cm^{-1}.mol^{-1}$ determined for the band of molecular CO_2 at 2346 cm^{-1} is 15% greater than that of Blank (1993). As a consequence, previous data based on Blank's calibration should be decreased by 15%. In addition, the new calibration indicates that the linear molar absorption coefficient does not depend on the amount of water dissolved in the glass.

H_2O and CO_2 solubilities in a natural rhyolite melt (EDF) in equilibrium with H_2O-CO_2 fluids were determined at 200 and 500 MPa and at 800 and 1100°C. The composition of the fluid phase after experiment was determined by gravimetry, except for extreme CO_2-rich fluids for which mass balance was used. Water and CO_2 contents of the glasses were measured using IR spectroscopy. At 200 MPa, the water solubility turn over from a square root dependence on mole fraction of H_2O in the fluid phase (X^f_{H2O}) at low X^f_{H2O} to a linear dependence above X^f_{H2O}=0.25. Up to about 5 wt% dissolved water in the melt (corresponding to $X^f_{H2O} \approx 0.5$) a similar trend is observed at 500 MPa. At higher X^f_{H2O}, however, the dependence of water solubility on X^f_{H2O} is more pronounced. A negative temperature dependence of water solubility is observed in the whole range of X^f_{H2O} at 200 MPa (e.g., the water solubility at X^f_{H2O}=1 decreases from 5.97 to 5.58 wt% when temperature rises from 800 to 1100°C). In contrast, at 500 MPa the temperature dependence of water solubility changes from positive at high X^f_{H2O} (e.g., increase from 9.84 to 11.04 wt% for a temperature increase from 800 to 1100°C) to negative at low X^f_{H2O}. An empirical model to predict water solubility in rhyolitic melts in the P-T range 75-500 MPa and 800-1100°C was derived from our new solubility data and data from Blank et al. (1993). The empirical model reproduces our data within ±2.5% relative, except at 500 MPa, 1100°C (±5% rel.).

The CO_2 solubility shows a non-linear dependence on X^f_{CO2} with deviation from linearity increasing with pressure. The maximum CO_2 solubilities (equilibrium with pure CO_2) predicted from the data trends are 0.28 ± 0.03 and 0.11 ± 0.01 wt% at 1100°C and 200 and 500 MPa, respectively. At 800°C, the melts are partially crystallised when using CO_2 rich fluids ($X^f_{CO2} > 0.65$ at 200 MPa, X^f_{CO2}

> 0.5 at 500 MPa) and prediction of the solubility of pure CO_2 is not possible. The temperature dependence of CO_2 solubility is found to be almost negligible at 200 and slightly positive at 500 MPa. Our experimental solubility data at 200 MPa are slightly better reproduced by the model of Papale (1999) than with that of Holloway and Blank (1994).

In addition, experiments have been carried out in order to characterise CO_2-diffusion in rhyolitic melts as a function of temperature, pressure and water content. Three series of experiments were conducted combining three different rhyolitic glasses and two different methods: (1) CO_2 sorption in water-poor natural EDF pieces at temperatures ranging from 580 to 1000°C and pressures of 100, 300 and 500 MPa, (2) CO_2 sorption in hydrous synthesised EDF pieces (with a water content before experiment of 2.2 wt%) at temperatures ranging from 580 to 900°C at 100 MPa, (3) CO_2 desorption from bubble-bearing hydrous CO_2-bearing synthesised EDF pieces at temperatures of 580 and 630°C and pressures of 100 and 500 MPa. Experiments were performed either in IHPV or in CSPV, depending on the run conditions. CO_2-diffusivities were derived from the fit of CO_2-concentration-distance profiles assuming the CO_2 diffusivity being constant along the profile. The data for water-poor rhyolitic composition at 100 MPa can be described in the whole temperature range by a simple Arrhenius relationship $D_{CO_2} = 2.14 \times 10^{-6}$ m^2/s $\exp(-17945/T)$. A 2.4 wt% increase in water content at 100 MPa and 900°C increases the CO_2-diffusivity by approx. half an order of magnitude. The effect of water on CO_2 diffusion seems to be more pronounced at lower temperature. The addition of 2.5 wt% water at 100 MPa and 580°C increases D_{CO_2} by about one and a half order of magnitude. Although experiments were carried out on different pressures, no clear trend of pressure dependence of D_{CO_2} could be seen. It is however possible to determine an apparent activation volume V_a of 3.4 ±1.7 cm^3/mole from data at 1000°C in the pressure range of 70-1000 MPa. Combining my data with that of Watson (1991) and Blank (1993),CO_2-diffusivity (in 10^{-12} m^2/s) in rhyolitic melts can be expressed as:

$$D_{CO_2} = \exp[(14.992-18.692\times X^m_{water})+(-19047.5+70193\times X^m_{water})/T-(0.632+7.543\times X^m_{water})P/T]$$

where T is in K, P in MPa, and X^m_{water} is the mole fraction of water on a single oxygen basis. Except for a few outlier points (data at 300 MPa), error of estimates is within 0.59 in terms of lnD for all data, covering a wide range of temperature (450-1100°C), pressure (72-1000 MPa) and water contents (0.13-11 wt%).

Zusammenfassung

In den magmatischen Schmelzen können beträchtliche Mengen an volatilen Komponenten gelöst sein. Dominierende Fluidkomponente in terrestrischen Magmen ist H_2O. Bis zu 8 Gew% gelöstes H_2O wurden in Glaseinschlüssen von hochdifferenzierte Magmen gefunden. Die zweithäufigste volatile Komponente ist CO_2. In der Natur sind in der Regel keine reinen sondern gemischte Volatile vorhanden (System C-H-O-S). Entgasungsprozesse von den ursprünglich in den Schmelzen gelösten Volatilen während des Magmenaufstiegs haben einen entscheidenden Einfluss auf den Verlauf vulkanischer Eruptionen. Die vorliegende Arbeit hat die Zielsetzung, thermodynamische und kinetische Eigenschaften von hochpolymerisierten Schmelzen, die für den explosiven Vulkanismus von fundamentaler Bedeutung sind, zu bestimmen und zu einem besseren Verständnis von vulkanischen Prozessen beizutragen.

In der Arbeit wurden die Wasser und CO_2-Lösligkeiten sowie die CO_2 Diffusion in rhyolitischen Schmelzen experimentell untersucht. Alle Experimente wurden je nach P-T Bedingungen in intern oder extern beheizten Gasdruckanlagen durchgeführt. In rhyolitischen Gläsern liegt CO_2 nur in Form von molekularem CO_2 vor. Es wurde zuerst eine Infrarot-Kalibration zur Messung von CO_2 in rhyolitischen Gläsern durchgeführt. Dafür wurden natürlichen rhyolitischen blasen- und kristallfreie Glasblöcke (aus Erevan Dry Fountain, Armenien) mit Silberoxalat (CO_2-Quelle) und Wasser (das Wasser erleichtert die Homogenisierung der Gläser) äquilibriert. Die Experimente wurden in Platinkapseln bei Drucken von 200 bis zu 800 MPa und Temperaturen von 1100°C oder 1200°C für 4-9 Tage durchgeführt. Die CO_2-Gehalte der Proben wurde mit IR-Spektroskopie und coulometrischer Titration analysiert. Der Absorptionskoeffizient wurde durch die Beer-Lamberts Beziehung aus den coulometrischen Messungen und den Peakhöhen der IR Absorptionsbanden durch eine lineare Regression der Daten bestimmt. Ein linearer molarer Absorptionskoeffizient von 1232 ± 36 $l.cm^{-1}.mol^{-1}$ wurde für den molekularen CO_2-Band bei 2346 cm^{-1} ermittelt (Fig. 3). Dieser Werte ist um 15% größer als der von Blank (1993) bestimmte Wert für rhyolitische Gläser und um 23% größer als der von Fine and Stolper (1985) bestimmte Wert für albitische Gläser. Als Folge sind der neuen Kalibration sind IR-spektroskopisch bestimmten CO_2-Gehalte für rhyolitische Gläser um 15% niedriger als in vorherigen Arbeiten, die auf Blank's Daten basieren. Es wurde keine Beeinflussung des molaren Absorptionskoeffizient durch gelöstes Wasser gefunden.

Ein Schwerpunkt der Arbeit lag in der experimentellen Bestimmung der Wasser- und CO_2-Löslichkeiten in rhyolitischen Schmelzen in Abhängigkeit von Druck, Temperatur, und Zusammensetzung der Fluidphase (= CO_2 + H_2O). Ausgangsmaterialen waren trockene und kristallfreie Glasstücke, zu denen bidestilliertes Wasser und eine CO_2-Quelle (entweder Oxalsäure oder Silberoxalat) zugegeben wurden. Die Fluidzusammensetzungen wurden nach dem Abschrecken

der Proben entweder durch Gaschromatographie oder Gravimetrie bestimmt. Wasser- und CO_2 Gehalte der Gläser wurden mit IR-Spektroskopie analysiert. Es wurde bei hohen Wassergehalten im Rahmen der Fehler eine lineare Abhängigkeit der Wasserlöslichkeit von X^f_{H2O} (Stoffmengenanteil von H_2O in der Fluidphase) bei 200 MPa, und eine nicht-lineare Abhängigkeit von X^f_{H2O} bei 500 MPa beobachtet (Fig. 7). Bei 200 MPa ist bei allen Fluidzusammensetzungen eine negative Temperaturabhängigkeit der Wasserlöslichkeit vorhanden. Im Gegensatz dazu wechselt die Temperaturabhängigkeit bei 500 MPa von positiv bei $X^f_{H2O}>0.75$ zu negativ bei $X^f_{H2O}<0.75$. Die CO_2-Lösligkeit ist bei 200 MPa direkt ungefähr proportional zu X^f_{CO2} (Stoffmengenanteil von CO_2 in der Fluidphase). Bei 500 MPa dagegen zeigt die CO_2-Lösligkeit eine starke nicht-lineare Abhängigkeit von X^f_{CO2} (Fig. 8). Die maximalen CO_2 Löslichkeiten wurden für die höchsten X^f_{CO2} erhalten. Die Temperaturabhängigkeit der CO_2-Löslichkeit in rhyolitischen Schmelzen ist nahezu vernachlässigbar bei 200 MPa und leicht positiv bei 500 MPa. Die experimentellen CO_2-Daten sind durch thermodynamische Modelle ziemlich gut reproduziert. Im Gegensatz dazu sind die experimentellen H_2O-Daten durch die Modelle entweder überschätzt oder unterschätzt (Fig. 9). Deshalb wurde ein neues empirisches Modell entwickelt, um die Wasserlöslichkeit in rhyolitischen Schmelzen im P-T Bereich von 75-500 MPa und 800-1100°C vorauszusagen. Das Modell wurde mit Literaturdaten zur Wasserlöslichkeit getestet (Silver et al., 1990, Zusammensetzungen PDIKS, KS); Holtz et al., 1992, 1995, Zusammensetzungen AOQ, HPG8); Yamashita, 1999, Zusammensetzung WOBS); Behrens and Jantos, 2001, Zusammensetzungen EDF, LGB, OT, LP). Das empirisches Model reproduziert 48 über 53 experimentelle Wasserlöslichkeiten innerhalb ±5.5% rel.. Zwei Experimente sind innerhalb ±7.5% rel. (AOQ) und drei innerhalb ±12.5-36% rel. (PDIKS, KS) reproduziert (Fig. 10).

Ein weiterer zentraler Bestandteil der Arbeit waren experimentelle Untersuchungen zur CO_2-Diffusion in rhyolitischen Gläsern und Schmelzen in Abhängigkeit von Druck, Temperatur und Wassergehalt. Dafür wurden drei Versuchsreihen mit drei verschiedenen Ausgangsmaterialen und zwei experimentellen Methoden durchgeführt: (1) Sorption von CO_2 in natürlichen, wasserarmen rhyolitischen Glasstücken bei Temperaturen von 580 bis zu 1000°C und Drucken von 100, 300 und 500 MPa, (2) Sorption von CO_2 in synthetisierten blasen- und kristallfreien, wasserhaltigen rhyolitischen Glasstücken bei Temperaturen von 580 bis zu 900°C und Drucken von 100 MPa, (3) Desorption von CO_2 aus synthetisierten blasenhaltigen, aber kristallfreien rhyolitischen Glasstücken, in denen zuvor sowohl Wasser als auch CO_2 gelöst wurde (Temperaturen: 580 und 630°C, Drücke: 100 und 500 MPa). Nach dem Abschrecken der Proben wurden CO_2-Profile senkrecht zur Plattenfläche mit einem IR-Mikroskop aufgenommen. CO_2-Profile wurden unter der Annahme ausgewertet, dass sich der Diffusionskoeffizient von CO_2 entlang des Profils nicht ändert (Fig. 11 bis 13). Daten für natürliche wasserarme rhyolitische Zusammensetzungen können in dem ganzen Temperaturbereich bei 100 MPa durch der folgende Arrhenius Beziehung beschrieben werden:

$D_{CO_2} = 2.14 \times 10^{-6}$ m^2/s exp(-17945/T).

Wenn 2.4 Gew% Wasser in dem Glas gelöst sind, dann vergrössert sich die CO_2-Diffusivität bei 100 MPa und 900°C um eine halbe Größenordnung. Der Einfluss des Wassers auf die CO_2 Diffusion scheint bei niedrigeren Temperaturen sehr viel ausgeprägter zu sein. Bei Einbau von 2.5 Gew% wird die CO_2-Diffusion bei 100 MPa und 580°C im Vergleich mit dem trockenen Glas sogar um 1.5 Grössenordnungen beschleunigt (Fig. 15). Die Druckabhängigkeit von D_{CO_2} ist relativ gering (Fig. 16). Die neuen experimentelle Daten sind konsistent mit früheren Ergebnisse und zeigen eine Ähnlichkeit der Diffusionsgeschwindigkeit von CO_2 mit Ar. Die Zusammenstellung meiner Daten mit den von Watson (1991) und Blank (1993) erlaubt die Herstellung eines Modells, um die Diffusion von CO_2 in rhyolitischen Schmelzen in Abhängigkeit von Druck, Temperatur und Wassergehalt zu berechnen:

$$D_{CO_2} = \exp[(14.992-18.692\times X^m_{water})+(-19047.5+70193\times X^m_{water})/T-(0.632+7.543\times X^m_{water})P/T]$$

Der Standardfehler für ln D_{CO_2} liegt bei ±0.59. Alle Daten werden durch das Modell innerhalb eines Faktors 4 reproduziert und 80% der Daten sogar innerhalb eines Faktors 2, wobei die Daten einen grossen Bereich der Temperatur (450-1100°C), des Druckes (72-1000 MPa) und des Wassergehaltes (0.13-11Gew%) umfassen.

Introduction

Volcanoes since long exert a fascination on men, leading them in turn to fear, to revere, to domesticate and then to understand it. Volcanic eruptions sometimes correspond to deadly catastrophes, as for example eruptions that destroyed Santorin in the Egean sea in the XVIIth century B.C. and Pompei (Vesuvio) in 79 A.C. or eruptions of the Tambora in 1815 that killed 92 000 people, that of the Montagne Pelée in 1902 or that of the Nevado del Ruiz in 1985 that made 29 000 and 25 000 victims, respectively. It appears from statistics recorded since the beginning of the XVIIIth century that volcanoes are not killing often, but dramatically. On an average, two cataclysmic eruptions occur per century. Volcanic eruptions are more especially killing as people keep living at their feet, sometimes neglecting all risks, because volcanoes are prosperity: they are source of valuable material (as ore deposits linked to ancient volcanism, native sulfur), energy, and indirectly source of abundant feeding (ashes are a recurrent rich natural fertilizer allowing intensive agriculture, and surroundings fresh or salty waters are enriched in nourishing elements from soil leaching favouring fish proliferation), of housing (troglodytic habitat, building stone), not to forget benefits from thermal waters.

Among the seven risks acknowledged by the IAVCEI (International Association of Volcanology and Chemistry of the Earth's Interior), namely lava flows, falls (volcanic ashes or bombs), pyroclastic flows, gas, lahars, landslides or avalanches, and tsunamis, pyroclastic flows are the most dangerous because of their instantaneity and power in the eruptive event. One of the causes of these eruptions explosive character is directly linked to the degassing abilities of the concerned magma. Degassing depends on magma composition and therefore on viscosity and density, temperature, volatile content and associated diffusivities, crystallisation degree, ascending rate, and the possibility of contact with another fluid phase (magma or different). The more difficult is the degassing, the more important is the eruptive character. This fact explains why explosive eruptions usually occur with felsic magma compositions (from dacitic to rhyolitic compositions). Volcanoes emit a lot of gases before, during and after eruptions. The main gases emitted from volcanoes are molecular combinations in the C-H-O-S system. Emissions occur from the crater as well as in a diffusive way from fractures in the volcano flanks (fumaroles) as well as simple emanations from the soil (mainly CO_2). Injected in high atmosphere in great quantities, these gases may sensibly modify the world climate (as for example during the spring 1816, when snow falls were recorded in June all over North America and West Europe after the Tambora eruption of 1815). Explosive volcanoes are mostly concentrated in the geodynamic context of subduction as the circle of fire (Pacific) or other insular arcs (Caribbean, Indonesian, Egean, Tyrrhenean).

Recent studies dealing with explosive eruptive dynamisms are oriented towards the understanding of degassing mechanisms taking place during the magma ascent, in order to define the conditions

under which this explosive character develops, and especially towards the definition of gas bubble nucleation, development conditions (Sparks, 1978), and consequences of nucleation on the magma physical, chemical and kinetic properties (e.g., viscosity). Workers explored different ways using: experimental petrology (e.g. Hurwitz and Navon, 1994; Navon et al., 1998; Liu and Zhang, 2000), experiments with analogue materials (e.g. Mourtada-Bonnefoi, 1998), analytical ways (e.g. Toramaru, 1995; Lyakhovsky et al, 1996; Proussevitch and Sahagian, 1998; Navon et al., 1998). However, for the total understanding of the phenomena, it is necessary, in addition to the characterisation of the involving parameters and their varying interactions, to quantify their individual effects and variations.

Volatile solubilities others than water (CO_2 in particular) are still poorly documented, as for their diffusivities, and especially in felsic compositions. Now it appears that their role in the bubble nucleation can not to be neglected (Papale and Polacci, 1999) because of their low solubility in magmas (one of the reason why they stayed so long in the shadow) and especially because their presence is diminishing the water activity, diminishing in the same time its solubility and enabling its exsolution.

The aim of my study is to contribute to a better understanding of volatile-bearing magmas. In particular the solubility and the diffusion of volatiles in magmas are investigated. On one hand the database for magmatic systems is increased by providing new information on the solubilities of water and CO_2 in rhyolitic melts is increased for melts and magmas coexisting with binary H_2O-CO_2 fluids and the diffusivities of CO_2 in the melt. On the other hand, new insights are obtained on the mechanism of volatile dissolution and migration in the melt. To quantify the CO_2 concentration in quenched rhyolitic glasses by IR absorption spectroscopy, a new calibration was performed to determine the molar absorption coefficients for the molecular CO_2 band at 2346 cm^{-1}. Implications of the new results for magmatic systems are discussed.

Ch. 1: Quantitative analysis of CO_2 contents in rhyolitic glasses using IR absorption spectroscopy

1. Introduction

Researchers in the glass sciences have long applied spectroscopic methods to the quantitative determination of volatiles in silicate glasses (e.g. Harrison, 1947; Scholze, 1960, 1966; Ernsberger, 1977; Bartholomew et al., 1980; Wu, 1980, see Ihinger et al., 1994 for a detailed review of analytical methods for volatiles in glasses). The measurement of water and CO_2 contents by infrared spectroscopy relies on characteristic vibrations of hydrous and carbon-bearing species: e.g., combination bands of hydroxyl group and molecular H_2O at 4520 and 5230 cm^{-1}, respectively (Scholze 1960, Stolper 1982, Behrens et al. 1996) and characteristic absorption bands between 1325 and 1625 cm^{-1} for carbonate group and 2350 cm^{-1} for molecular CO_2 (cf. Mysen, 1976; Mysen et al., 1976; Brey, 1976; Taylor, 1990; Fine and Stolper, 1985). The absorption peak heights of these bands obey the Beer-Lambert law. However, in the absence of good theoretical model for absolute peak intensities, a calibration of this method is required using standard samples with volatile contents determined by bulk techniques. Infrared spectroscopic studies only became a routine method for rapid and reliable analysis in geosciences since Stolper and co-workers refined and developed the near-infrared (NIR) absorption technique in a series of studies on water speciation and solubility with melts and glasses of geological interest, later followed by many research teams (e.g. Stolper, 1982; Newman et al., 1986; Silver and Stolper, 1989; Stolper, 1989; Silver et al., 1990; Ihinger, 1991; Behrens, 1995; Nowak and Behrens, 1995; Yamashita, 1999; Zhang, 1999). Infrared spectroscopic studies have been also applied successfully to the investigation of dissolved CO_2 in natural and synthetic silicate glasses, e.g., in the works of Fine and Stolper (1985, 1986). This technique has subsequently been used to measure carbon contents in natural samples from a variety of localities (e.g. Dixon et al., 1988; Newman et al., 1988; Stolper and Newman, 1994) and in synthetic glasses to produced in a wide range of experimental conditions (Fogel and Rutherford, 1990; Pan et al., 1991; Pawley et al., 1992; Blank et al., 1993).

In this chapter, I have re-investigated the quantitative determination of CO_2 contents in rhyolitic glasses by IR spectroscopy. In doing so, the linear molar absorption coefficient of the fundamental CO_2 vibration band at 2346 cm^{-1} was re-calibrated using coulometric CO_2 titration.

2. Synthesis of standards

2 1. Starting material

The starting material was an obsidian from Erevan Dry Fountain (EDF), Armenia. The glass was chosen because it contains only minor amounts of crystals (less than 1 vol%), very few bubbles, and little iron. Genesis and rheological properties of the EDF obsidian are described by Bagdassarov and Dingwell (1993) and Stevenson et al. (1995). The composition of the glass is almost metaluminous (Table 1), close to the natural rhyolitic compositions investigated by Blank et al. (1993) and Fogel and Rutherford (1990) and close to well characterised synthetic quartzofeldspathic compositions (such as HPG8 and AOQ, e.g., Holtz et al., 1995; Hess et al., 1995; Dingwell et al., 1998). A water content of the obsidian of 0.22 wt.% was derived from the peak height of the near infrared combination band at 4520 cm^{-1} using the calibration of Zhang et al. (1997). A similar value (0.24 wt% H_2O) was obtained from the peak height of the fundamental OH vibration band at 3550 cm^{-1} band using a linear molar absorption coefficient of 78 $L.mol^{-1}.cm^{-1}$ determined for haplogranitic glasses (Behrens and Schmidt, 1998). No CO_2 was detected by IR spectroscopy in the EDF starting glass. Sulfur content was analysed at SARM, CRPG-CNRS in Nancy (F) using coulometric titration and was found to be below the detection limit (50 ppm).

2.2. Experimental procedure

Glass pieces (ca. 1×3×15 mm, approx. 115 to 120 mg) were loaded with a CO_2 source and double-distilled water into a Pt-capsule (inner diameter: 3-4 mm, wall thickness: 0.2 mm, length: 2.5-3.5 cm). I chose to prepare mixed volatile bearing glasses because H_2O enhances the CO_2 diffusivity (e.g. Watson, 1991, 1994). The proportion of fluid in the charge ranged from 5 to 27 % (by weight). Different techniques were used to generate CO_2 during the experiment. In the first set of synthesis, silver oxalate ($Ag_2C_2O_4$) was loaded directly into the Pt-capsule. However, I found that Ag produced by decomposition of silver oxalate formed an alloy with the Pt-capsules, which can lead to leakage of the capsules. Therefore, in the further sets of experiments, silver oxalate was isolated from the Pt-capsule walls. Furthermore, direct contact of the silver oxalate with melt must be avoided to limit the dissolution of Ag into the melt. To isolate silver oxalate, it was loaded into a small Pt-capsule (wall thickness: 0.1 mm, inner diameter 2.5 mm, length: 1-1.5 cm), which was carefully squeezed at both ends and placed beside the glass block. Silver oxalate was stored in a desiccator to prevent any water adsorption. However, some remaining water (< 1 wt.%) can not be avoided. During welding, the capsules were cooled using liquid nitrogen to prevent any loss of water or CO_2. For each sample, the technique used to generate CO_2 is specified in Table 2.

2.3. Run conditions

Three sets of synthesis were performed in a vertically oriented internally heated pressure vessel (IHPV) pressurised with argon at 1100°C (Becker et al., 1998). Run conditions depended on the CO_2 and water content: 200 MPa/1100°C, 500 MPa/1100°C and 800 MPa/1200°C. The experiments were always fluid saturated. Run duration ranged from 4 to 9 days (Table 2). Temperature was measured with an accuracy of ±10°C (taking temperature gradients and accuracy of thermocouples into account) using K type thermocouples and pressure with an accuracy of ±5 MPa using a strain gauge manometer.

Samples were quenched by turning off the heating power of the furnace resulting in an initial cooling rate of 150°C/min. All runs were quenched isobarically.

3. Analytical techniques

3.1. Sample preparation

Three chips were cut off from the middle and both ends of the run products except for samples 1P and 2P, which were broken into several pieces after the experiment. In the latter case, I decide to pick up only one piece, thought to be the most representative one, in order to preserve enough sample for the bulk extraction. The chips were prepared for IR spectroscopy: doubly polished down to a thickness of 35 to 95 μm. The thickness of the polished sections was measured using a digital micrometer. An estimate of ±0.0003 cm was assumed for the uncertainty in thickness. In addition, I used the thickness determination method described chapter 2 § 3.4.1. to measure the sample thickness. The rest of the sample was saved for bulk extraction.

3.2. IR spectroscopy

3.2.1. Analysis conditions

Spectra were collected with a Bruker IFS 88 FTIR spectrometer coupled with an IR microscope A590. The spot size used in our measurements was approximately 80-100 μm (Nowak and Behrens, 1997). Operation conditions were: light source - W lamp and Glowbar for NIR and MIR, respectively; beamsplitter - CaF_2 and KBr, for NIR and MIR, respectively; detector - narrow band MCT with NIR equipment (range 600-10000 cm^{-1}); number of accumulated scans - 100. For CO_2 acquisition, increasing the number of scans up to 600 scans was tested with no improvement of the quality of the

spectra (no attenuation of scattering). In order to lower atmospheric effects, especially during MIR analysis, the sample stage of the IR microscope was isolated from the atmosphere in a chamber. Both the whole microscope and the chamber were purged with dry air. Furthermore, a new background was taken before each sample measurement.

3.2.2. Spectroscopic determination of CO_2 contents

The quantification of the molecular CO_2 was made using the heights (see Table 2) of the baseline corrected MIR absorption band at 2346 cm^{-1} as described in chapter 2 § 3.4.3.. 5 to 24 measures were taken to test the homogeneity of each section. The long-range homogeneity along the axis of the synthesis sample was tested by comparing the results with the other sections of the same sample. A typical MIR spectrum is displayed Fig. 1.

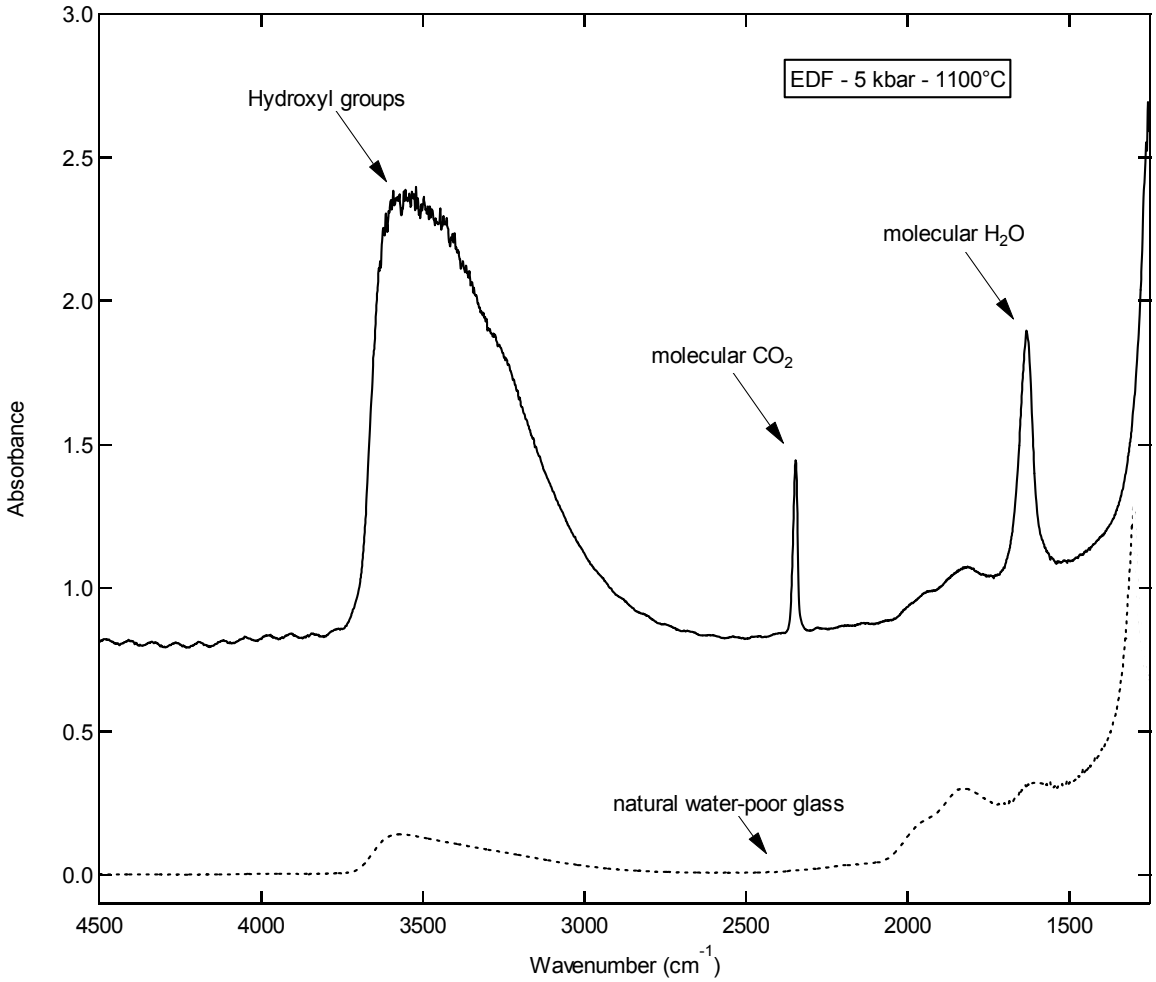

Fig. 1: Typical MIR-spectrum of a hydrous CO_2-bearing sample. A spectrum of the natural water-poor glass is shown for comparison in dotted line. Sample thicknesses: 50 µm.

A major problem in our measurements has been that the IR beam could not be completely isolated from the atmosphere. Thus, the CO_2 content of the air in the beam path may vary during the measurements. To quantify this variation, we have compared 92 spectra collected without sample. These spectra were recorded in two ways over a period of several days: (1) series of around 10 spectra without sample were recorded without opening the sample chamber of the IR microscope, (2) one or several spectra without sample were directly collected after the IR measurements performed on each glass sample. The variation in peak intensity was found to be random, suggesting rapid changes of atmospheric CO_2 concentrations with time. Therefore, the average of 0.014 ±0.0010 absorbance units in peak intensity corresponding to the atmospheric CO_2 band at 2349 cm^{-1} was used to determine the precision of our CO_2 measurements.

3.3. Bulk extraction

The C contents of the glasses were measured by CO_2-titration. A schematic illustration of the CO_2-titration device (Deltromat 500, Deltronik) is given in Fig. 2. For clarity, not all details of the apparatus are included. The advantage of this method is that only small quantities of material are required to get a reliable analysis. Only 70 mg of material with a concentration of a few hundred ppm give reliable results. The method is based on the quantitative reaction of CO_2 with barium hydroxide forming barium carbonate, which is insoluble in the aqueous liquid:

$$Ba^{2+} + CO_2(g) + 2\,OH^- \Leftrightarrow BaCO_3(s) + H_2O \quad (1)$$

The amount of hydroxyl groups necessary for this reaction is generated electrolytically (coulometric titration). The titration is controlled by the pH-value of the solution in the cathode cell (basic barium perchlorate). The pH-value is measured by a glass electrode with an Ag|AgCl half-cell as reference (Fig. 2). Hydroxyl groups are produced by the following reaction:

$$2\,H_2O + 2\,e^- \Rightarrow H_2 + 2\,OH^- \quad (2)$$

The CO_2 content can be directly determined from the quantity of electrons required for the electrolyses. One mole of CO_2(g) reacts quantitatively with one mole of Ba^{2+} and 2 moles of hydroxyl groups and, therefore, 1 mg of CO_2 is equivalent to 4.39 coulombs. At the anode (chamber I, Fig. 2), the reaction (1) proceeds in the opposite direction. OH^- is consumed by the following reaction:

$$4\,OH^- \Rightarrow O_2 + H_2O + 4\,e^- \quad (3)$$

The current stream is ensured by the flux of ions Ba^{2+} through the clay membrane (diaphragm) towards chamber II and I, respectively.

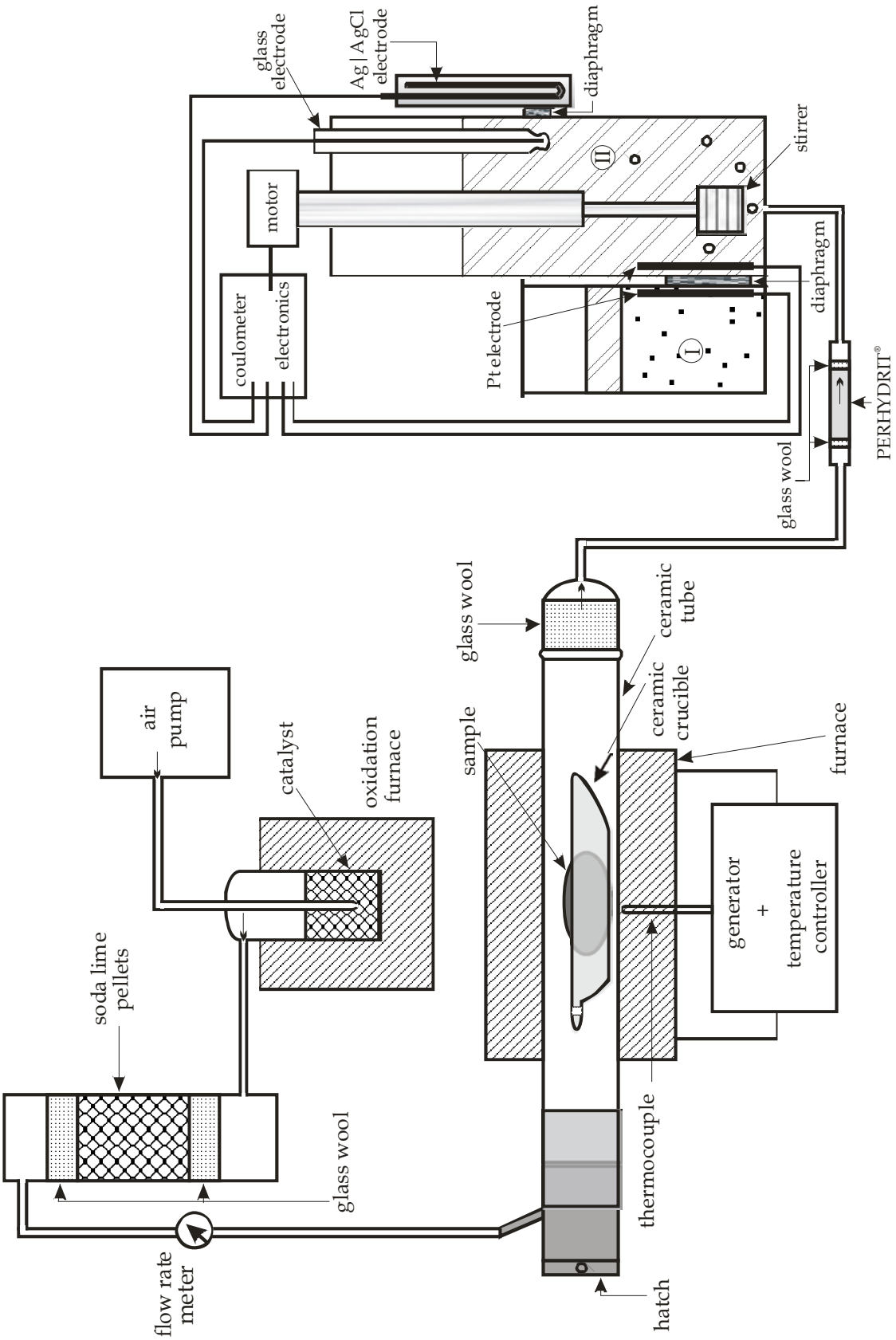

Fig. 2: Schematic illustration of the CO_2-titration device (Deltromat 500, Deltronik). Item scale is not respected. See text for working explanations.

In principle, no standards are necessary for the calibration of this method. However, for the analyses of solid materials, additional steps are involved in the measurement procedure besides the titration itself. C must be released from the sample by heating and must be transported to the titration cell. Tests are necessary to guarantee that really the entire C content of the sample is detected. The materials used for testing were separately analysed by two others bulk extraction ways, in three different places, in Köln and Göttingen using coulometric titration, and in Bristol using a LECO CS-300 (LECO® corporation, St Joseph, MI), based on IR measurements of carbon dioxide. All measurements are consistent within 5%.

In standard measurements an air stream is used for oxidising carbon of the sample. Organic components from the air stream are oxidised in an oven heated up to 800°C. Soda lime pellets absorb the so-produced CO_2 as well as the initially present CO_2. Thus, the air stream is essentially C-free when reaching the sample and low background levels can be achieved (typical background: 0.0003 ±0.0001 units, corresponding to 1.5 ±0.5 µg C, or 5.5 ±1.8 µg CO_2).

For sample loading, the flow of air leading to the cell is interrupted and a counter flux of decarbonated air prevents contamination of the system by carbon species from outer atmosphere. The coarse grained sample is inserted in a ceramic crucible (12×80×9) which was pre-annealed for 5 min at 1200°C. The crucible is placed in the hot zone of the tube furnace which is held at a constant temperature of ca. 1200°C. Temperature is measured by a thermocouple located close to the ceramic tube. After closing the chamber the apparatus is flushed with a flow rate of ca. 50 L/hour. On its path to the titration cell the gas stream passes through glass wool to remove any flowing particles as iron oxides, and PERHYDRIT® to oxide SO_2. All C is released from the sample and carried off to the cell as CO_2 gas within 90 s. The analyses are terminated automatically by the dead-stop method, if the titration current falls below 5 mA.

The uncertainty on a single measurement given by the constructor is ± 0.0004 units corresponding to 2 µg C. To test which accuracy of the determination can be obtained in practice, we performed repeated series of measurements using a similar sample mass of a given sample. We explore four different materials (TW64d, GD62, 22V and 45V) containing between 0.4 to 6 wt.% equivalent CO_2. Standard samples analysis are given in Table 3. It comes out that the value given by the constructor can be taken as an appropriate estimate of the error of the C-content.

A critical aspect in all decarbonation techniques for the determination of volatile contents is whether or not all CO_2 is released from the sample. It is difficult to answer that question because IR spectroscopy could not be performed on the analysis products. I assumed, that the CO_2 remaining in the glass structure was negligible after the heating. However, it can not be excluded that some CO_2 was still present in the glasses after extraction as observed for H_2O after determining water contents in granitic and feldspathic glasses by Karl-Fischer titration (Behrens 1995).

Another important problem in C analysis may be that C-bearing species are adsorbed on the sample surface as polluters before bulk extraction. Step heating was not possible with the Deltromat,

so that dissolved and adsorbed CO_2 could not be discriminated. I consider this as a minor problem in my study because of the high CO_2 contents involved (up to 3893 ppm versus 870 ppm in Blank's study, 1993).

4. Results and discussion

4.1. Quenched products

The run products were bubble- and crystal-free glass blocks, weakly coloured to colourless except for samples 1P and 2P, which came out almost red and broken into pieces. The coloration is due to the dissolution of Ag, and the breaking is the result of a too quick decompression.

Absorbances from MIR spectroscopy and CO_2 contents from the bulk extraction are given Table 2. All chips, based on MIR spectroscopy, show a fairly homogeneous distribution of CO_2 (absorbances on the same chip agree within 6%), with no detectable difference between rim and core of glasses outside the analytical error. An exception is sample std5, in which absorbances vary between 0.717 (middle piece, showing itself differences up to 40% between core and rim) and ca. 0.950 (extremity pieces), for similar sample thicknesses. In this run, the fluid was extremely poor in water. I assume that the run duration was not sufficient to homogenise the melt. See chapter 2 § 4.1..

In addition given Table 2 are water contents of the samples determined either by NIR spectroscopy (as described chapter 2 § 3.4.2.) or by KFT (as described chapter 2 § 3.3.).

4.2. Calibration

The relationship between the coulometric and IR measurements was evaluated by the Lambert-Law using a linear, least squares regression of the data (Fig. 3) taking into account both errors of both the abscise and the ordinate. The molar absorption coefficient ε for CO_2 in rhyolite, ε_{2350}, was determined from the slope of the line using the following expression:

$$\varepsilon_{2346} = \frac{\mathrm{K}}{c_{CO_2}} \tag{4}$$

where

$$\mathrm{K} = \frac{4401 \times A_{2346}}{\rho \times d} \tag{5}$$

with c_{CO_2} the CO_2 contents of the glasses in wt%, A is the absorbance (peak height), ρ the glass density in $g.l^{-1}$, and d the thickness of the doubly polished chips for IR measurements in cm.

First an average *K* value was determined for each chip (see Table 2), and then an average value was calculated for each sample. The latter one was used in the regression. The error on each *K* was determined by taking into account the error on the absorbance, as described in § 3.2.2., the error on the density as described in chapter 2 § 3.2., and the error on the thickness as explained in chapter 2 § 3.4.1.. The error on the averages *K* for the regression is obtained by error propagation.

All data are well reproduce by a signal regression line except of the sample std1, which has the lowest CO_2-content. The water content of the other samples vary widely (0.5 – 6.8 wt%) and the consistency of the data indicate that water is not influencing noticeably the linear molar absorption coefficient. Data from Blank (1993) could not be included in the regression, because of the lack of clarity in the samples thicknesses.

The value of ε_{2346} obtained in this study for rhyolitic glasses is 1232 ±36 $l.cm^{-1}.mol^{-1}$. This value is 15% higher than the value of 1066 ±20 $l.cm^{-1}.mol^{-1}$ determined by Blank (1993) for rhyolite and 23% higher than the value of 945 $l.cm^{-1}.mol^{-1}$ determined by Fine and Stolper (1985) for albite composition (Fig. 3). CO_2 concentrations reported in former works (Fogel and Rutherford, 1990 and Blank, 1993) should all be decreased by 23% and 15%, respectively.

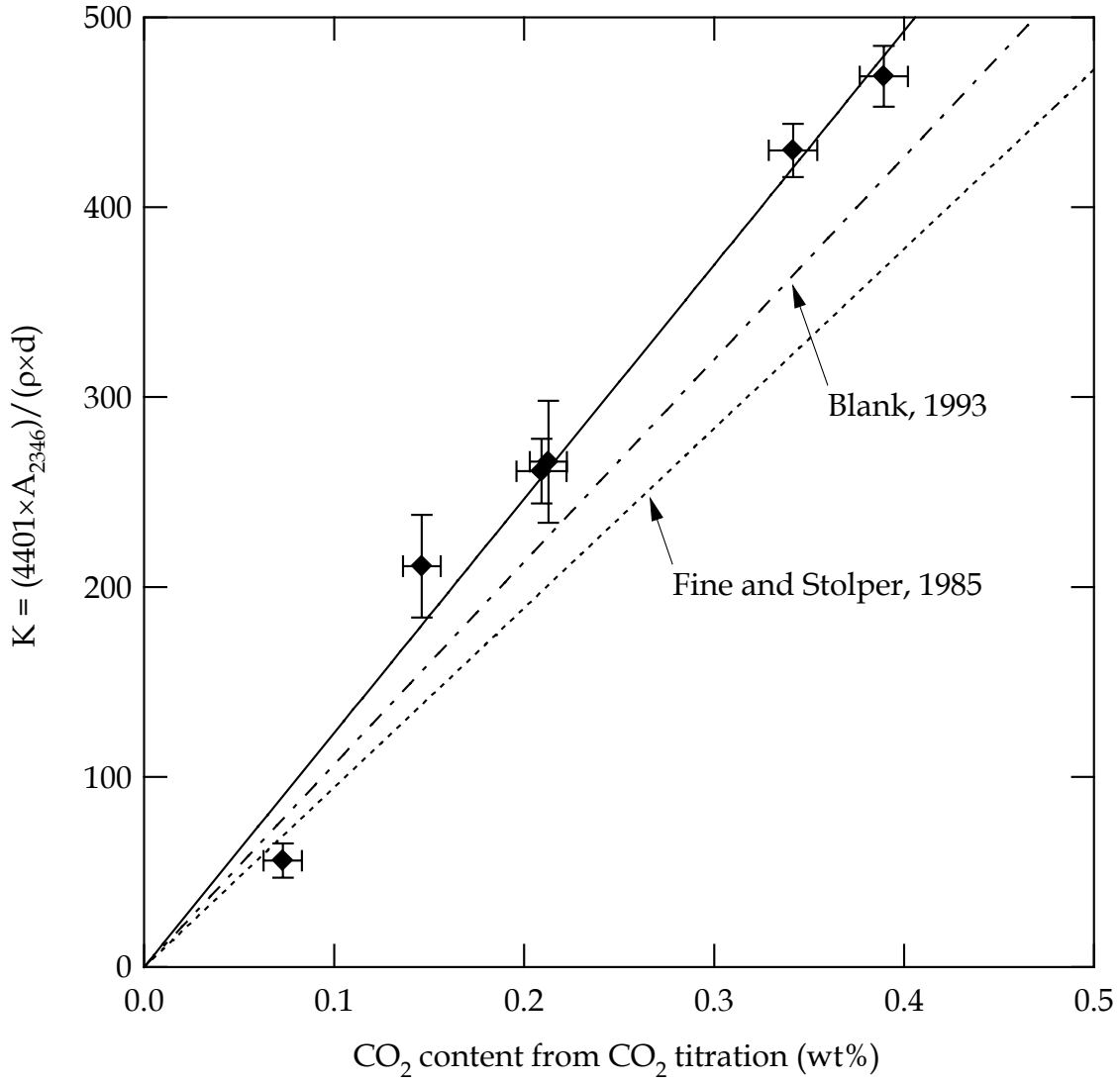

Fig. 3: Determination of the molar absorption coefficient ε for the CO_2 band at 2346 cm^{-1} using bulk extraction and IR measurements. ε is obtained by a linear, least squares regression of the data taking into account errors in both coordinates. Regressions of Fine and Stolper (1985) determined for albitic compositions and Blank (1993) determined for rhyolitic compositions are displayed for comparison. Outlier at low C_{CO2} may be explained by contamination from organic material of the sample used for coulometric titration.

Ch. 2: The solubility of H_2O and CO_2 in rhyolitic melts in equilibrium with a mixed CO_2-H_2O fluid phase

1. Introduction

Volatiles (especially water) dissolved in silicate melts influence dramatically the chemical and physical properties of magmas. Because of its high solubility in silicate melts, water is of particular interest for understanding properties of magmas. Water solubility in rhyolitic melts coexisting with pure H_2O fluid were investigated by several authors in the last decades (see McMillan, 1994; Zhang, 1999) using different techniques (see reviews in Ihinger et al., 1994; Kohn, 2000). CO_2 is the second most important volatile which is usually present in natural magmas. The CO_2 solubility in rhyolitic melts is not as well documented as the H_2O solubility (see Blank and Brooker, 1994) because it is significantly lower than that of water. Its presence reduces significantly water solubility (Blank et al., 1993) and can influence degassing processes. To model degassing during volcanic eruptions a detailed knowledge of mixing properties of volatile components in the fluid and in the melt is required. So far, only a few studies have been performed to investigate the solubility of volatiles in rhyolitic or in synthetic analogs in equilibrium with mixed fluids melts (Wyllie and Tuttle, 1959; Kadik et al., 1972; Blank et al., 1993; Schmidt et al., 1998, 1999). Because of the lack of experimental data, the solubilities of H_2O and CO_2 are often calculated using the model of Holloway and Blank (1994). However, the application of this model is limited to relatively low pressure (<200 MPa). An alternative to this model is that of Papale (1999), which has not been experimentally tested in the pressure range 200-500 MPa.

In this chapter, the solubility of H_2O and CO_2 was investigated at 200 and 500 MPa and 800 and 1100°C to constrain the solubility behaviour of mixed fluids in melts of rhyolitic compositions. An empirical model to calculate the H_2O content of the melt between 75 and 500 MPa as a function of the fluid phase composition, pressure and temperature is derived from our new data and solubility data from Blank et al. (1993).

2. Sample preparation

2.1. Starting material and experimental procedure

The starting material was the same assimilated bubble- and crystal-free obsidian (EDF) that was used for the determination of the linear molar absorption coefficient described chapter 1 § 2.1..

Small glass pieces (1.5×2.5×5.5 and 1×2×5 mm, approx. 45 to 30 mg) were loaded with a CO_2 source and double-distilled water into a noble metal capsule (Au or Pt, inner diameter: 3-4 mm, wall thickness: 0.2 mm, length: 2-4.5 cm). The proportion of fluid in the charge ranged from 6 to 23 % (by weight). Different techniques were used to generate CO_2 during the experiment depending on run temperature. For runs at 800°C silver oxalate ($Ag_2C_2O_4$) was loaded directly into the Au-capsule. In the very first runs at 1100°C Pt capsules were used and showed some leakages. Therefore, as described chapter 1 § 2.2., silver oxalate when used as the CO_2 source was isolated from the Pt-capsule walls. An alternative source of CO_2 used is oxalic acid ($H_2C_2O_4$), produced by dehydration of $H_2C_2O_4 \cdot 2\ H_2O$ in a drying-oven at 105°C. Oxalic acid can be directly loaded in Pt-capsules as only volatiles (H_2 and CO_2) are generated by thermal decomposition. CO_2 sources were stored in a desiccator to prevent any water adsorption. However, some remaining water (< 1 wt.%) can not be avoided. During welding, the capsules were cooled using liquid nitrogen to prevent any loss of water or CO_2. For each sample, the technique used to generate CO_2 is specified in Table 4.

2.2. Run conditions

Four sets of experiments were performed: 200 MPa/800°C, 200 MPa/1100°C, 500 MPa/800°C and 500 MPa/1100°C with run durations ranging from 3 to 12 days (Table 4). Two different kind of pressure vessels were used: (1) cold seal pressure vessel (CSPV) pressurised with water at 800°C, (2) vertically oriented internally heated pressure vessel (IHPV) pressurised with argon at 1100°C (Becker et al., 1998). Temperature was measured with an accuracy of ±10°C (taking temperature gradients and accuracy of thermocouples into account) using K type thermocouples and pressure with an accuracy of ±5 MPa using a strain gauge manometer.

The oxygen fugacity in CSPV was buffered by the NNO (Ni-NiO) assemblage. An intrinsic oxygen fugacity (expressed as $\Delta \log f_{O_2}$) of NNO +2.3 was determined at 500 MPa and 850°C in the IHPV by Wilke and Behrens (1999) using Ni-Pd solid sensors (Taylor et al., 1992). The same technique was applied at 500 MPa and 1100°C and the calculated intrinsic oxygen fugacity was NNO +3.5.

In CSPV, samples were quenched from experimental conditions to room conditions using a flux of compressed air and the initial cooling rate is approximately 200°C/min. In IHPV, samples were quenched by turning off the power resulting in an initial cooling rate of 150°C/min. All runs were quenched isobarically.

3. Analytical techniques

3.1. Determination of the fluid composition after experiment

The fluid composition after the experiment was determined by weighing the capsule using the following procedure: (1) the capsule was weighed, (2) the water from the fluid phase was frozen using liquid nitrogen, (3) the capsule was punctured with a needle, (4) after warming to room temperature, the capsule was weighed to determine the mass of CO_2 (+N_2 from air enclosed during loading the capsule), (5) the capsule was placed into a drying oven and subsequently weighed to determine the mass of water. The capsule weight-loss was periodically checked (approximately 10 min interval) until the weight remained constant. At this point, the water from the fluid phase was considered to be entirely extracted. The temperature of the drying oven was 110°C, except for glass samples with expected water concentrations exceeding 6 wt% H_2O. For these glasses, the oven temperature was between 50-70°C.

The mole fractions of H_2O and CO_2 in the fluid (Table 4) were calculated as follows:

$$X^{f}_{H_2O} = \frac{\left(\frac{m_{H_2O}}{18.02}\right)}{\left(\frac{m_{CO_2}}{44.01} + \frac{m_{H_2O}}{18.02} + \frac{m_{N_2}}{28.01}\right)} \tag{6}$$

$$X^{f}_{CO_2} = \frac{\left(\frac{m_{CO_2}}{44.01}\right)}{\left(\frac{m_{CO_2}}{44.01} + \frac{m_{H_2O}}{18.02} + \frac{m_{N_2}}{28.01}\right)} \tag{7}$$

In these calculations we take into account that atmospheric N_2 was trapped in the experimental charge during preparation of the capsule. We estimate the resulting mole fraction of N_2 in the fluid phase (X^{f}_{N2}) to be in the range 0.5 to 4 mol%. This variation is due to varying melt/fluid ratios and capsule lengths. The estimated X^{f}_{N2} are consistent with the X^{f}_{N2} determined by gas chromatography on the remaining fluid phase of similar solubility experiments performed with haplogranitic melts (Behrens, unpublished data). Furthermore, minor amounts of CO (< 0.12 mol%) were detected in CO_2 rich fluids. However, as concentrations of additional components are low we consider the fluid phase as a two-component gas mixture of CO_2 and H_2O.

Using the gravimetric method (described above), the individual weights of CO_2 and N_2 could not be distinguished. Therefore, the enclosed N_2 represents the main source of error in the determination of X^{f}_{CO2} and X^{f}_{H2O}. To account for N_2 we assumed an average X^{f}_{N2} of 0.02 ±0.02 for all experiments,

except for experiments with pure water where X^f_{N2} was negligible (<0.01). As N_2 and CO_2 are measured together but H_2O is measured independently the error is larger in X^f_{CO2} than in X^f_{H2O}. The maximum error on X^f_{CO2} is given by X^f_{N2} in the fluid phase. The corresponding error on X^f_{H2O}, resulting from the difference in molar mass between N_2 (28.01 g.mol^{-1}) and CO_2 (44.01 g.mol^{-1}), is $0.36 \times X^f_{N2}$. To calculate the errors on X^f_{CO2} and X^f_{H2O} given in Table 4, we have taken into account the weighing uncertainty (0.1 and 0.05 mg for CO_2 and H_2O, respectively) and the error induced by atmospheric N_2 (0.02 and 0.007 mol% for CO_2 and H_2O, respectively).

The gravimetric method was found to be accurate for fluid compositions $0.1 < X^f_{H2O} < 0.9$. However, for extreme CO_2 or H_2O rich fluids, this method is not suitable because water and CO_2 can not be properly separated. Therefore, in these cases we have used mass balance to determine the composition of the fluid phase.

3.2. Density determination

Densities of the rhyolitic glasses were measured by weighing the single glass pieces in air and in water. The principal error of the method arises from weighing the sample in water, where problems related to surface creep introduce 0.2 mg uncertainty, estimated by repeated measurements on standards. For the relatively small samples obtained in the solubility experiments (20-40 mg) the resulting error is typically 2% relative. Densities of a total number of 22 hydrous rhyolitic samples including two samples synthesised at 150 MPa were measured. The density data of 9 glasses obtained from our solubility experiments are given in Table 5. As already observed by several authors (e.g. Silver et al., 1990; Richet et al., 1996; Schulze et al., 1996; Behrens et al., 1996; Richet and Polian, 1998) the dependence of density on water content can be modelled by a linear equation:

$$\rho = \rho_0 + m \cdot C_{water} \tag{8}$$

where ρ is the density of the hydrated glass, ρ_0, the density of the dry glass, m a constant and C_{water} the total water content (expressed in wt%). An updated weighted least square regression was performed for the EDF rhyolitic composition using our 22 samples and data from Withers and Behrens (1999). The density data of Withers and Behrens (1999) are systematically higher than those determined in our study (Fig. 4). This deviation can be explained by the difference in synthesis pressure (Withers and Behrens, 1999: 500 MPa; this study: 150–500 MPa) and sample size (smaller samples and therefore higher uncertainty on density determination in our study), and a possible effect of dissolved CO_2 in the glasses.

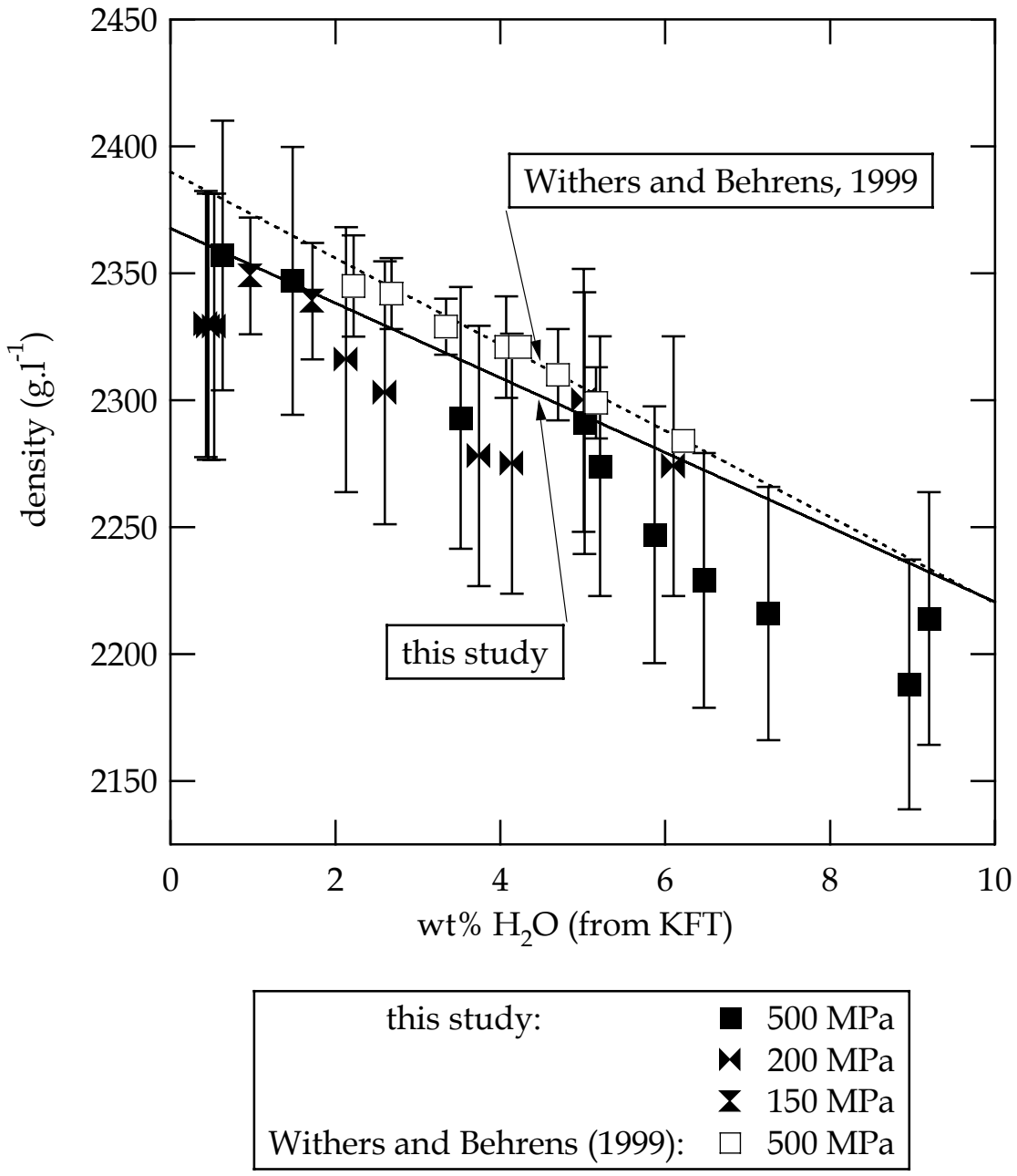

Fig. 4: Density-water content relationship for rhyolitic glasses. The linear fit of Withers and Behrens (1999) considers data of glasses synthesised at 500 MPa only (dashed line). In our new fit (solid line) we combined the data from Withers and Behrens with our new data obtained at 150, 200 and 500 MPa.

Fitting all the data to equation (8) we have calculated ρ_0 and m to be 2367.7 (±15.6) and -14.72 (±3.50), respectively, for rhyolitic glasses (see Fig. 4). To be internally consistent, the glass densities required for determination of volatile concentrations from IR spectra always were calculated by this density-water content relationship. It is emphasised that the density-water content relationship defined

by Withers and Behrens (1999) may predict adequately densities at 500 MPa. However, to calculate densities of rhyolitic glasses produced over a wide pressure range (150-500 MPa), the new relationship is recommended.

3.3. Karl-Fischer titration

The water contents of some of the experimental glasses were measured by pyrolysis and subsequent Karl-Fischer titration (KFT). The apparatus and analytical technique are described in detail by Behrens et al. (1996). One or two chips of glass (15-30 mg) are heated to 1300°C in order to extract the dissolved water. The released water is transported by an Ar-flux to a titration cell and analysed by a coulometric method (KFT). Uncertainties in measured water contents were calculated on the basis of ±0.02 $\mu g.s^{-1}$ uncertainty in titration rate (Behrens et al., 1996), taking also into account a residual (unextracted) water content of 0.10 ±0.05 wt% (Behrens, 1995).

3.4. IR spectroscopy

3.4.1. Sample preparation and analysis conditions

Small pieces were cut from the middle of the sample and doubly polished down to a thickness of either 480-1000 μm for NIR or 35-125 μm for MIR spectroscopy. The thickness of each glass chip was measured using a digital micrometer. An estimate of ±0.0003 cm was assumed for the uncertainty in thickness. The thicknesses of the polished sections were in part difficult to measure with the micrometer due to bending of the glass. Therefore, we have used the interference fringes in the IR spectra for thickness determination of the samples investigated with MIR spectroscopy (Fig. 5). This method has the advantage that peak intensities and thicknesses are measured exactly at the same position of the sample.

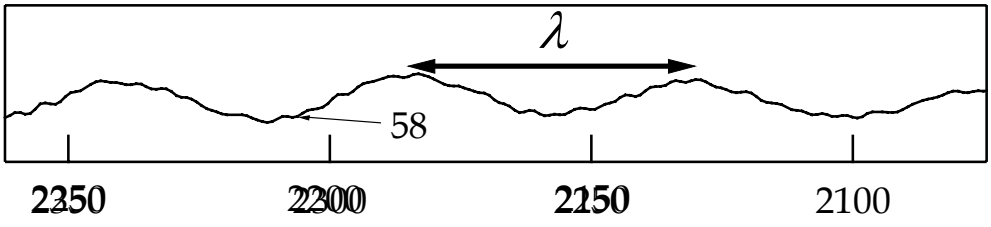

(5-b)

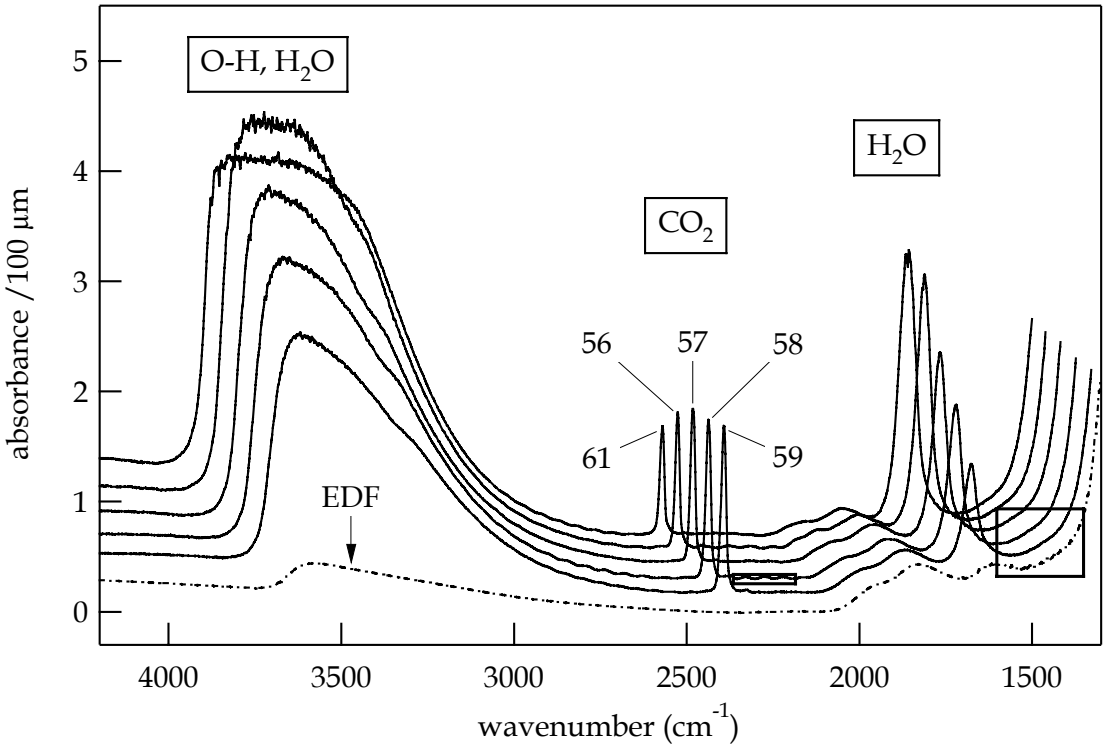
O-H, H2O
H2O
CO2
56
57
58
61
59
EDF
absorbance /100 µm
wavenumber (cm-1)
0
1
2
3
4
5
4000
3500
3000
2500
2000
1500

(5-a)

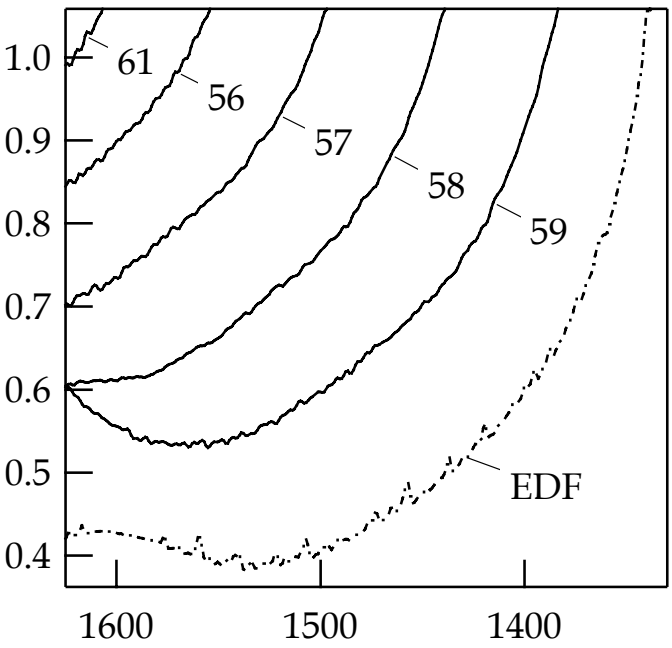
61
56
57
58
59
EDF
0.4
0.5
0.6
0.7
0.8
0.9
1.0
1600
1500
1400

(5-c)

Fig. 5a-c: (**a**) Typical MIR spectra of hydrous CO_2-bearing rhyolitic glasses normalised to 100 µm thickness. A linear base line fitted to the feet of the CO_2 peak was subtracted. A spectrum from natural EDF is shown for comparison (dashed line). For clarity, spectra of experimental glasses are plotted with x/y offsets. Numbers refer to the experimental runs in Table 2 and Table 3. (**b**) detail showing the interference fringes in the domain where sample thicknesses were determined. (**c**) detail showing the 1325-1625 cm^{-1} area where carbonate doublets were observed in glasses of other compositions. No evidence of carbonate could be found in any of the rhyolitic glasses.

If the measurement beam is oriented perpendicular to the glass chip, the wavelength λ of the interference fringes is given by:

$$\lambda = \frac{1}{2 \cdot d \cdot n} \tag{9}$$

where d is the thickness and n the refractive index. This equation can not be directly applied for thickness determination because (1) the refractive indexes of the rhyolitic glasses are not exactly known in the MIR (only a value of $1.48<n<1.51$ in the visible is given by Tröger, 1959) and (2) the beam of the IR microscope is focused at the sample position. Thus, the factor, which links the thickness and the inverse of the wavelength, has to be determined experimentally. Using a set of 53 samples for which we have measured interference fringes in the range 2070-2270 cm^{-1} we found a linear relationship of d and $1/\lambda$ (Fig. 6). By linear regression we obtained:

$$d = \frac{0.3176(\pm 0.0024)}{\lambda} \tag{10}$$

Equation (10) was used throughout our study for determination of thicknesses of MIR sections.

See § 3.2.1. chapter 1 for a description of the devices used for spectra collection.

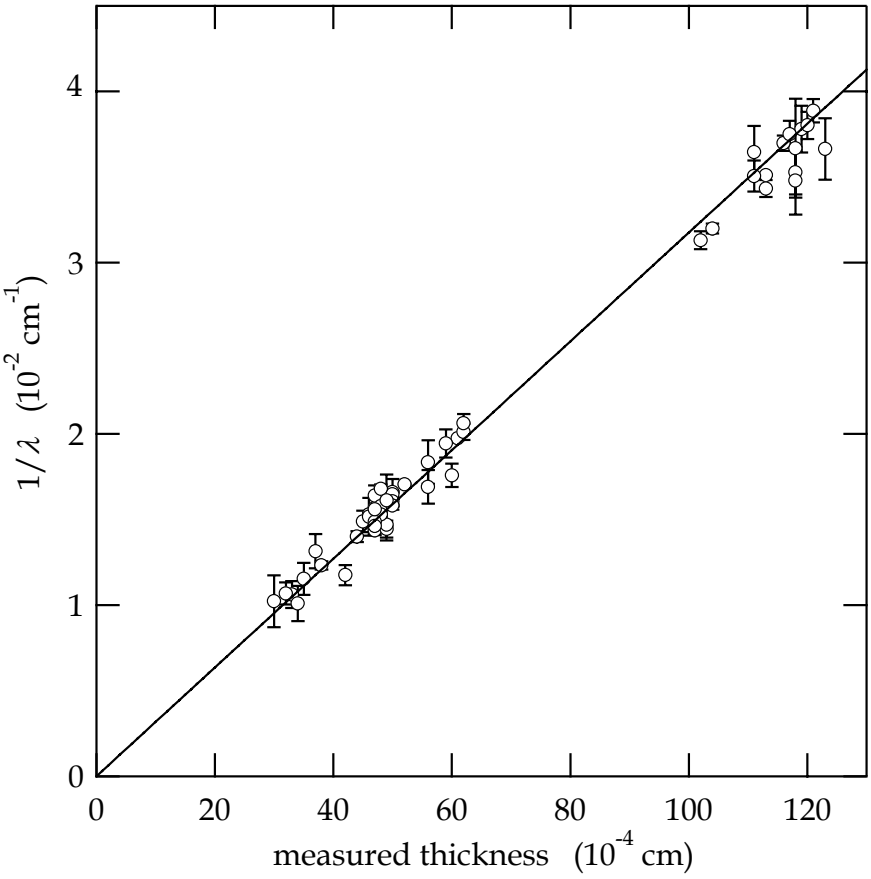

Fig. 6: Calibration curve of sample thickness as a function of the inverse wavelengths of interference fringes.

3.4.2. NIR spectroscopic determination of water contents

The concentrations of H_2O and OH were determined from the heights (see Table 5) of the baseline corrected absorption bands at 5230 cm^{-1} and at 4520 cm^{-1} which are attributed to the combination stretching + bending mode of molecular H_2O and combination stretching + bending mode of OH groups (Scholze, 1960; Bartholomew et al., 1980; Stolper, 1982) by using the Lambert-Beer law. We used an appropriate automated two linear tangent baseline subtraction method (described in detail in Withers and Behrens, 1999), to increase the reliability of the method. Linear molar absorption coefficients of 1.41 $L.cm^{-1}.mol^{-1}$ and 1.66 $L.cm^{-1}.mol^{-1}$ for the 4520 cm^{-1} and 5230 cm^{-1} bands, respectively (Withers and Behrens, 1999) are used to calculate the total water contents.

3.4.3. MIR spectroscopic determination of CO_2 contents

The concentrations of carbon species were determined from the heights (see table 5) of the baseline corrected MIR absorption band at 2346 cm^{-1} assigned to the fundamental ν_3 vibration of CO_2 molecules (Fig. 5a). No carbonate species was detected in any of the rhyolitic glasses (Fig. 5c). This is consistent with former studies on CO_2 solubility in rhyolite (cf. Fogel and Rutherford, 1990; Blank et al., 1993). The height of the 2346 cm^{-1} peak was determined using an automated linear tangent baseline subtraction method. We used the linear molar absorption coefficient of 1232 ±36 $g.cm^{-1}.mol^{-1}$ determined chapter 1.

We encountered the same random unavoidable change in CO_2 atmospheric concentration during measurements. The average peak intensity of the atmospheric CO_2 band at 2349 cm^{-1} corresponding to 0.014 ±0.0010 absorbance unit determined for our measurement conditions corresponds to an equivalent CO_2 content of 19 ppm for a 100 μm thick sample. This is considered to be the precision of CO_2 absorbance measurement.

4. Results and discussion

4.1. Quenched products

The solid run products consist of clear, weakly coloured to colourless glasses (except sample 11, which contains up to 2 wt% Ag), which were mostly bubble and crystal free. Bubbles are only observed in two samples (Ech22 and Ech24) synthesised in an experiment, which was started twice (due to failure of the furnace), and are small and homogeneously distributed. Few crystals were observed at 800°C and 200 MPa for X^f_{H2O}<0.35 (Table 4). The crystals were too small to be analysed by microprobe but no noticeable change in the melt composition was observed. The composition of each glass was checked by electron microprobe for possible changes during the experiments. Only a loss of iron in experiments performed with Pt-capsules was observed, especially at rimes of the glasses. However, as the iron content in the starting glass is low, we assume that the depletion of iron has no significant effect on volatile solubilities.

The H_2O and CO_2 contents of glasses are given in Table 5. All samples analysed by IR spectroscopy show a homogeneous distribution of water and CO_2 with no detectable difference between rim and core of glasses within analytical error. An exception is sample Ech75 in which CO_2 concentration varied between 0.203 (core) and 0.254 wt% (rim). In this run the fluid was extremely water poor and we assume that the run duration was insufficient to homogenise the melt. This interpretation is supported by diffusion data (Watson, 1994; Zhang and Behrens, 2000) showing a strong decrease of CO_2 and H_2O diffusivity with decreasing water content in the melt. The CO_2

solubility of Ech75 given in table 5 corresponds to the average of the five highest solubilities measured in rime of the sample. This value is assumed to be close to the equilibrium solubility.

It can be noted that for water contents >7 wt%, the NIR spectroscopy method tends to under-estimate water contents as shown by comparison to the KFT data (maximum difference: 0.77 wt%, Ech36). A possible explanation is that some water was lost during sample preparation (before polishing, samples are heated up to 60-70°C). This interpretation is supported by the results obtained for the most water rich sample (Ech49) which was not polished and for which the NIR and KFT values are almost within the error-bar. Therefore, we decided to take the KFT data as representative for the water solubility in water rich samples (Ech36, Ech49).

4.2. H_2O solubility

Fluid compositions and the corresponding water and CO_2 contents of the quenched glasses are presented in Table 4 and Table 5, respectively. At both 200 and 500 MPa, a square root dependence of water solubility on X^f_{H2O} is observed at low X^f_{H2O} (Fig. 7). At 200 MPa, a linear function between water solubility and X^f_{H2O} allows to model all data within uncertainty for $0.25<X^f_{H2O}<1$. At 500 MPa, the water solubility shows a non linear dependence on X^f_{H2O} in the whole X^f_{H2O} range. The 500 MPa data indicate a point of inflexion at around $X^f_{H2O}\sim0.5$.

The temperature dependence of water solubility is different at 200 and 500 MPa. At 200 MPa, the water solubility decreases with increasing temperature, regardless of the composition of the fluid phase. The water solubility variation as a function of temperature is constant in the investigated range of X^f_{H2O} ($0.25<X^f_{H2O}<1$) and corresponds to -0.16 wt% H_2O per 100°C. This value is similar to that observed for a haplogranitic composition at $X^f_{H2O}=1$ (Holtz et al., 1992). At 500 MPa, the temperature dependence of water solubility changes from positive for $X^f_{H2O}>0.75$ to negative for $X^f_{H2O}<0.75$. Water solubility is found to be independent of temperature at a water content of approximately 7 wt%.

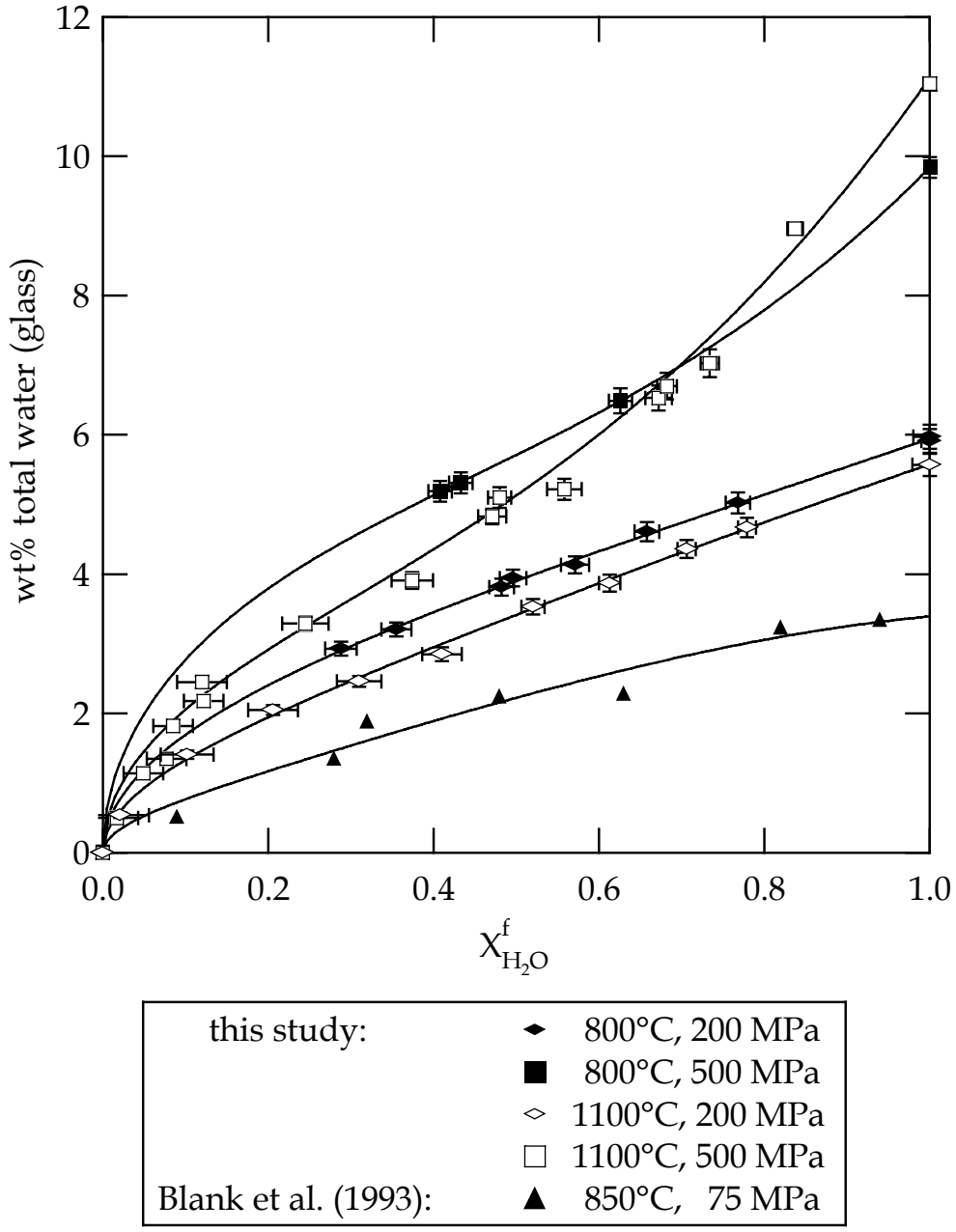

Fig. 7: Relationship between the mole fraction of H_2O in the fluid phase and the concentration of total water dissolved in the melt at various temperatures and pressures. Solids lines are the fits of the data used for the empirical model developed in this study. Data from Blank et al. (1993) are shown for comparison.

Behrens et al. (2000b) showed that the pressure at which water solubility at $X^f_{H2O}=1$ is independent on temperature depends on the melt composition and especially on the aluminum charge balancing cation (compare also results from Paillat et al., 1992; Holtz et al., 1995). For a subaluminous composition with approximately the same Na/K ratio as EDF, the water solubility at $X^f_{H2O}=1$ is

independent on temperature at approximately 350 MPa (composition AOQ, Holtz et al., 1995), which corresponds to a water content of about 8 wt%. This amount of water is close to the water content at which water solubility in rhyolitic melts coexisting with mixed fluids is independent on temperature at 500 MPa (7 wt%). The small difference may be attributed to compositional differences of the melts and experimental uncertainties. Thus, for a given composition, the temperature dependence of water solubility does not depend on total pressure but on the prevailing f_{H2O}.

4.3. CO_2 solubility

CO_2 solubility increases with increasing X^f_{CO2} in the fluid phase (Fig. 8) and increasing pressure. The variation of CO_2 solubility with X^f_{CO2} is non-linear. The deviation from linearity increases with pressure and is espacially pronounced at 500 MPa. Extrapolating our data set to X^f_{CO2}=1, the maximum solubility are 0.09 ± 0.01 and 0.24 ± 0.03 wt% at 1100°C and 200 and 500 MPa, respectively. At 800°C, the melts are partially crystallised when using CO_2 rich fluids (X^f_{CO2} > 0.65 at 200 MPa, X^f_{CO2} > 0.5 at 500 MPa) and prediction of the solubility of pure CO_2 is very uncertain.

To compare our CO_2 solubility data with those from Fogel and Rutherford (1990), we have interpolated their data, and for internal consistency corrected them taking into account the difference in absorption coefficient (Fogel and Rutherford used absorption coefficients for albitic glasses from Fine and Stolper, 1985). The so-obtained CO_2 solubility for $X^f_{CO2} \approx 1$ at 1100°C, 200 and 500 MPa are 15-20 % lower than our extrapolated data (Fig. 8 and 9). The differences may result from experimental uncertainties in the study of Fogel and Rutherford (1990). Gradients of CO_2 and/or H_2O were observed even in long term experiments, and extrapolating the CO_2 diffusion profiles to determine CO_2 solubility may underestimate the equilibrium solubility. Furthermore, the composition of the fluid was not analysed. As noted by the authors, the fluid contained minor amounts of H_2O and possibly up to 30 mol% CO. Assuming an X^f_{CO2} of 0.7, the solubility data of Fogel and Rutherford are in a good agreement with our data.

Within the uncertainty of the data, no obvious effect of temperature on CO_2 solubility is observed at 200 MPa (Fig. 8). However, the data indicate a slight positive temperature dependence on CO_2 solubility at 500 MPa (for X^f_{CO2}<0.5). It is interesting to note that this effect of temperature on CO_2 solubility for X^f_{CO2}<0.5 differs from that observed by Fogel and Rutherford (1990) at X^f_{CO2}=1. These authors found that increasing temperature from 950 to 1150°C the CO_2 solubility decreases at both 200 and 500 MPa.

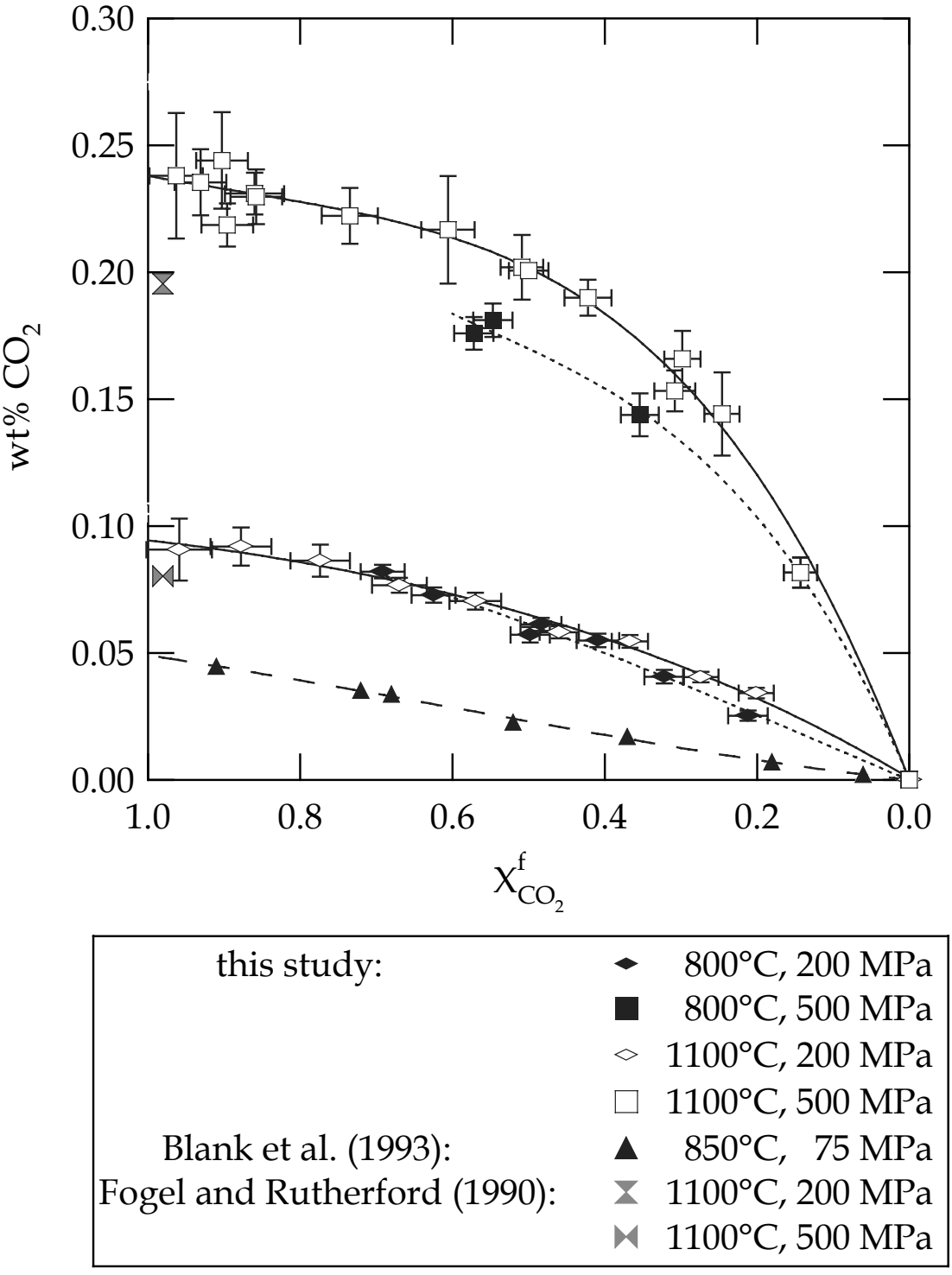

Fig. 8: Relationship between the mole fraction of CO_2 in the fluid phase and the concentration of CO_2 in the melt at various pressures and temperatures. Data from Fogel and Rutherford (1990) and Blank et al. (1993) are shown for comparison. Solid lines represent trends at 1100°C and dotted lines at 800°C. The dashed line show the trend of the data obtained at 850°C and 75 MPa by Blank et al. (1993).

4.4. Comparison with calculations

Figure 9 shows the experimental data for H_2O and CO_2 solubility in rhyolitic melts coexisting with H_2O-CO_2 fluids in comparison to predictions of thermodynamic models from Holloway and Blank (1994) and Papale (1999).

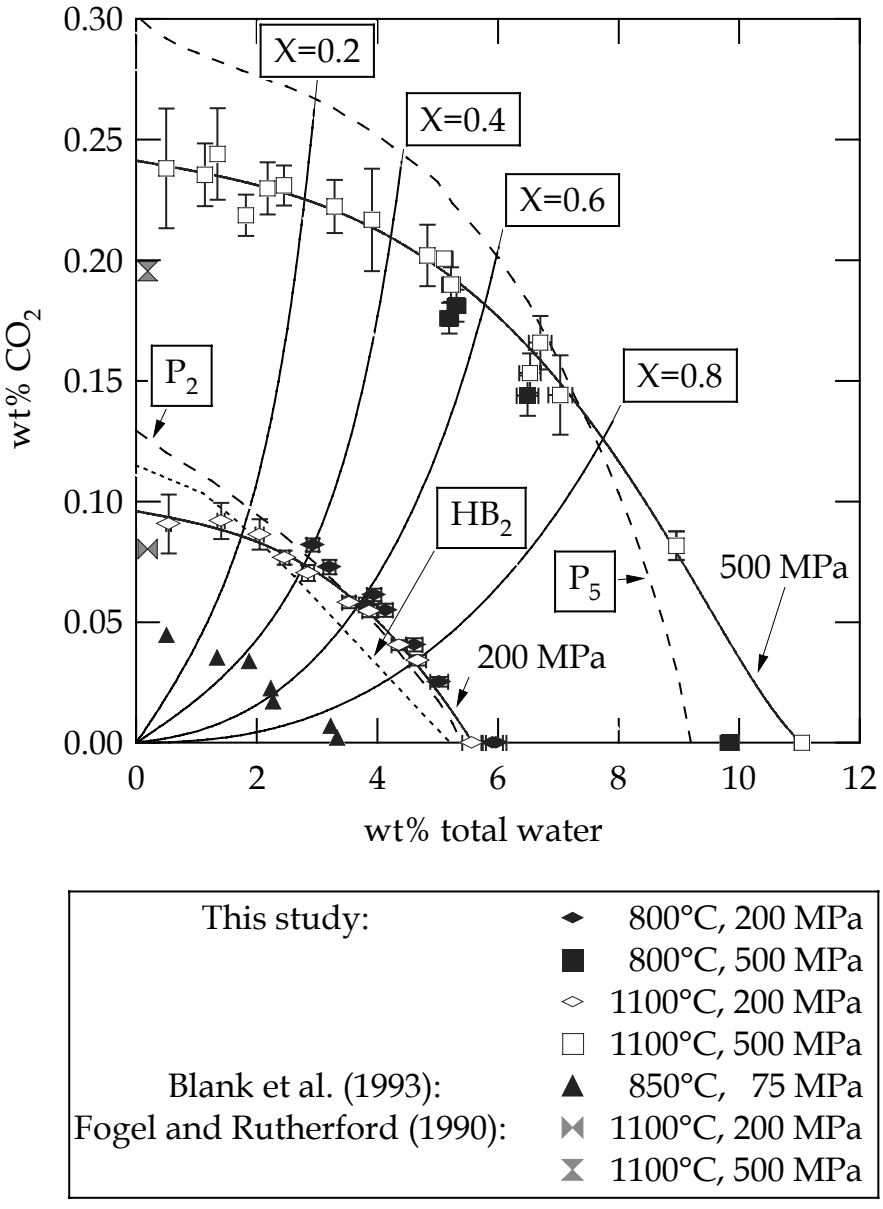

Fig. 9: Relationship between total water and CO_2 contents dissolved in rhyolitic melt at various pressures and temperatures. Data from Fogel and Rutherford (1990) and Blank et al. (1993) are shown for comparison. The solid lines are isotherms fitted to experimental data at 1100°C. X values correspond to the mole fraction of water in the fluid phase. The dotted line labelled by HB_2 shows the predictions of Holloway and Blank (1994) at 900°C-200 MPa and the dashed lines labelled by P_2 and P_5 the predictions of Papale (1999) at 900°C-200 and 500 MPa, respectively.

The model of Holloway and Blank (1994) is based on the water solubility model of Burnham (1979) and the CO_2 solubility models of Spera and Bergman (1980) and Stolper et al. (1987). The calculated data for rhyolitic melts at 200 MPa and 850°C are slightly lower than the water and CO_2 solubilities determined experimentally at 200 MPa and 800°C (approx. 8-10 % relative, for water solubility). The temperature dependence of volatile solubility is too small to account for this deviation. A possible explanation is the use of the model of Burnham (1979), which underestimates the water solubility, especially at high pressure (Holtz et al., 1995). Thus, the model of Holloway and Blank (1994) probably allows the prediction of H_2O and CO_2 solubilities with a precision better than ±10% rel. below 200 MPa. It is emphasised that more significant deviations are expected if the model is used at higher pressures. At 500 MPa, the calculated and experimentally determined water solubilities for X^f_{H2O}=1 differ by 15% relative at 800°C. These differences are more pronounced at higher temperatures, because the strong positive temperature dependence of water solubility at 500 MPa is not predicted by the model of Burnham (1979).

The model of Papale (1999) reproduces our experimental data at 200 and 500 MPa much better than the model of Holloway and Blank (1994) if the CO_2 contents predicted are lowered of 15% (to account for the change in linear molar extinction coefficient). At 200 MPa, the predicted and experimental determined values agree within experimental error. At higher pressure, however, the model of Papale tends to underestimate the water solubility. For example, at 500 MPa our data for pure H_2O solubility interpolated to 900°C are 1 wt% higher than the prediction of Papale (1999). It is interesting to note that despite the relatively small CO_2 solubility database of the model, the predictions of CO_2 solubility are close to our experimental data also at high pressure.

4.5. Empirical model for water solubility between 75 and 500 MPa

In order to improve the prediction of water solubility as a function of the fluid phase composition, we have developed an empirical model based on our data set and that of Blank et al. (1993). At a given temperature and pressure, the data plotted in Fig. 7 can be fitted adequately by an equation of the form:

$$C_{water}(wt.\%) = A \cdot x^2 + B \cdot x^{2.5} + C \cdot x^{0.5} \qquad (11)$$

where C_{water} is the total water content of the glass, A, B, C empirical coefficients, and x the composition of the fluid phase in equilibrium with the melt (x=X^f_{H2O}). The curves in Fig. 7 result from the fit of each data set to equation (11).

At low water fugacity, the third term in equation (11) is dominating and water solubility varies with the square root of X^f_{H2O}. This is consistent with water speciation data that demonstrate that water

is preferentially incorporated in silicate melts as OH-groups at low water contents (Nowak and Behrens, 1995; Sowerby and Keppler, 1999). At high water fugacity, the first and second term in equation (11) becomes increasingly important. This behaviour may be related to increasing amounts of molecular H_2O with increasing water content.

To model the temperature dependence, a linear variation of water solubility as a function of temperature was assumed. Such a temperature dependence has been observed experimentally over a wide temperature range for P<500 MPa. As the data from Blank et al. (1993) are only given at 850°C, their data were extrapolated to 1100°C using the temperature dependence of water solubility found at 200 MPa (Holtz et al., 1995, have shown that the temperature dependence of water solubility is almost identical between 50 and 200 MPa, at least for X^f_{H2O}=1). The pressure dependence has been modelled assuming a third order polynomial dependence of water solubility on pressure. The equation (11) can be rewritten as:

$$C_{water}(wt.\%) = A_{P,T} \cdot x^2 + B_{P,T} \cdot x^{2.5} + C_{P,T} \cdot x^{0.5} \tag{12}$$

where

$$A_{P,T} = (\alpha_{a_A} + \beta_{a_A} \cdot P + \gamma_{a_A} \cdot P^2) + (\alpha_{b_A} + \beta_{b_A} \cdot P + \gamma_{b_A} \cdot P^2) \cdot T \tag{13a}$$

$$B_{P,T} = (\alpha_{a_B} + \beta_{a_B} \cdot P + \gamma_{a_B} \cdot P^2) + (\alpha_{b_B} + \beta_{b_B} \cdot P + \gamma_{b_B} \cdot P^2) \cdot T \tag{13b}$$

$$C_{P,T} = (\alpha_{a_C} + \beta_{a_C} \cdot P + \gamma_{a_C} \cdot P^2) + (\alpha_{b_C} + \beta_{b_C} \cdot P + \gamma_{b_C} \cdot P^2) \cdot T \tag{13c}$$

The values of the empirical coefficients $\alpha_{i,j}$, $\beta_{i,j}$, $\gamma_{i,j}$ are given Table 6. P is given in MPa, and T in °C.

The empirical model reproduces our data within ±2.5% relative, except at 500 MPa, 1100°C (±5% rel.). We have tested the validity of the model from experiments performed in synthetic and natural rhyolitic compositions obtained for X^f_{H2O}=1 in the pressure range 75-500 MPa and temperature range 800-1100°C. The data sets that have been considered are from: Silver et al. (1990, compositions PDIKS, KS), Holtz et al. (1992, 1995, compositions AOQ, HPG8), Yamashita (1999, composition WOBS), Behrens and Jantos (2001, compositions EDF, LGB, OT, LP). All the compositions are quartzofeldspathic or close to subaluminous rhyolitic compositions. The empirical model reproduces 48 of 53 experimental water solubility data within ±5.5% rel.. Two experiments are reproduced within ±7.5% rel. (AOQ) and three are within ±12.5-36% rel. (PDIKS, KS). The comparison of calculated and experimentally determined water solubilities for X^f_{H2O}=1 is shown in Fig. 10.

It is emphasised that this model is valid only between 75 and 500 MPa and 800 and 1100°C. As polynomians are used in the model an extrapolation out of this range has a large error, e.g., the calculated water solubility at 800°C and 800 MPa is 20 % lower than the experimental solubility determined for haplogranitic melts (Holtz et al., 1995). Although our model is empirical, we believe that it is nethertheless useful for application in geoscience to predict water solubilities in rhyolitic melts at various X^f_{H2O} because it has high precision and can be easily run.

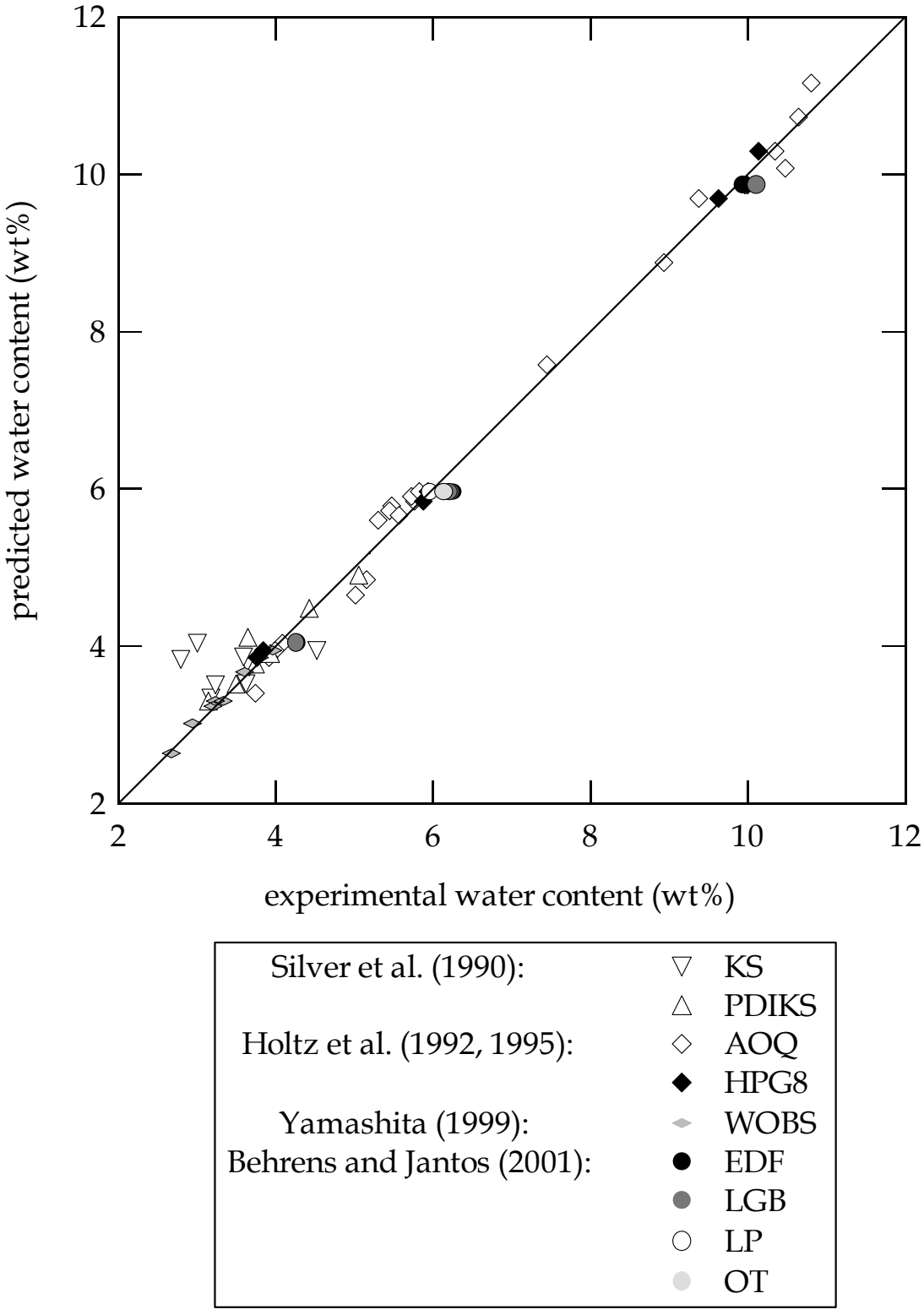

Fig. 10: Comparison of water solubilities calculated from the empirical model given by equation (7) with experimental water solubility data in the range $75 < P < 500$ MPa and $800 < T < 1100$°C. The model reproduces most of water solubility data within ±5.5%.

Ch. 3: Diffusivity of CO_2 in rhyolitic melts

1. Introduction

Papale and Polacci (1999) have shown the importance of the relative insoluble CO_2 component in the location of the volatile-saturation and magma-fragmentation levels as in the distribution of the flow variables in the volcanic conduit. In order to understand and furthermore to model the dynamics of magma ascent, it is necessary to constrain parameters like viscosity of the melt, volatile contents (solubilities) and diffusivities. Viscosities as well as water solubilities are well documented (e.g. for viscosities Persikov, 1991; Lejeune and Richet, 1995; Schulze et al., 1996; Holtz et al, 1996; Dingwell et al., 1998; Lejeune et al., 1999; and for water solubilities see McMillan, 1994; Zhang, 1999). The chapter 2 of the present study provide an extensive CO_2 data set in addition to few previous studies (cf. chapter 2). However, only two previous works concern CO_2 diffusivity in rhyolitic compositions (Watson, 1991 and Blank, 1993, an abstract of latter one was published by Blank and Zhang, 1991).

In order first to improve our knowledge on the CO_2 diffusivities and second to constrain the effect of temperature, pressure and water content on CO_2 diffusion, I performed three different types of experiments on nominally anhydrous and water-bearing samples at temperatures ranging from 580°C to 1000°C and at pressures of 100, 300 and 500 MPa. This chapter exposes the experimental results and suggests a model for the prediction of CO_2 diffusivities as a function of temperature, pressure and water content, derived from my new data and CO_2 diffusivities reported by Watson (1991) and Blank (1993).

2. Starting materials

2.1. Natural CO_2-free and water poor glasses

The starting material was the same bubble- and crystal-free obsidian (EDF) that was used in previous chapters. See chapter 1 § 2.1. for a precise description of that glass.

2.2. Synthesis of hydrous glasses

A large hydrous glass (25 mm in length and 5 mm in diameter) was synthesised from anhydrous EDF and doubly distilled water, using an internally heated pressure vessel (IHPV). A 1:1 mixture of EDF powder with different grain size (200-500 μm and <200 μm) was sealed in a platinum capsule and held at 1225°C and 500 MPa for 17 hours to produce a glass containing 2.2 wt% water. The obtained glass is crystal- and bubble-free with a lighter brown coloration than the natural obsidian,

suggesting that a part but not all of the iron was lost from the melt into the capsule walls during the experiment. Presence of CO_2 in the glass was checked with middle infrared spectroscopy and was found to be ca. 0.010 wt%. I assume that this CO_2 is due to air and impurities enclosed in the capsule during the synthesis of the hydrous glass.

2.3. Hydrous CO_2-bearing glasses

A large hydrous and CO_2-bearing glass (25 mm in length and 6 mm in diameter) was synthesised in two steps:

(1) Synthesis of a CO_2-bearing glass from anhydrous EDF and oxalic acid as the CO_2 source using an IHPV. A 1:1 mixture of EDF powder with grain sizes of 200-500 µm and <200 µm was sealed in a platinum capsule and held at 1100°C and 500 MPa for 10 hours to produce a glass containing 0.18 wt% CO_2 (by IR spectroscopy). The produced glass was brittle, showed a large amount of vesicles (attributed to the air enclosed in the capsule) and a clear concentric colour partition: a colourless ring, ca. 1 mm thick enclosed a dark brown core. I interpret this being the result of a total loss of iron in the rim. Ghost grain boundaries are visible by optical microscopy. This is attributed to absence of convective flow in the capsule due to the high melt viscosity.

(2) Synthesis of hydrous CO_2-bearing glass using the glass obtained in step (1), the carbon-free starting rhyolite and doubly distilled water. Carbon-free and carbon-bearing glasses were mixed in a ratio of 1:1. Again both constituents are composed of 1:1 mixtures of grain size fractions 200-500 µm and <200 µm. The reagents were sealed in a platinum capsule and held at 1100°C and 500 MPa for 10 hours in an IHPV. The CO_2 and water contents of the run product were not analysed, to preserve enough material for the diffusion experiments. The run product is a greenish glass enclosing large amounts of spherical vesicles which can be distinguished in three main families: (a) small vesicles (ca. 1 µm in diameter) occurring in clouds inside the glass, outlining the remaining ghost grain pattern (b) randomly distributed large vesicles (ca. 15 µm in diameter), (c) few very large vesicles (ca. 80 µm in diameter) which are also randomly distributed. The proportion of bubbles is difficult to estimate because of inhomogeneities caused by the ghost grains. The colour change of the sample is suggesting a change in the oxidation state of iron from Fe^{3+} to Fe^{2+}. Inhomogeneities in bubble size suggest that in addition to air bubbles (usually identified by their inhomogeneous size and random distribution), there must be bubbles of partly exsolved CO_2. I attribute this phenomena to the addition of water combined with a relative short experimental duration (equilibrium could not obtained). Initial inhomogeneities of the volatiles in the sample could not equalise and parts of the sample were still fluid-oversaturated at the end of the synthesis. In addition to the spherical vesicles, some dark irregular-shaped inclusions of a size of ca. 30-40 µm are

disseminated all over the sample. I attribute them to the result of pyrolysis of some foreign organic material that initially polluted the glass powder during grinding.

3. Experimental and analytical procedures

3.1. Desorption experiments

Desorption experiments were conducted in a rapid-quench cold seal pressure vessel (CSPV) pressurised with argon. Samples were rapidly quenched by turning the furnace upside down so that the sample drops into the water-cooled part of the vessel. The heating-up duration was about 30 min. The estimated cooling rate was about 30°C/s (Zhang and Behrens, 2000). In these experiments doubly polished plates (ca. 2×2.5×5 mm) from the hydrous CO_2-bearing glass were directly exposed to the pressure medium Ar. Thus both, water and CO_2, diffused out of the sample and Ar diffused into the sample. In the experiment, a piece of glass was fixed in an open gold capsule, one polished face in contact with argon, the other in part loosely covered by gold. The capsule was clamped into a groove at the tip on a Ni rod. The assemblage is then placed into the CSPV, and brought to the specified pressure and temperature. Temperature was measured with a K-type thermocouple with a typical fluctuation of ±3°C over the course of an experiment. Accuracy of temperature is estimated to be 10°C (including sample position uncertainty) and accuracy of pressure to be 50 MPa. The pressures and temperatures investigated are reported Table 7.

Desorption experiments can not be conveniently conducted over a large range of temperatures and water contents, because of sample crystallisation and sample flow. Hydrous samples rapidly crystallise above 630°C and deformation by viscous flow becomes important above 900°C. Water-poor rhyolitic glasses also show noticeably crystallisation after long term experiments at temperatures between 630 and 800°C but their shape remain usually unchanged towards higher temperature (due to high viscosities) so that sorption and desorption experiments are possible even above 1000°C (Behrens and Zhang 2001). Typical run temperatures suitable for desorption runs are around 600°C ±100°C for samples containing from 1 to 4 wt% water, depending on pressure and composition investigated. To investigate CO_2 diffusion over a wide range of temperature, it is therefore needed to combine this method with others.

3.2. Sorption experiments

Sorption experiments were conducted in a standard CSPV pressurised with argon. Samples were quenched from experimental conditions to room conditions using a flux of compressed air. The initial cooling rate was approximately 200°C/min. Temperature was measured with a K-type thermocouple

in a bored hole of the autoclave. Accuracy of temperature and pressure are the same as for the rapid quench CSPV. Pressures and temperatures investigated are reported Table 7.

3.2.1. Sorption in dry glasses

The natural water-poor and CO_2-free EDF glass was cut into plates 1×4×4 mm in size, doubly polished and corners slightly rounded. Glass pieces were loaded with silver oxalate as the CO_2-source (isolated in a separate capsule made of the same noble metal that the outer capsule, similarly to what is described chapter 1 § 2.2.) into a noble metal capsule (Au or Pt, depending on the P-T conditions, 4 mm inner diameter; 0.2 mm wall thickness; 2.5 mm length). During welding, the capsules were cooled using liquid nitrogen to prevent any loss of CO_2.

3.2.2. Sorption in hydrous glasses

Slices (4×5 mm, 2 mm in thickness) were cut off the synthesised hydrous glass and doubly polished. Glasses were loaded with water and silver oxalate as the CO_2-source (isolated in a separate Au-capsule, similarly to what is described chapter 1 § 2.2.) into a Au-capsule (4 mm inner diameter; 0.2 mm wall thickness; 2.5 mm length). The water content of each slice was determined by near infrared spectroscopy (as described in chapter 2 § 3.4.2.) and is reported in Table 7. The H_2O/CO_2 ratio in the vapour phase was adjusted to be close to the equilibrium value corresponding to the water content of the glass to prevent water diffusion in or out off the melt during the run. The equilibrium mole fraction of water in the fluid ($X^f_{H_2O}$) was calculated using the empirical equation derived in the solubility study (chapter 2). For most of the sorption experiments the conditions are in the P-T range as used for solubility experiments so that the equilibrium fluid composition could be reliably predicted. In one case (run h15834j at 580°C) a large extrapolation of the water solubility equation towards low temperature was required. In this run $X^f_{H_2O}$ was too high and water diffused into the glass. During welding, the capsules were cooled using liquid nitrogen to prevent any loss of water or CO_2. After the run, the final $X^f_{H_2O}$ was checked by gravimetry. $X^f_{H_2O}$ before and after experiment are reported in Table 7.

3.3. IR spectroscopy

After quenching, the glass piece was sectioned perpendicular to its polished surfaces near the center. This provided a glass slice with the complete diffusion profile. The slice was then doubly polished down to a thickness of 40-312 μm (see Table 7). CO_2 concentration profiles were determined from IR spectra measured with an IR microscope A590 connected to a FTIR spectrometer Brucker

IFS88. A slit aperture between the objective and the detector was used to limit the analysis sample volume. In the focus plane, the area selected by the slit was typically 16-29 µm wide and 100 µm long (the width of the slit used for each measurement is specified Table 7). The sample was fixed to a translation stage, and the slice aligned so that the rim was parallel to the slit. The slide can be moved in x and y direction by micrometer drives. The position of the rim of the sample was read on the micrometer display (precision ±10 µm) and on the ocular scale of the microscope to define the start point of the diffusion profile. The distance away from this start point was determined using the microscope reading when the rim is still in view (≤ 180 µm, with a precision of ±5 µm). Longer distances were determined from the difference between the micrometer reading at the start point and that at the position measured. Positions measured in this way are reproducible to better than 20 µm on a 1000-µm distance. The microscope scale was calibrated in each measurement by regressing the microscope reading and the micrometer reading at distances of ≤180 µm. This insured self-consistency of the two methods. There are two difficulties near the edge of the slices. One is that the base planes of the polished slices are never perfectly flat near the edges due to chipping during cutting and polishing. The second is that the edge may not be perfectly vertical (e.g. due to flowing of the melt during the experiment), leading to uncertainties in distance determinations. Hence, the uncertainty on the distance from the start point can be much larger than the 5 µm cited above, and CO_2 concentrations could usually only be measured precisely at more than ~ 30 µm from the edge, the exact distance depending on the particular glass wafer.

CO_2 concentrations were determined from the peak height of the absorption band at 2346 cm^{-1} as described in chapter 2 § 3.4.3. using the linear molar absorption coefficient determined Chapter 1. The relative precision of CO_2 concentrations along one profile is about 6 %. The problem of the random background in the spectra due to atmospheric CO_2 (encountered in Chapter 1 and 2) is not that critical because of the large relative changes of CO_2 concentration along the diffusion profile. Thus, no special care in regard to atmospheric CO_2 was required to protect the samples during measurements.

4. Results

4.1. Quenched products

4.1.1. Desorption experiments

All samples came out with brown coloration, mainly non-deformed, but sometimes slightly smoothed (from very long time experiments). The change in color from greenish to brownish is suggesting a re-oxidation of iron in the glass. The implications of a change in the valence of Fe on the CO_2 diffusivity/solubility are not known and can not be elaborated from the results of this study, though it may be important. The sections prepared for IR slides showed the same features as the

starting glasses, namely large amounts of bubbles inhomogeneous in size and distribution, with apparent ghost grains. Raw inspection by microscope suggests that bubbles change neither in size nor in number. However, in detail it is impossible to exclude changes in the sample due to the inhomogeneous initial distribution of bubbles in the starting glass on a large scale. In first approximation I assume the bubbles being unchanged during the run so that diffusion occurs in an effective medium composed of bubbles and glass. However, in a more precise evaluation partitioning of CO_2 between the bubbles and the glass has to be taken into account. This problem is discussed by Behrens and Zhang (2001) for Ar diffusion vesicle-bearing rhyolitic glass.

4.1.2. Sorption experiments

Diffusion experiments conducted with dry glasses produced clear (bubble- and crystal-free) light brown quenched products. Diffusion experiments conducted with hydrous glasses all produced bubble-bearing crystal-free light brown glasses. Two kinds of bubble distribution have been observed: (1) a ca. diffusion-length thick ribbon of numerous very small bubbles (upper rim on the right part of Photo 1) and (2) non-homogeneously distributed bigger bubbles, leading to ghost-grain patterns (right part of Photo 1). A possible explanation of the former kind of bubbles may be directly linked to CO_2 diffusion into the hydrous glass, as assumed by Mourtada-Bonnefoi (1998). The temperature dependence of volatile solubility is changed through CO_2 penetration, so that a local oversaturation occurs during quenching. Therefore, I assume that these bubbles do not much alter diffusivity results. The later kind of bubbles may be due to the different temperatures at which glass synthesis and diffusion experiments were performed. At the temperature of the synthesis, the air enclosed in the capsule between grains was dissolved in the melt, leading to a bubble-free quenched product. The temperature dependence of nitrogen (the major constituent of air) solubility in hydrous rhyolitic melts is unknown (see Carroll & Webster 1994) so that it only can be speculated about the evolution of a N_2 and H_2O bearing melt during cooling and low-temperature annealing. An explanation for the large bubbles and the ghost pattern in the interior of the diffusion samples may be a retrograde decrease in volatile solubility. An exception is sample h18718h (conditions: 870°C, 100 MPa, 65336 s) for which ghost-grain patterns didn't occur. I assume that in that case the experimental duration was long enough to reach homogenisation of the melt.

All dry glasses processed at temperatures ≥900°C and all hydrous glasses processed at temperatures ≥800°C became rounded at the edges and the sample thickness increased by up to 26%, depending on the P/T conditions of the experiments. The assumption made by Behrens and Zhang (2001) in Ar diffusion experiments with rhyolitic melts that the deformation occurs mainly at the beginning of the diffusion experiment and, therefore, is not dependent on the experimental duration, could not be verified in my study. However, I consider that thickening did not dramatically alter diffusivity results if the measurements are taken in the central area of the plate. Deformation was

especially dramatic for sample h1876h, (Photo 1). I assume that the convections appeared during the short over-heating of the sample. However, it is noteworthy that the diffusion rim (as indicated by the zone with small bubbles) has a similar width around the sample and along the cracks. Therefore, I suggest that measurements of diffusion profiles perpendicular to planar areas of the samples are a good approach to quantify CO_2 diffusion.

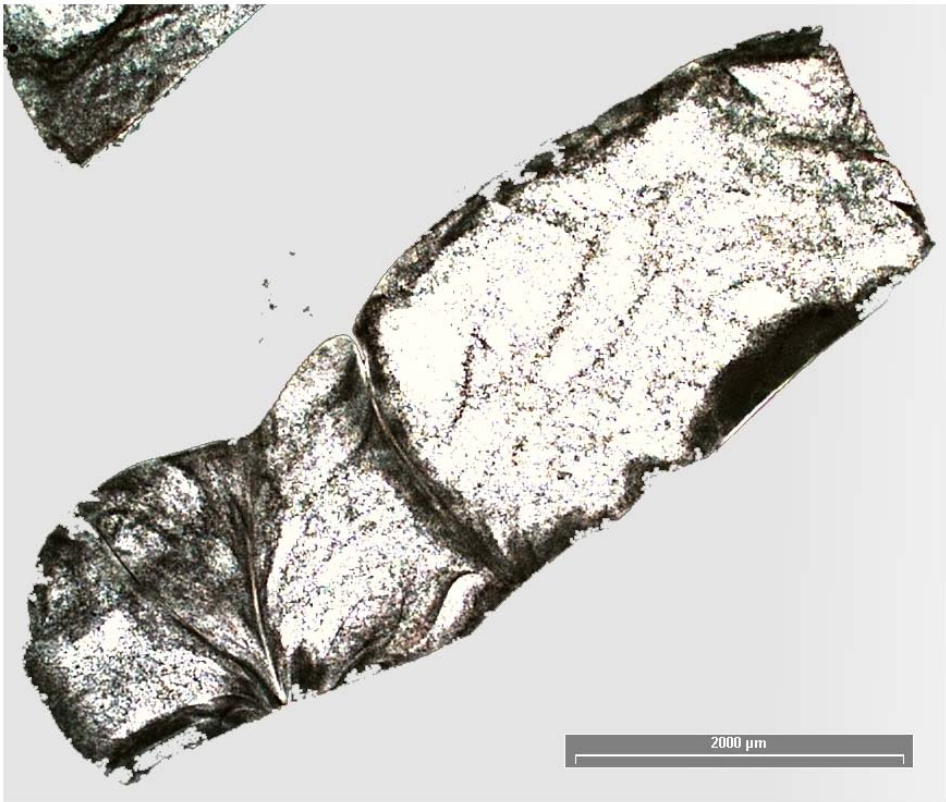

Photo 1: dramatic deformation of sample h1876h.

4.2. Effective duration at the experimental temperature

All experimental durations have been corrected to take into account the effect of diffusion during heating up and cooling down. Time corrections were made as described by Zhang and Behrens (2001) assuming a constant activation energy of diffusion in the whole temperature range. Integrating the diffusivity over time and dividing the results by the diffusivity at run temperature $D_{T_{exp}}$ gives the effective duration t_{eff} of the experiment: $t_{eff} = \int Ddt/D_{T_{exp}}$. The uncertainty in this treatment results from that in the activation energy of diffusion.

4.3. Determination of diffusion coefficients

Diffusion profiles were analysed for 5 desorption experiments and 16 sorption experiments (including 6 experiments with hydrous glasses). In most of the samples I realised a transverse measurement, so that I obtained two diffusion profiles at two opposite locations. Total water profiles as by-products in desorption experiments were also measured by MIR spectroscopy, using the peak height of the fundamental –OH stretching vibration at 3550 cm^{-1}, converted to concentrations using a molar absorption coefficient of 78 $l.mol^{-1}.cm^{-1}$ determined by Behrens and Schmidt (1998) for a haplogranitic glass. Unfortunately, water diffuses much faster than CO_2 (Zhang and Behrens 2000, Behrens and Zhang 2001), and the samples were not thick enough to produce semi-infinite diffusion profiles of both H_2O and CO_2. As the experiments were optimised to measure CO_2-diffusion, none of the water diffusion profiles enables a reliable determination of water diffusion coefficients (because all water diffusion profiles were much longer than half of the sample thickness). Nevertheless, the water profiles are very useful for a precise determination of the true density of the glass, needed in the quantification of peculiar CO_2-contents. In the same way, water contents were taken into account in the density determination of hydrous samples. All densities were determined using equation (8), defined in chapter 2. Water contents of the samples are listed in Table 7.

4.3.1. Sorption in dry glasses

I considered as dry material samples from sorption experiments containing less than 0.6 wt% and samples from desorption experiments, because water contents were low close to the surface, in the crucial part of the profile. CO_2 profiles were evaluated assuming a constant surface concentration in the glass $C_{0,CO2}$ and a concentration-independent diffusion coefficient D_{CO_2}. If the initial concentration of CO_2 in the glass is zero (in sorption experiment), the solution of Fick's second law for one-dimensional diffusion into a plate of thickness 2λ is (Crank, 1975, eqn. 2.15):

$$C_{CO_2} = C_{0,CO_2}\, erfc\frac{x}{\sqrt{4D_{CO_2}t}} \qquad (14)$$

where C_{CO_2} is the concentration of CO_2 at the distance x from the center and t the run duration, and erfc(x)=1-erf(x). To fit the profiles, C_{0,CO_2} and D_{CO_2} were adjustable parameters. C_{0,CO_2} can be interpreted as the equilibrium solubility of CO_2 at the experimental conditions. Fitted values of C_{0,CO_2} are mostly in the magnitude order of CO_2 concentrations expected from the solubility study (chapter 2), though not accurately reproducible (up to 38% variations in the C_{0,CO_2} recorded, see Table 7). Thus, this method does not enable accurate C_{0,CO_2} determination due to the uncertainty in extrapolation of the profile to the surface and in the determination of the surface position (see Fig. 11).

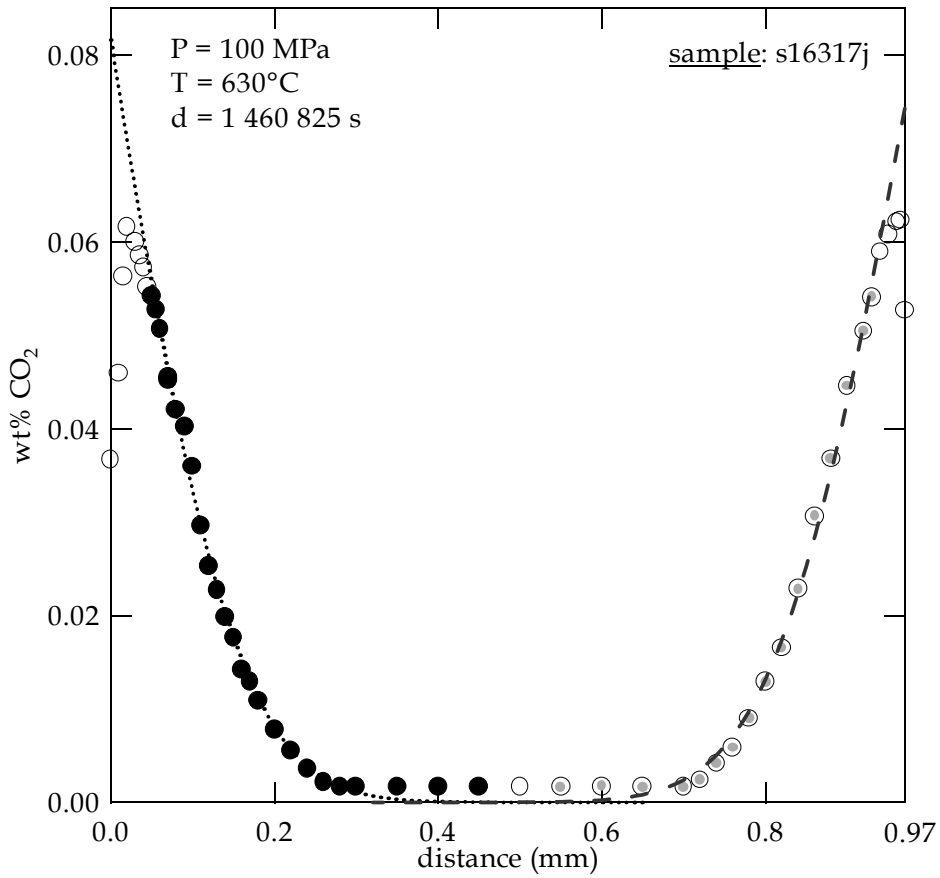

Fig. 11: Concentration-distance profile of CO_2 in a natural rhyolitic glass after CO_2 sorption. Profiles on both sides were fitted independently with eqn. (14). Black symbols indicate data used to fit the profile on the left and grey symbols indicate data used to fit the profile on the right.

Assuming that the surface concentration is zero in the desorption experiments the solution of Fick's second law for one-dimensional diffusion is (Crank, 1975):

$$C_{CO_2} = C_{0,CO_2} erf \frac{(x-\delta)}{\sqrt{4D_{CO_2}t}} \tag{15}$$

where C_{CO_2} is the concentration of CO_2 at the distance x from the surface, C_{0,CO_2} is the CO_2 content in the middle of the sample, and δ is the deviation between the starting point of the profile (where C_{CO_2}=0) and the surface of the sample. To fit the profiles, C_{0,CO_2}, δ, and D_{CO_2} were adjustable parameters. δ was always within 12 µm, which is roughly the uncertainty in the measurement location.

The CO_2 profiles of all but two (samples s39028h, s59014h) sorption experiments are well fitted by equation (14). Even experiments at high temperature in which flow of the sample occurred do not

show any systematic deviation between data points and the fitted curve. This supports the conclusion that CO_2 sorption is then still controlled by diffusion and that flow of the sample during experiment has no significant influence on CO_2 transport into the glass. An example of such a profile and fit is displayed Fig. 11. All Profiles and fits are displayed in annex 2, Fig. 1(a-i). The small variations in water contents do not produce significant deviation from the CO_2 profile from simple error function shape. Samples s39028h and samples s59014h show overlapping profiles. The solution of Fick's second law for one-dimensional diffusion is in that case (Crank, 1975) written as:

$$C_{CO_2} = C_{0,CO_2}\left[(1-erf\frac{\lambda-x}{\sqrt{4D_{CO_2}t}})+(1-erf\frac{\lambda+x}{\sqrt{4D_{CO_2}t}})\right] \quad (16)$$

where C_{CO_2} is the concentration of CO_2 at the distance x from the center and t the run duration. To fit the profiles, C_{0,CO_2} and D_{CO_2} were adjustable parameters. C_{0,CO_2} can be again interpreted as the equilibrium solubility of CO_2 at the experimental conditions. λ is a fixed parameter (2 λ being the sample thickness), corresponding to the distance from one surface of the sample to the crossing point of the 2 overlapping diffusion profiles. Still sample s59014h is not perfectly fitted (annex 2, Fig 1-h). This may be attributed to a slight overlapping in the third direction.

The CO_2 profiles of all desorption experiments are well fitted by equation (15). Initial sample heterogeneities are sometimes occulting parts of diffusion profiles. I chose either to select the best representative points for the fit (Fig. 11) or to neglect the whole profile (e.g. sample d16317j, annex 2 Fig. 2-b: only one profile could be fitted). All Profiles and fits are displayed in annex 2, Fig. 2(a-d).

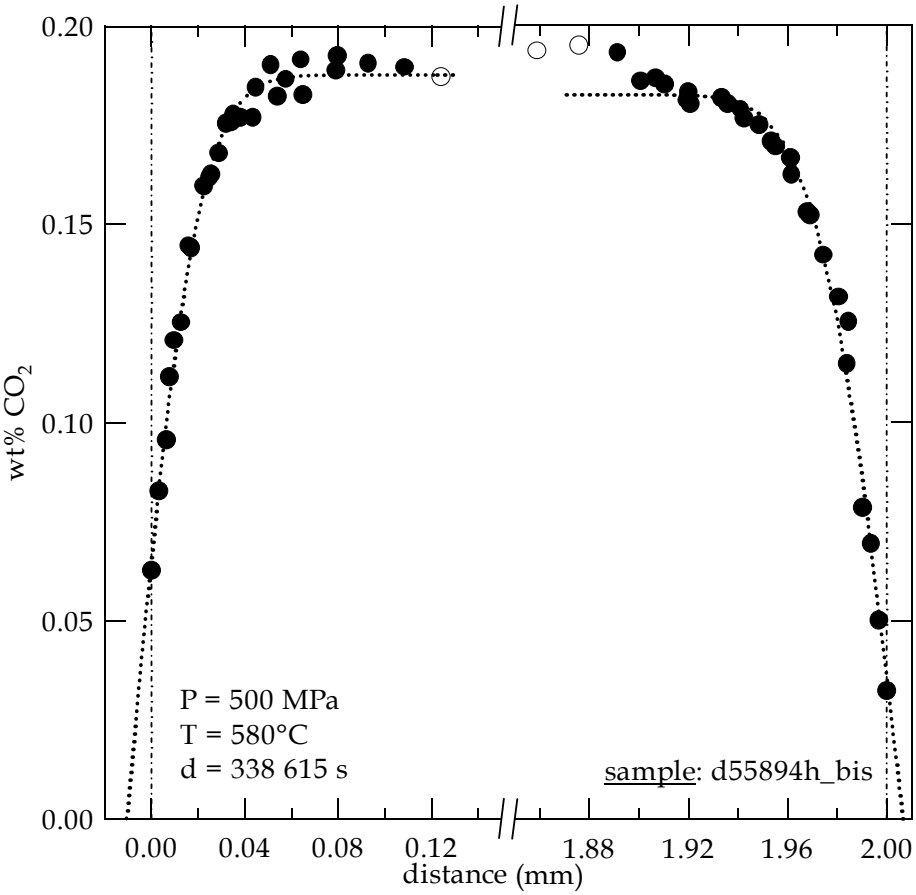

Fig. 12: Concentration-distance profile of CO_2 in hydrous CO_2-bearing rhyolitic glasses after CO_2 desorption. Profiles on both sides were fitted independently with eqn. (14). Points chosen for the fit are shown in black. Surfaces of the sample are shown by two vertical dotted lines.

4.3.2. Diffusion in hydrous material

CO_2 contents of the profiles were evaluated assuming a water-dependent density of the sample. CO_2 profiles were evaluated assuming a constant surface concentration in the glass C_{0,CO_2} and a concentration-independent diffusion coefficient D_{CO_2}. All my samples contained some CO_2 before diffusion experiments were conducted (cf. this chapter § 2.2.). The solution of Fick's second law for one-dimensional diffusion in that case is (Crank, 1975):

$$C_{CO_2} = C_i + C_{i,CO_2} erfc \frac{x}{\sqrt{4D_{CO_2} t}} \qquad (17)$$

where C_{CO_2} , x and t are the same parameters as in equation (14). To fit the profiles, C_{i,CO_2} and D_{CO_2} were adjustable parameters. C_i is the initial CO_2 content of the sample which can be measured in the

center. $C_{0,CO_2} = C_{i,CO_2} + C_i$ can be interpreted as the equilibrium solubility of CO_2 at the experimental conditions. Fitted values of C_{0,CO_2} are again mostly in the magnitude order of CO_2 concentrations expected from the solubility study (chapter 2), though still not accurately reproducible (up to 38% variations in the C_{0,CO_2} recorded, see Table 7). All samples but sample h15834j are well fitted by equation (17). An example of such a profile and fit is displayed Fig. 13.

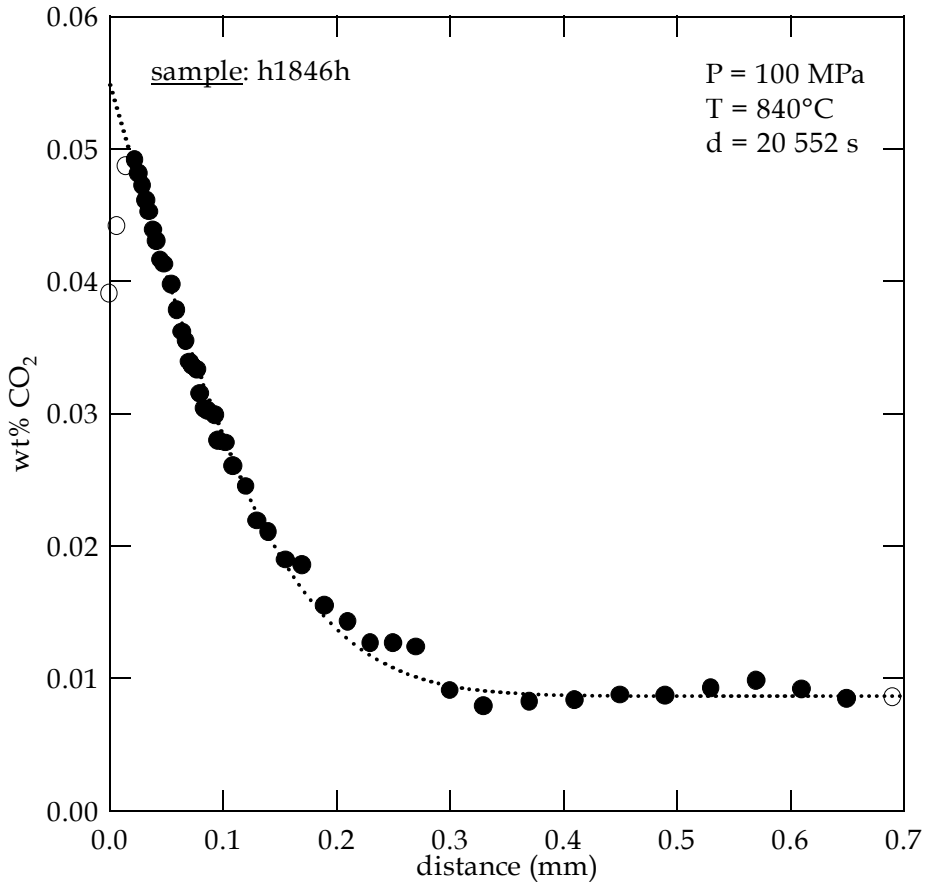

Fig. 13: Concentration-distance profile of CO_2 in hydrous rhyolitic glass after CO_2 sorption. On this sample, only one profile could be used and was fitted with eqn. (17). Points chosen for the fit are shown in black. Note that the core of the sample is not CO_2-free. See text for more details.

Sample h15834j shows overlapping profiles. The solution of Fick's second law for one-dimensional diffusion is in that case (Crank, 1975) is a variation of equation (16), to take into account the initial CO_2 content:

$$C_{CO_2} = C_i + C_{i,CO_2}\left[(1 - erf\frac{\lambda - x}{\sqrt{4D_{CO_2}t}}) + (1 - erf\frac{\lambda + x}{\sqrt{4D_{CO_2}t}})\right] \quad (18)$$

This equation is the same than equation (16) if $C_i = 0$. To fit the profiles, C_{i,CO_2} and D_{CO_2} were again adjustable parameters. C_i corresponds again to the initial CO_2 content of the sample and is in this case fixed to the average of initial CO_2 contents from all other hydrous samples. Equation (18) fits adequately diffusion profiles of sample h15834j. All Profiles and fits are displayed in annex 2, Fig. 3(a-e).

4.3.3. Uncertainty in diffusion coefficient

A major uncertainty in CO_2 diffusion experiments is linked to the determination of the diffusion profile length. It takes into account: (1) the position of the sample surface. Rims are slightly rounded or rough due to polishing so that the original diffusion surface (which is the zero point of the distance axis after sectioning) cannot be exactly determined. I estimate the uncertainty to be at the most ±6 µm. I assume that slight deviation of the measured profile from diffusion direction has only a minor influence on diffusion data, as shown by Behrens and Zhang (2001) for Ar-diffusion data. (2) The precision of the micrometer drives, estimated to ±10 µm; (3) the effective slit width on the sample (estimated to ±30 µm). For short diffusion profiles, the resulting relative error of diffusivity can be large, between 17% and 49% for desorption experiments, up to 19% in sorption experiments (e.g. sample d55894h_bis, Fig.12; sample s310030m, annex2 Fig. 1-f).

Another uncertainty is related to the presence of bubbles in desorption experiments and sorption experiments in hydrous material. Bubbles are generated in two different ways: during starting material synthesis for hydrous-CO_2 bearing samples and during diffusion experiments itself for hydrous samples. Size, concentration and distribution of the bubbles in desorption run products appear to be unchanged compared to initial bubbles in the starting glasses. As assumed by Behrens and Zhang (2001) for Ar diffusion, I don't expect rapid CO_2 diffusion in the bubbles affect much CO_2 diffusivities measured in this study since bubbles are not interconnected and the volume relatively small (cf § 2.3.). In the case of hydrous sorption samples, the formation of bubbles during the diffusion experiment might slow the fluxes and lead to an underestimation of the true fluxes and diffusivities.

Uncertainty in pressure has no significant influence on the diffusion data because of the relatively small pressure dependence of CO_2 diffusivity. Temperature uncertainty, on the opposite has a larger effect. Based on an activation energy of 149 kJ/mol for CO_2 diffusion, the uncertainty of ±10°C in temperature corresponds to errors in D_{CO_2} of 50% at around 600°C and 18% at 1000°C.

Uncertainty on run duration is hidden in the time correction for the determination of effective run duration considering heating and cooling times. The calculation for time correction is shortly depicted this chapter § 4.2. after Zhang and Behrens (2000), assuming an activation energy for CO_2 diffusion of 149 kJ/mol. The uncertainty on run duration is estimated to be about 10-15 min. Another error source

is related to the assignment of water content to an average CO_2 diffusivity. This water content is estimated to the average of water contents strictly along the profile. The error is estimated to be less than one half of this water content.

Errors of the diffusion coefficients calculated by error propagation based on these estimates are included in Table 7.

5. Discussion

5.1. Validity of CO_2 solubilities derived from diffusion data fits

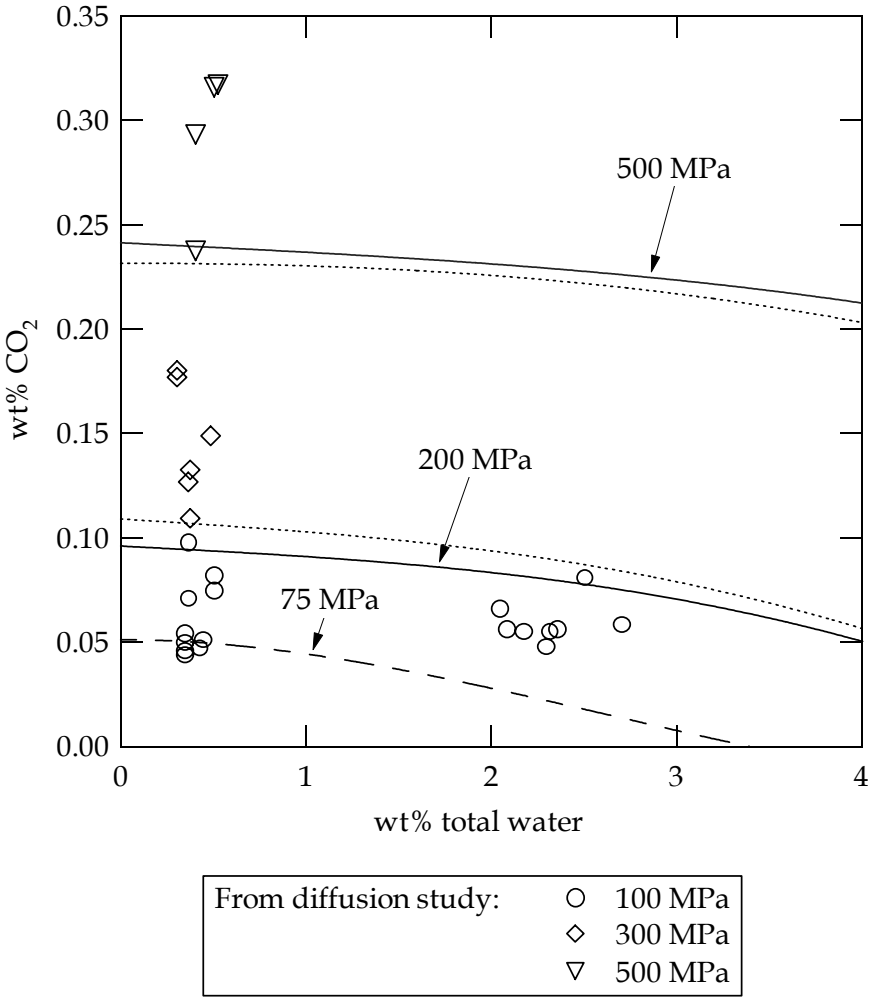

Fig. 14: Comparison of surface solubilities derived from the fit of the diffusion profiles with equilibrium solubilities (lines) determined in chapter 2. The solid lines are isotherms at 1100°C. Dotted lines are extrapolations of experimental data at 800°C. The dashed line is the isotherm fitted to experimental data at 850°C from Blank, 1993.

CO_2 solubility data from chapter 2 does not allow us a precise prediction of CO_2 solubilities at pressures and temperatures at which diffusion experiments were conducted. It is however possible to determine whether estimations derived from the fit of the diffusion profiles (Table 7) are reliable. It appears that CO_2 solubilities derived from CO_2 diffusion profiles are both over- and underestimated, by about ±15-20% (Fig. 14) except at 500 MPa, pressure at which all but one CO_2 solubilities derived from CO_2 diffusion profiles are overestimated by about 20-35%. As assumed chapter 2, differences between my data set and data from Fogel and Rutherford (1990) probably come from the use of diffusion profiles to determine CO_2 solubilities. A precise determination of CO_2 solubility from diffusion profiles is not possible, because: (1) sorption profiles can not be measured to the surface and are therefore extrapolated, (2) the position of the surface can not be precisely defined, and (3) the surface of the samples may be chemically altered during high temperature experiments. However, it is to mention that solubility determination derived from diffusion profiles can lead to satisfying results as for example with H_2O in haplogranitic melts (Schmidt et al., 1999) and with Ar in sorption experiments bellow 1000°C (temperature above which sample surfaces altered, Behrens and Zhang 2001).

5.2. CO_2 diffusion in nominally anhydrous and water-bearing rhyolite

Diffusion data for water-poor rhyolitic glasses are in good agreement with data from Blank (1993) and Watson (1991) if differences in run pressure are not taken in account (Fig. 15). The data obtained for rhyolitic composition at 100 MPa can be described (considering only sorption experiments) in the whole temperature range of 580 to 1000°C by a simple Arrhenius relationship

$$D_{CO_2} = D_0 \exp(-E_a / RT) \qquad (19)$$

where D_0 is the pre-exponential factor and Ea is the activation energy for diffusion. The fitted values are log D_0 = -5.67 ± 0.16 (D_0 in m^2/s) and E_a = 149 ± 3 kJ/mol. These values are consistent with previous data of Blank (1993) at 72 MPa (log D_0 = -5.42 where D_0 is in m^2/s; E_a = 152 kJ/mol).

Desorption data were not taken into account to determine the Arrhenius relationship because the data scatter widely. This scattering may come from various non-well constrained parameters as: (1) the changing amounts of water along the CO_2-profiles (in first approximation samples are assumed to be completely dehydrated in the diffusion zone) is not considered, (2) the presence of bubbles in the starting material (its effect on CO_2 diffusion may not be negligible, as assumed), (3) the inhomogeneity in CO_2-content of the starting materials, (4) the CO_2 content in the Ar gas, assumed to be negligible (organic material may have contaminated the gas, e.g. the oil of the screws sealing the autoclave), (5) the change in oxygen fugacity over the different stages.

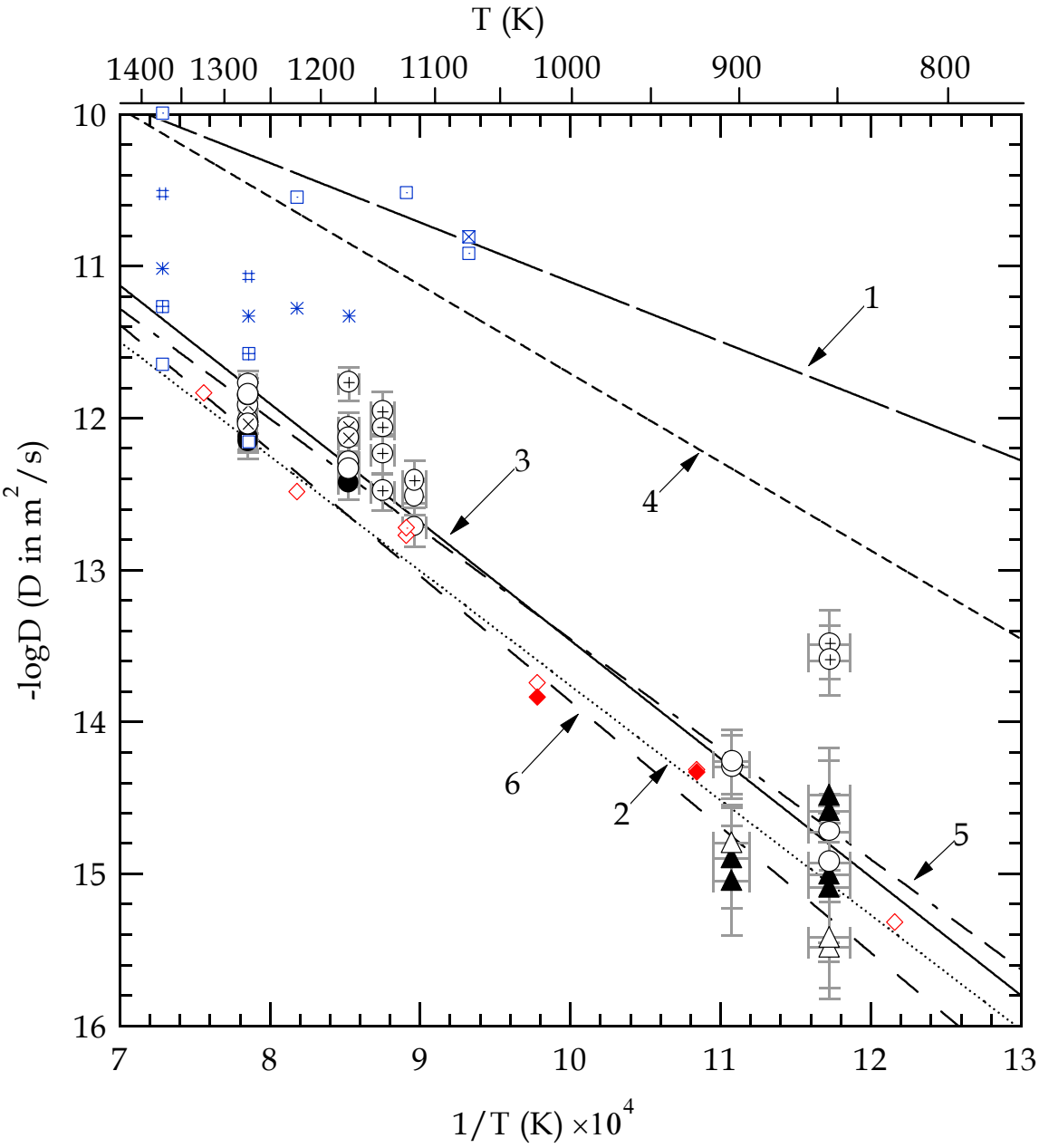
T (K)
1400 1300 1200 1100 1000 900 800
10
11
12
13
14
15
16
-logD (D in m^2/s)
7 8 9 10 11 12 13
1/T (K) ×10^4
1
2
3
4
5
6

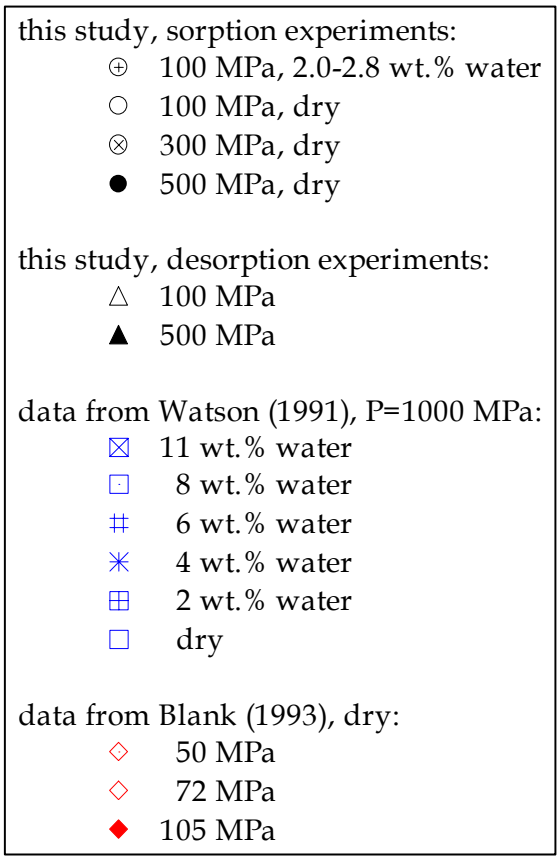

Fig. 15: Arrhenius plot for CO_2-diffusion in rhyolitic glasses and melts. Data obtained by Watson (1991) and Blank (1993) are shown for comparison. Lines 1-3 represent the different trends derived from CO_2 diffusion data with (1) hydrous samples (8 wt%) at 1000 MPa, Watson (1991), (2) water-poor samples at 72 MPa, Blank (1993), (3) water-poor samples at 100 MPa, this study. For comparison (lines 4-6), I displayed trends derived from: (4) molecular H_2O diffusion at 100 MPa, Zhang and Behrens (2000), (5) Ar diffusion in water-poor samples at 100 MPa, Behrens et al. (2000), (6) Ar diffusion in water-poor samples at 500 MPa, Behrens and Zhang (2001). It is noteworthy that CO_2- and Ar-diffusion are very similar.

The effect of dissolved water on CO_2 diffusivity observed in this study is consistent with results from previous studies (Watson, 1991; Blank, 1993): adding water to the dry melt always increases D_{CO_2} (Fig. 14). However, it seems that the effect of dissolved water is more pronounced at lower temperature (e.g. the addition of 2.4 wt% water to the dry melt at 100 MPa and 900°C increases D_{CO_2} by about half an order of magnitude, compared to the addition of 2.5 wt% water at 100 MPa and 580°C that increases D_{CO_2} by about one and a half order of magnitude), although the uncertainty on D_{CO_2} is larger at low temperature and that there is only one experiment to constrain the effect of water content. However, this is to be proven by additional low temperature experiments. Three experiments (h1846h, h1876h and h18718h) do not show any particular increasing of D_{CO_2} with the addition of

more than 2 wt% water. This may be explained by a technical problem: a part of the sample was stick to the capsule so that diffusion conditions vary around the sample. Another explanation may be that the quantity of CO_2 in the fluid phase was not sufficient to provide constant CO_2 fugacity during the experiments.

In addition, it comes out this study that the pressure effect is rather small (Fig. 16). It is however possible to determine an apparent activation volume V_a from data at 1000°C in the pressure range of 70-1000 MPa with the Arrhenius relation $D = D_{0'} \exp(PV_a/TR)$ where $D_{0'}$ is the diffusion coefficient at T and 1 bar. The V_a value is 3.4 ±1.7 cm^3/mole.

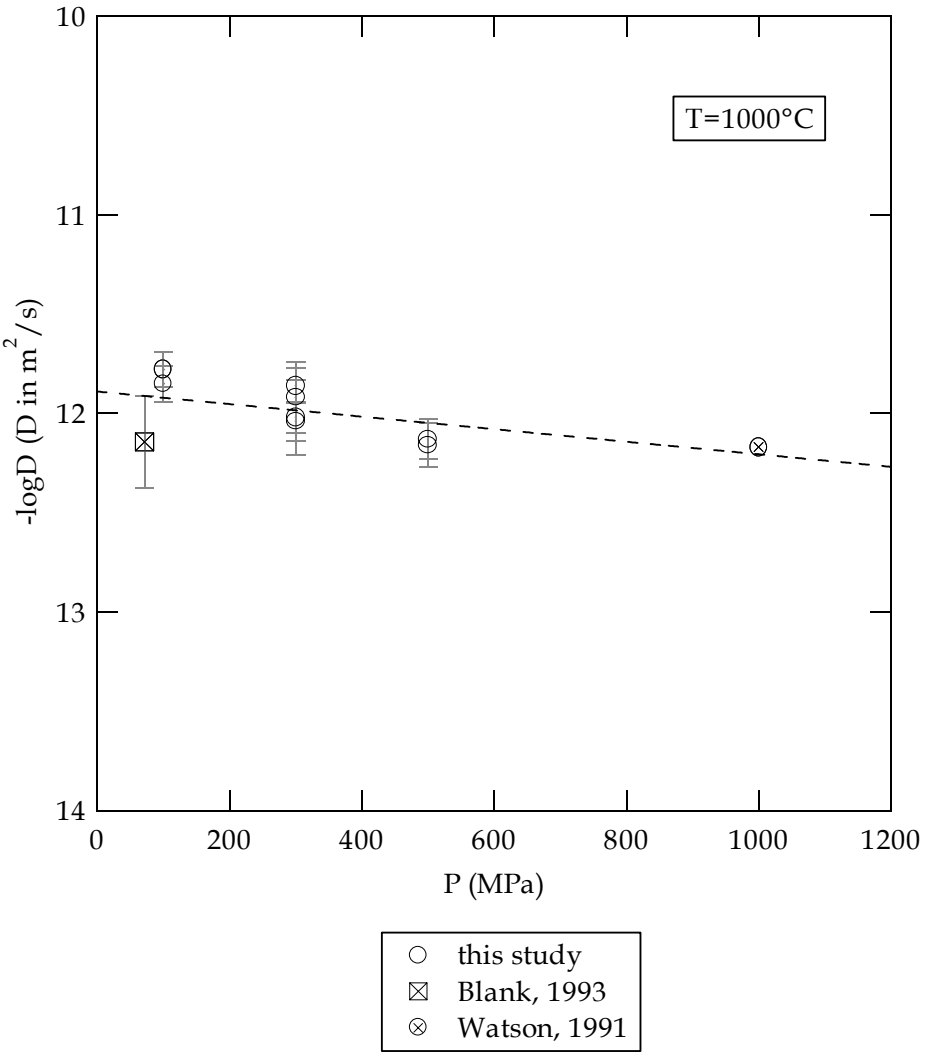

Fig. 16: Pressure dependence of CO_2-diffusion in water-poor rhyolitic glasses/melts at 1000°C. Data from Blank is calculated according the Arrhenius equation given in Blank (1993). Data in the range 70 – 1000 MPa are fitted by the dotted line resulting in an apparent activation volume of 3.4 ± 1.7 cm^3/mole.

5.3. Modelling CO_2 diffusion as a function of T, P and X^m_{water}

To describe the pressure, temperature and water content (expressed as the molar fraction of water dissolved into the melt, calculated on a single oxygen basis) dependence of diffusivity, I followed Behrens and Zhang (2001) by taking an equation of the type:

$$D_{CO_2} = \exp(a_0+a_1/T+a_2P/T) \quad (20)$$

The parameters a_0, a_1 and a_2 are related to the pre-exponential factor, the activation energy and the activation volume, respectively. I assume that as for Ar (Behrens and Zhang, 2001), CO_2 diffusivity varies exponentially with water concentration. This assumption is supported by the results of Watson (1991). However, the compositional variation may be dependent on pressure and temperature. The simplest expression accounting for this is:

$$D_{CO_2} = \exp[(a+bX^m_{water})+(c+dX^m_{water})/T+(e+gX^m_{water})P/T] \quad (21)$$

where X^m_{water} is the molar fraction of water on a single oxygen basis. The parameters a, b, c, d, e, and g are to be obtained by fitting experimental data to equation (21). Water contents taken into account for the fit were (1) the measured water contents for sorption experiments and (2) for desorption experiments a constant water content equal to the average of water contents along the CO_2 profiles. Combining my data with the data of Watson (1991) and Blank (1993), the following equation was obtained for CO_2 diffusivity (in 10^{-12} m^2/s) in rhyolitic melts as a function of pressure (in MPa), temperature (in K) and mole fraction of water:

$$D_{CO_2} = \exp[(14.992-18.692\times X^m_{water})+(-19047.5+70193\times X^m_{water})/T \\ -(0.632+7.543\times X^m_{water})P/T] \quad (22)$$

The equation is based on 32 data for water-poor melts and 30 data for hydrous melts. The standard error of estimate is 0.59 for $\ln D_{CO_2}$. The fit equation reproduces 80% of the diffusion data within a factor of 2 and all data within a factor of 4 (Fig. 17). The comparison of the model to experimental data as a function of water contents is also shown Fig. 18. The activation energy E_a for CO_2 diffusion is calculated as $-(c+dX^m_{water})R$ with R being the gas constant (8,3144 J/mole.K). At ambient pressure, E_a decreases from 158 kJ/mole for the anhydrous melt to 100 kJ/mole for a melt with X^m_{water}= 0.1. At 500 MPa, E_a decreases from 161 kJ/mole for the anhydrous melt to 106 kJ/mole for a melt with X^m_{water} = 0.1. The apparent activation volume V_a for CO_2 diffusion is calculated as $-(e+gX^m_{water})R$. The apparent activation volume for CO_2 diffusion increases from 5.3 cm^3/mole for the anhydrous melt to 11.5 cm^3/mole for a melt with X^m_{water} = 0.1. The V_a value for the hydrous melt is close to the value of 11 cm^3/mole found by Watson et al. (1982) for basaltic composition and significantly lower than the value of 25 cm^3/mole suggested by Blank (1993) for rhyolitic

composition. However, it has to be emphasized, as acknowledged by the author herself, that the range of pressure was to small in the experiments of Blank to reliably constrain the pressure dependence of CO_2 diffusivity.

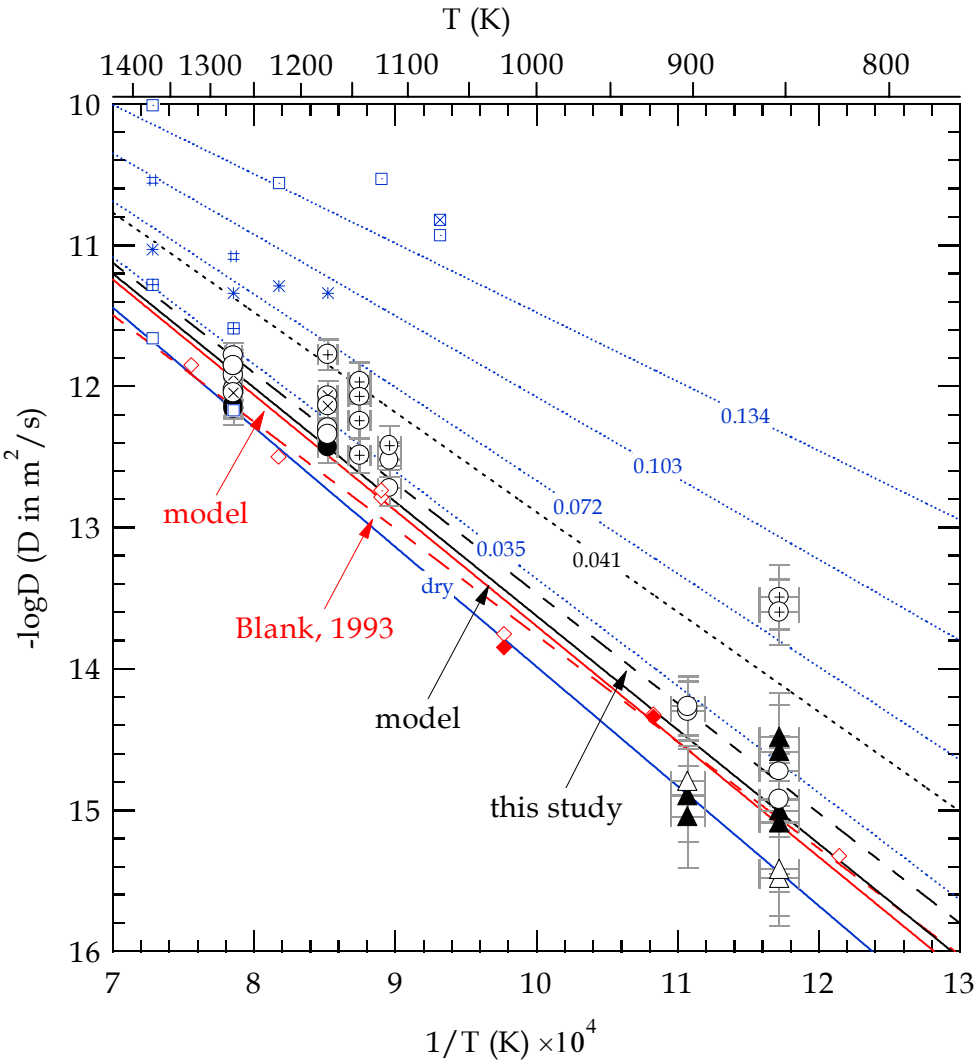

Fig. 17: Arrhenius plot for CO_2-diffusion. Solid lines are CO_2-diffusivity predictions for water-poor rhyolitic glasses at 72 (in red), 100 (in black) and 1000 MPa (in blue) from eqn. (22). Red and black dashed lines are the Arrhenius relationships derived for water-poor glasses at 72 MPa by Blank (1993) and at 100 MPa in this study, respectively. Dotted lines illustrate the effect of dissolved water on CO_2-diffusion. Lines in blue are calculated for 1000 MPa and the line in black for 100 MPa. Line numbers refer to the molar fraction of water dissolved. Numbers in blue correspond to dry, 2, 4, 6, 8 wt% water at 1000 MPa. The number in black corresponds to the average water content for all hydrous experiment of this study. Symbols are the same as in Fig. 15.

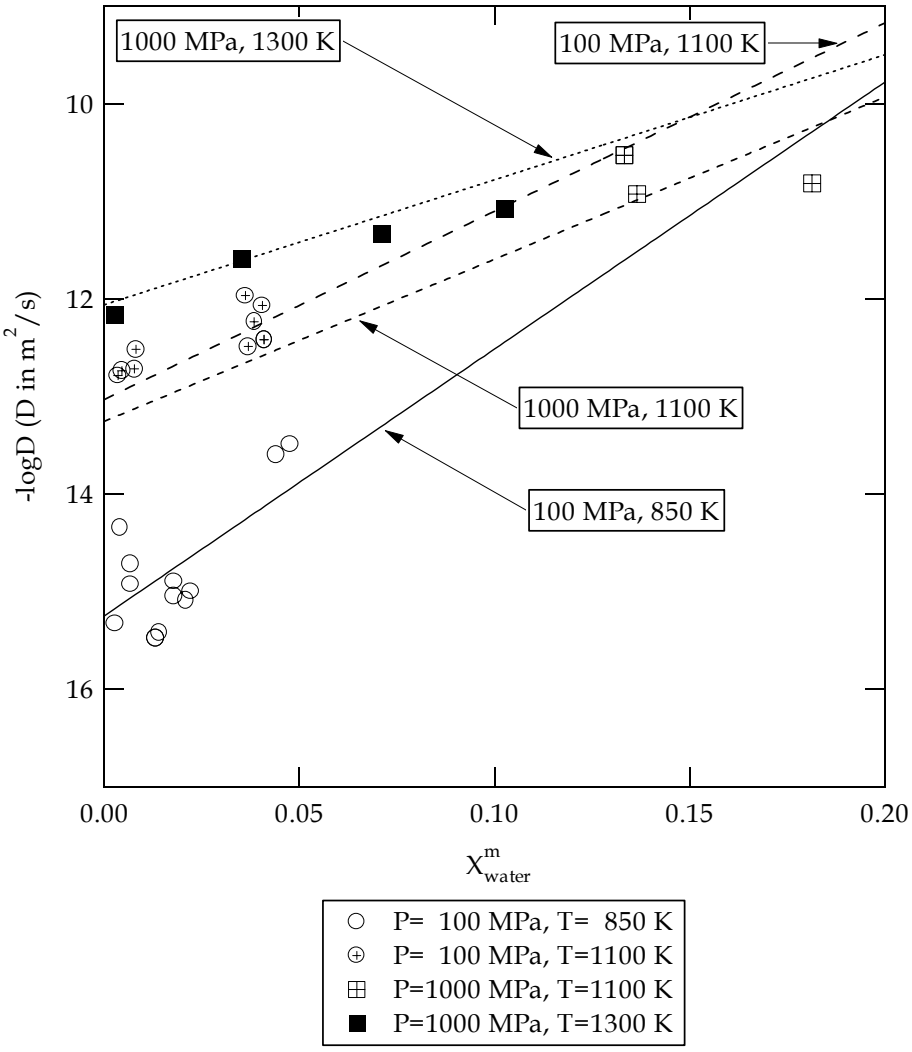

Fig. 18: Dependence of CO_2-diffusion in rhyolitic melts on dissolved water. Lines are calculated with the new diffusion model, eqn. (22).

The diffusivities of CO_2 and Ar are almost identical in water-poor rhyolitic melts over a wide range of temperature and pressure (Fig. 15). Although CO_2 diffusivities are similar to Ar diffusivities, and to other uncharged particles (such as molecular H_2O), the increase of activation volume with water content contrasts the dependence derived for molecular H_2O diffusion (Zhang and Behrens, 2000) and Ar diffusion (Behrens and Zhang, 2001). The pressure dependence becomes smaller for both Ar and molecular H_2O diffusion with increasing water content. Note that the pressure dependence is not well constrained for CO_2 at high H_2O contents.

The similarity between Ar and CO_2 diffusivity implies that the linear CO_2 molecule (base radius: 1.4 Å; half-length: 2.5 Å) moves as an oriented molecule to minimize expansion of the doorways of the silicate network (Behrens and Zhang, 2001).

Conclusions

(1) As found in previous studies, CO_2 dissolve in rhyolite only as molecular CO_2 species. I determined a new value of 1232 ± 36 $l.cm^{-1}.mol^{-1}$ for the linear molar absorption coefficient of the MIR baseline corrected band at 2346 cm^{-1} assigned to the fundamental ν_3 vibration CO_2 molecules. This value is 15% higher than the value of 1066 ± 20 $l.cm^{-1}.mol^{-1}$ determined by Blank (1993) on rhyolite. In addition, water does not influence the linear molar absorption coefficient.

(2) At both 200 and 500 MPa, a square root dependence of water solubility on X^f_{H2O} is observed at low X^f_{H2O}. At 200 MPa, a linear function between water solubility and X^f_{H2O} allows to model all data within uncertainty for $0.25<X^f_{H2O}<1$. At 500 MPa, the water solubility shows a non linear dependence on X^f_{H2O} in the whole X^f_{H2O} range. The 500 MPa data indicate a point of inflexion at around X^f_{H2O}~0.5. The temperature dependence of water solubility is different at 200 and 500 MPa. At 200 MPa, the water solubility decreases linearly with increasing temperature by -0.16 wt% H_2O per 100°C, regardless of the composition of the fluid phase (investigated range $0.25<X^f_{H2O}<1$). At 500 MPa, the temperature dependence of water solubility changes from positive for $X^f_{H2O}>0.75$ to negative for $X^f_{H2O}<0.75$. Water solubility is found to be independent of temperature at a water content of approximately 7 wt%. By comparing these results to that of Holtz et al., 1995 for a haplogranitic composition (AOQ), it was deduced that the temperature dependence of water solubility is not determined by total pressure but by the prevailing f_{H2O}.

(3) CO_2 solubility increases with increasing X^f_{CO2} in the fluid phase (Fig. 7) and increasing pressure. The variation of CO_2 solubility with X^f_{CO2} is non-linear. The deviation from linearity increases with pressure and is espacially pronounced at 500 MPa. Extrapolating our data set to $X^f_{CO2}=1$, the maximum solubility are 0.09 ±0.01 and 0.24 ±0.03 wt% at 1100°C and 200 and 500 MPa, respectively. Within the uncertainty of the data, no obvious effect of temperature on CO_2 solubility is observed at 200 MPa (Fig. 7). However, the data indicate a slight positive temperature dependence on CO_2 solubility at 500 MPa (for $X^f_{CO2}<0.5$). This effect of temperature on CO_2 solubility for $X^f_{CO2}<0.5$ differs from that observed by Fogel and Rutherford (1990) at $X^f_{CO2}=1$.

(3) Water and CO_2 solubilities found in this study are generally well reproduced by the model of Papale (1999) if CO_2 solubilities are lowered of 15% to take into account the change in linear molar absorption coefficient, except for high water contents (above about 6 wt%), for which water contents are systematically underestimated. Therefore, an empirical model was developed to predict water

contents from the composition of the fluid phase coexisting with the melt, based on the present data set and that of Blank (1993).

(4) Using CO_2 diffusion profiles to derive CO_2 solubilities has a large uncertainty due to the extrapolation of the profile to the surface. Deviation between equilibrium solubilities and extrapolated surface concentrations is in the range 15-35 % rel..

(5) CO_2 diffusion in water-poor samples can be described at 100 MPa by a simple Arrhenius relationship. My new results indicate that the effect of dissolved water on CO_2 diffusion may be more pronounced at low than at high temperatures. However, this is to be proven by additional low temperature experiments. Combining my data with those from the studies of Watson (1991) and Blank (1993) indicate that the effect of pressure on CO_2 diffusion only is weak. Similarity of diffusion of CO_2 and Ar (Behrens and Zhang, 2001) implies that the smaller size of the elongated CO_2 molecule (compared to the spherical Ar atom) compensates for the length and that CO_2 moves oriented through the silicate network to minimize strain.

(6) From my data set and those of Watson (1991) and Blank (1993), I developed a model to calculate CO_2 diffusion as a function of temperature, water content (as molar fraction) and pressure. At ambient pressure, E_a decreases from 158 kJ/mole for the anhydrous melt to 100 kJ/mole for a melt with X^m_{water}= 0.1. At 500 MPa, E_a decreases from 161 kJ/mole for the anhydrous melt to 106 kJ/mole for a melt with X^m_{water} = 0.1. The apparent activation volume V_a for CO_2 diffusion increases from 5.3 cm^3/mole for the anhydrous melt to 11.5 cm^3/mole for a melt with X^m_{water} = 0.1. The V_a value for the hydrous melt is close to that of 11 cm^3/mole found by Watson et al. (1982) for basaltic composition and significantly lower than that of 25 cm^3/mole suggested by Blank (1993) for rhyolitic composition.

The new experimental data on volatile solubility and diffusivity can be used as an input to develop or improve models to predict thermodynamic and kinetic properties of magmas and melts at various conditions. Especially degassing models for magmas (e.g. Navon et al., 1998; Papale and Polacci, 1999) may be tested and improved. This is an important step towards the prediction of volcanic hazards.

Appendix 1: Tables

Table 1
Composition of the starting material determined by electron microprobe

	EDF	standard deviation
SiO_2	77.04	0.77
TiO_2	0.11	0.01
Al_2O_3	12.76	0.13
FeO	0.68	0.07
MnO	0.07	0.01
MgO	0.08	0.01
CaO	0.58	0.06
Na_2O	4.07	0.20
K_2O	4.79	0.24
H_2O^*	0.22	
total	100.40	

* The initial total H_2O content of the natural glass was determined by IR spectroscopy. See text for more details.

Table 2
CO_2 calibration data

sample[a]	CO_2 Source[b]	P (MPa)	T (°C)	run duration (h)	C_{water} (wt%)[c]	CO_2 titration: glass weight (mg)	C_c (wt%)	C_{CO_2} (wt%)	MIR spectroscopy: A_{2346}	measured density ($g.l^{-1}$)[e]	thickness (cm)[f]	K = (4401×A)/(ρ×thickness)
std1 v	1+	200	1100	208	[d]	82.82	0.0199 (28)	0.0730 (101)	0.160 (17)	2264 (51)	0.0059 (3)	54 (8)
m					4.45 (0.23)				0.276 (6)		0.0090 (1)	60 (3)
s					4.30 (0.08)				0.260 (6)		0.0094 (1)	54 (3)
												56 (9)
std3 v	1+	500	1100	168	[d]	89.00	0.0399 (27)	0.1462 (99)	0.715 (16)	2250 (51)	0.0064 (1)	219 (6)
m					6.87 (0.57)				0.542 (29)		0.0051 (3)	207 (17)
s					6.75 (0.46)				0.595 (35)		0.0056 (4)	207 (20)
												211 (27)
std5 v	1+	500	1100	168	0.55 (0.06)	90.44	0.0580 (27)	0.2127 (98)	0.942 (15)	2343 (53)	0.0060 (1)	294 (6)
m					0.51 (0.05)				0.717 (88)		0.0063 (2)	215 (28)
s					0.53 (0.05)				0.955 (29)		0.0062 (2)	288 (13)
												266 (32)
std7 v	1+	500	1100	168	[d]	66.56	0.0571 (36)	0.2092 (132)	0.791 (10)	2277 (51)	0.0058 (1)	266 (7)
m					4.79 (0.20)				0.809 (14)		0.0062 (1)	252 (8)
s					4.75 (0.33)				0.735 (28)		0.0054 (1)	264 (13)
												261 (17)
1P	1	800	1200	96	6.95 (0.07)	69.72	0.0932 (35)	0.3415 (128)	0.842 (16)	2269	0.0038 (1)	430 (14)
2P	1	800	1200	96	4.32 (0.07)	70.60	0.1062 (35)	0.3893 (127)	0.860 (7)	2306	0.0035 (1)	469 (16)

[a] Letters v, m, and s indicate the chip distance from the CO_2-source during the experiment:
v is the piece opposite to the source
m is the middle piece of the run product
s is the piece closest to the source

[b] CO_2 was generated in two different ways by decomposition of inorganic materials:
1 Silver oxalate was added directly to the sample.
1+ Silver oxalate was placed in a separate unwelded capsule beside the sample.

[c] Water content was determined using NIR spectroscopy, except for samples 1P and 2P, for which KFT was used. See chapter 2, § 3.4.2. and § 3.3., respectively, for more details.
[d] Not determined.
[e] Except for the samples 1P and 2P for which densities are calculated using equation (8).
[f] Thicknesses are calculated using equation (10). See chapter 2 § 3.4.1. for more details.

Table 3
Analysis of the samples used for the CO_2-titration calibration

	LECO analysis (Bristol)		coulometric titration			
			C content (wt%)			
	C content (wt%)	number of analysis	Köln (K)/ Göttingen (G)	Hannover	number of analysis	typical weight (mg)
TW64d	1.69 ±0.01	4	1.61 (G)	1.61 ±0.02	36	23-36
GD62	0.51 ±0.01	5	0.491 (G)	0.489 ±0.009	37	25-32
22V	0.122 ±0.008	3	0.145 (K)	0.110 ±0.006	30	72-86
45V	0.042 ±0.006	5	0.034 (K)	0.026 ±0.001	10	70-110

Table 4
Conditions and sample characterisation for volatile solubility experiments.

sample	CO_2 source [a]	run duration (h)	P (MPa)	T (°C)	$X^f_{H_2O}$	$X^f_{CO_2}$	C_{water}, KFT (wt%)
Ech1 [b] [c]	1	240	200	800	0.288 (19)	0.692 (29)	-
Ech7 [b] [c]	1	283	200	800	0.355 (18)	0.625 (29)	-
Ech6 [c]	1	260	200	800	0.482 (15)	0.498 (26)	-
Ech2 [c]	1	240	200	800	0.496 (16)	0.484 (27)	3.84 (07)
Ech8 [c]	1	283	200	800	0.571 (17)	0.409 (28)	3.78 (07)
Ech9	1	227	200	800	0.658 (15)	0.322 (26)	4.32 (07)
Ech10 [c]	1	227	200	800	0.768 (15)	0.212 (26)	5.01 (07)
Ech3	-	240	200	800	1.000 (10)	0.000 (22)	6.12 (07)
Ech4	-	240	200	800	1.000 (20)	0.000 (-)	6.10 (07)
Ech66	1+	208	200	1100	0.021 (35)	0.959 (43)	-
Ech65	1+	208	200	1100	0.102 (32)	0.878 (40)	-
Ech64	1+	208	200	1100	0.206 (30)	0.774 (39)	-
Ech63	1+	208	200	1100	0.310 (27)	0.670 (36)	-
Ech62	1+	208	200	1100	0.410 (24)	0.570 (34)	-
Ech17	2	72	200	1100	0.520 (14)	0.460 (26)	-
Ech18	2	72	200	1100	0.613 (13)	0.367 (24)	3.74 (07)
Ech19	2	72	200	1100	0.706 (11)	0.274 (23)	4.14 (07)
Ech20	2	72	200	1100	0.779 (11)	0.201 (23)	-
Ech21	-	72	200	1100	1.000 (21)	0.000 (-)	-
Ech37	1	98	500	800	0.408 (14)	0.572 (26)	5.02 (07)
Ech38	1	98	500	800	0.433 (14)	0.547 (26)	5.21 (07)
Ech39	1	96	500	800	0.626 (14)	0.354 (25)	6.47 (07)
EDF(1) [d]	-	144	500	800	1.000 (-)	0.000 (-)	9.84 (15)
Ech75	1+	120	500	1100	0.017 (26)	0.963 (35)	-
Ech74	1+	120	500	1100	0.084 (24) [0.049]	0.896 (34) [0.931]	-
Ech73	1+	120	500	1100	0.107 (24) [0.077]	0.873 (34) [0.903]	-
Ech72	1+	120	500	1100	0.114 (24) [0.085]	0.866 (34) [0.896]	-
Ech59	1+	156	500	1100	0.120 (30)	0.860 (39)	-
Ech71	1+	120	500	1100	0.122 (24)	0.858 (34)	-
Ech58	1+	156	500	1100	0.245 (28)	0.735 (37)	-
Ech57	1+	156	500	1100	0.374 (25)	0.606 (35)	-
Ech11[e]	1	96	500	1100	0.471 (17)	0.509 (28)	4.83 (11)
Ech22[f]	2	72	500	1100	0.480 (14)	0.500 (26)	-
Ech56	1+	156	500	1100	0.558 (21)	0.422 (31)	-
Ech61	1+	156	500	1100	0.672 (16)	0.308 (27)	-
Ech24[f]	2	72	500	1100	0.682 (12)	0.298 (24)	-
Ech41	2	96	500	1100	0.734 (11)	0.246 (23)	7.25 (07)
Ech36	2	96	500	1100	0.837 (09)	0.143 (22)	8.96 (07)
Ech49	-	96	500	1100	1.000 (-)	0.000 (-)	11.04 (06)

C_{water},KFT is the concentration of total water in the glass determined by Karl Fischer titration. Uncertainty of pressure is ±5 MPa and uncertainty of temperature is ±10°C. The $X^f_{H_2O}$ and $X^f_{CO_2}$ given in square brackets correspond to the values obtained by mass balance calculation. See text for more details.

(a) CO_2 was generated in three different ways by decomposition of inorganic materials:
1 Silver oxalate was added directly to the sample.
1^+ Silver oxalate was placed in a separate unwelded capsule beside the sample.
2 Dehydrated oxalic acid was directly added to the sample.

(b) Glass partially crystallised (<10 vol%)

(c) Quenched glass contains aggregates of metallic silver.

(d) Data from Behrens and Jantos (2001)

(e) Dark coloured glass due to dissolution of silver (up to 2 wt%)

(f) Sample contains bubbles (<10 vol%)

Table 5
Spectroscopic data of volatile solubility experiments

sample	measured density ($g.l^{-1}$)	calculated density [b] ($g.l^{-1}$)	MIR			NIR				
			thickness (cm) [c]	A_{2346}	C_{CO_2} (wt%)	thickness (cm)	A_{4520}	A_{5230}	C_{OH} (wt%)	C_{H_2O} (wt%)
Ech1[a]	-	2325	0.0112 (1)	0.598	0.082 (3)	0.0500	0.128	0.163	1.41 (0.08)	1.52 (0.06)
Ech7[a]	-	2321	0.0111 (3)	0.525	0.073 (3)	0.0493	0.129	0.186	1.44 (0.08)	1.76 (0.06)
Ech6[a]	-	2312	0.0112 (4)	0.414	0.057 (3)	0.0486	0.134	0.237	1.52 (0.09)	2.29 (0.08)
Ech2[a]	-	2310	0.0109 (2)	0.432	0.061 (3)	0.0495	0.138	0.253	1.54 (0.09)	2.40 (0.08)
Ech8[a]	-	2307	0.0111 (3)	0.393	0.055 (3)	0.0492	0.137	0.271	1.54 (0.09)	2.59 (0.09)
Ech9	-	2300	0.0116 (5)	0.304	0.041 (3)	0.0484	0.140	0.308	1.61 (0.09)	3.00 (0.10)
Ech10[a]	2300 (52)	2294	0.0117 (1)	0.190	0.025 (2)	0.0495	0.144	0.356	1.62 (0.09)	3.40 (0.11)
Ech3	-	2281	-	-	-	0.0496	0.142	0.449	1.60 (0.09)	4.31 (0.14)
Ech4	2274 (51)	2280	-	-	-	0.0496	0.147	0.449	1.66 (0.09)	4.31 (0.14)
Ech66	-	2360	0.0077 (7)	0.461	0.091 (12)	0.0810	0.073	0.009	0.49 (0.03)	0.05 (0.02)
Ech65	-	2347	0.0077 (4)	0.465	0.092 (8)	0.0814	0.148	0.074	0.99 (0.05)	0.42 (0.02)
Ech64	-	2337	0.0095 (4)	0.537	0.086 (6)	0.0810	0.179	0.147	1.21 (0.07)	0.84 (0.03)
Ech63	-	2331	0.0096 (1)	0.481	0.077 (3)	0.0805	0.194	0.198	1.32 (0.07)	1.14 (0.04)
Ech62	-	2326	0.0088 (2)	0.404	0.070 (3)	0.0810	0.205	0.253	1.39 (0.08)	1.46 (0.06)
Ech17	-	2316	0.0117 (2)	0.441	0.058 (2)	0.0500	0.139	0.213	1.53 (0.09)	2.00 (0.07)
Ech18	2278 (51)	2311	0.0121 (3)	0.427	0.055 (3)	0.0504	0.142	0.248	1.56 (0.09)	2.31 (0.08)
Ech19	2275 (51)	2303	0.0123 (2)	0.321	0.040 (2)	0.0492	0.145	0.285	1.64 (0.09)	2.73 (0.09)
Ech20	2273 (51)	2299	0.0119 (3)	0.262	0.034 (2)	0.0489	0.147	0.311	1.67 (0.09)	3.00 (0.10)
Ech21	-	2286	-	-	-	0.0489	0.151	0.396	1.73 (0.09)	3.85 (0.13)
Ech37	2291 (52)	2291	0.0053 (1)	0.598	0.176 (6)	0.0496	0.146	0.371	1.64 (0.09)	3.54 (0.12)
Ech38	2274 (51)	2289	0.0051 (1)	0.592	0.181 (7)	0.0495	0.145	0.384	1.64 (0.09)	3.68 (0.12)
Ech39	2229 (50)	2272	0.0047 (2)	0.430	0.144 (8)	0.0494	0.145	0.500	1.65 (0.09)	4.84 (0.16)
EDF(1)	-	2223	-	-	-	-	-	-	-	-
Ech75	-	2360	0.0036 (2)	0.566	0.238 (25)	0.0975	0.082	0.010	0.45 (0.03)	0.05 (0.01)
Ech74	-	2351	0.0044 (1)	0.682	0.235 (13)	0.0962	0.153	0.059	0.86 (0.05)	0.28 (0.02)
Ech73	-	2348	0.0056 (3)	0.898	0.244 (19)	0.0956	0.168	0.083	0.95 (0.05)	0.40 (0.02)
Ech72	-	2341	0.0063 (2)	0.903	0.219 (9)	0.0957	0.198	0.143	1.13 (0.06)	0.69 (0.03)
Ech59	-	2332	0.0064 (2)	0.965	0.231 (8)	0.0579	0.139	0.141	1.32 (0.07)	1.13 (0.04)
Ech71	-	2336	0.0060 (2)	0.901	0.230 (11)	0.0953	0.215	0.193	1.24 (0.07)	0.94 (0.03)
Ech58	-	2319	0.0058 (2)	0.837	0.222 (11)	0.0586	0.155	0.229	1.46 (0.08)	1.83 (0.06)
Ech57	-	2310	0.0051 (5)	0.715	0.217 (21)	0.0589	0.162	0.299	1.52 (0.08)	2.39 (0.08)
Ech11	-	2297	0.0052 (3)	0.675	0.202 (13)	-	-	-	-	-
Ech22[d]	-	2293	0.0058 (4)	0.747	0.201 (15)	0.0511	0.147	0.377	1.60 (0.09)	3.49 (0.12)
Ech56	-	2291	0.0050 (1)	0.609	0.190 (7)	0.0591	0.172	0.448	1.62 (0.09)	3.59 (0.12)
Ech61	-	2272	0.0062 (3)	0.604	0.153 (8)	0.0601	0.176	0.614	1.65 (0.09)	4.88 (0.16)
Ech24[d]	-	2269	0.0054 (3)	0.569	0.166 (11)	0.0502	0.149	0.528	1.67 (0.09)	5.03 (0.17)
Ech41	2216 (50)	2264	0.0051 (5)	0.466	0.144 (16)	0.0501	0.147	0.562	1.66 (0.09)	5.38 (0.18)
Ech36	-	2247	0.0050 (2)	0.257	0.082 (6)	0.0500	0.141	0.682	1.60 (0.09)	6.59 (0.22)
Ech49	-	2212	-	-	-	0.0249	0.080	0.443	1.86 (0.12)	8.73 (0.31)

Concentrations on C_{OH} and C_{H2O} are given in terms of wt% of H_2O component. Total water determined from NIR is the sum of C_{OH} and C_{H_2O}. See text for details about error calculations.

[a] Quenched glass contains aggregates of metallic silver.

[b] Densities are calculated using equation (8). See text for more details.

[c] Thicknesses are calculated using equation (10). Sample thickness and peak heights are average values derived from 3 to 9 spectra measured in different areas of the samples, including rim and core. See text for more details.

[d] Sample with bubbles (<10 vol%)

Table 6
Fit parameters of equation (12) to describe the water solubility in rhyolitic melts

	$A_{(P,T)}$		$B_{(P,T)}$		$C_{(P,T)}$	
	a_A	b_A	a_B	b_B	a_C	b_C
$\alpha_{i,j}$	-14.749	$2.7296\ 10^{-2}$	12.615	$-2.3041\ 10^{-2}$	5.4181	$-6.11323\ 10^{-3}$
$\beta_{i,j}$	$7.67\ 10^{-2}$	$-1.3688\ 10^{-4}$	$-6.3322\ 10^{-2}$	$1.1396\ 10^{-4}$	$1.2838\ 10^{-2}$	$2.0095\ 10^{-5}$
$\gamma_{i,j}$	$-2.0868\ 10^{-4}$	$2.5324\ 10^{-7}$	$1.5411\ 10^{-4}$	$-1.747\ 10^{-7}$	$1.4632\ 10^{-5}$	$-4.8208\ 10^{-8}$

Table 7
Experimental data for CO_2 diffusion experiments

sample	P/T (MPa)/(°C)	effective duration (s)	C_{water_i} (wt.%)[a]	$X^f_{H_2O}$ [b] initial	final	slide thickness (µm)	profile	slit width (µm)	C_{water} along the profile[c] (µm)	C_{CO_2} surface (fit)** (wt.%)	- log D (m^2/s)[d]
CO_2 –desorption from hydrous CO_2-bearing samples											
d15834j	100/580	2578532				60 (1)	A	19	0.27-1.2		15.48 (± 0.34)
							B	19	0.24-1.1		15.42 (± 0.33)
d16317j	100/630	1460825				63 (2)	A	19	0.16-0.7		14.80 (± 0.25)
d5589j	500/580	764849				57 (5)	A	16	0.30-1.7		14.90 (± 0.33)
							B	16	0.30-1.7		15.05 (± 0.36)
d55894h_bis	500/580	338615				79 (1)	BA	16-26	0.25-2.1		15.09 (± 0.49)
							BB	16-26	0.25-2.3		15.00 (± 0.45)
d56378h	500/630	279397				60 (1)	A	16	0.25-1.8		14.59 (± 0.33)
						60 (1)	B	16	0.25-1.8		14.48 (± 0.31)
CO_2 –sorption from pre-hydrated natural samples											
h15834j	100/580	2578532	2.24	0.27	0.24	140 (1)	A	19	2.71	0.0582	13.49 (± 0.23)
				0.27	0.24		B	19	2.51	0.0805	13.60 (± 0.23)
h1846h	100/843	20552	2.23	0.39	0.38	154 (4)	A	26	2.32	0.0550	12.42 (± 0.14)
h1872h	100/870	7433	2.23	0.38	0.38	226 (1)	A	19	2.05	0.0656	11.97 (± 0.14)
				0.38	0.38		B	19	2.30	0.0475	12.07 (± 0.15)
h1876h*	100/870	22106	2.18	0.40	0.39	150 (2)	A	29	2.18	0.0548	12.24 (± 0.12)
h18718h	100/870	65336	2.23	0.38	0.38	250 (5)	B	19	2.09	0.0559	12.49 (± 0.12)
h1904h	100/900	14565	2.21	0.40	0.39	151 (2)	A	29	2.36	0.0357	11.78 (± 0.11)
CO_2 –sorption from natural samples											
s15834j	100/580	2578532				243 (3)	A	19	0.32-0.42	0.0976	14.93 (± 0.26)
							B	19	0.32-0.42	0.0708	14.72 (± 0.25)
s16317j	100/630	1460825				246 (4)	A	17	0.47-0.56	0.0816	14.30 (± 0.21)
							B	17	0.47-0.56	0.0743	14.26 (± 0.21)
s18418h	100/843	63942				312 (2)	A	25	0.33-0.53	0.0469	12.72 (± 0.13)
							B	25	0.33-0.58	0.0508	12.52 (± 0.12)
s19012h	100/900	41565				308 (1)	A	26	0.27-0.43	0.0455	12.29 (± 0.11)
							B	26	0.27-0.42	0.0539	12.34 (± 0.11)
s11004h	100/1000	14528				308 (2)	A	20	0.21-0.49	0.0494	11.78 (± 0.09)
							B	20	0.21-0.48	0.0436	11.85 (± 0.09)
s39028h	300/900	110910				77 (1)	A	20	0.21-0.42	0.1797	12.06 (± 0.10)
							B	20	0.21-0.41	0.1765	12.14 (± 0.10)
s310030m	300/1000	1992				115 (3)	A	22	0.21-0.53	0.1263	12.12 (± 0.19)
							B	22	0.21-0.56	0.1321	11.92 (± 0.18)
s31004h	300/1000	14528				98 (2)	A	20	0.31-0.58	0.1484	11.86 (± 0.09)
							B	20	0.31-0.48	0.1089	12.04 (± 0.09)
s59014h	500/900	50510				40 (1)	A	19	0.50-0.56	0.3167	12.33 (± 0.11)
							B	19	0.49-0.52	0.3154	12.43 (± 0.11)
s51004h	500/1000	14528				65 (1)	A	20	0.25-0.52	0.2928	12.13 (± 0.10)
							B	20	0.25-0.52	0.2370	12.16 (± 0.11)

Notes.

Thicknesses of samples used in diffusion experiments are 2 and 1 mm for desorption and sorption experiments, respectively.

[a] Water content measured with KFT for samples used in desorption experiments, and equals 2.34 ± 0.06. For pre-hydrated samples used in sorption experiments, water contents were determined by IR spectroscopy.

[b] In the desorption experiments the samples are in contact with the pressure medium Ar which has an unknown water content. Fluid composition in sorption experiments using mixed H_2O-CO_2 fluids are calculated as explained in Chapter 2 § 3.1.. In the sorption experiments using natural samples a pure CO_2 fluid was generated containing a small but unknown amount of H_2O.

[c] Determined by IR spectroscopy

[d] Determined from the fit. See text for more details.

* A problem occurred when starting the experiment: the oven heated too quick and went for 15-20 min to 900°C before being set back to input run temperature.

** These CO_2 concentrations were derived from the fit of the diffusion profiles. In the desorption experiments the CO_2 content at the sample surface is assumed to be zero.

Appendix 2: Diffusion profiles and fits

Fig. 1-(a-i): Concentration-distance profiles of CO_2 in natural rhyolitic glasses after CO_2 sorption. Two profiles were fitted independently for each sample using eqn. (14) or eqn (16) depending whether the profiles from both sides do overlap or not. Points chosen for the fits are shown in black for the first fit and in grey for the second.

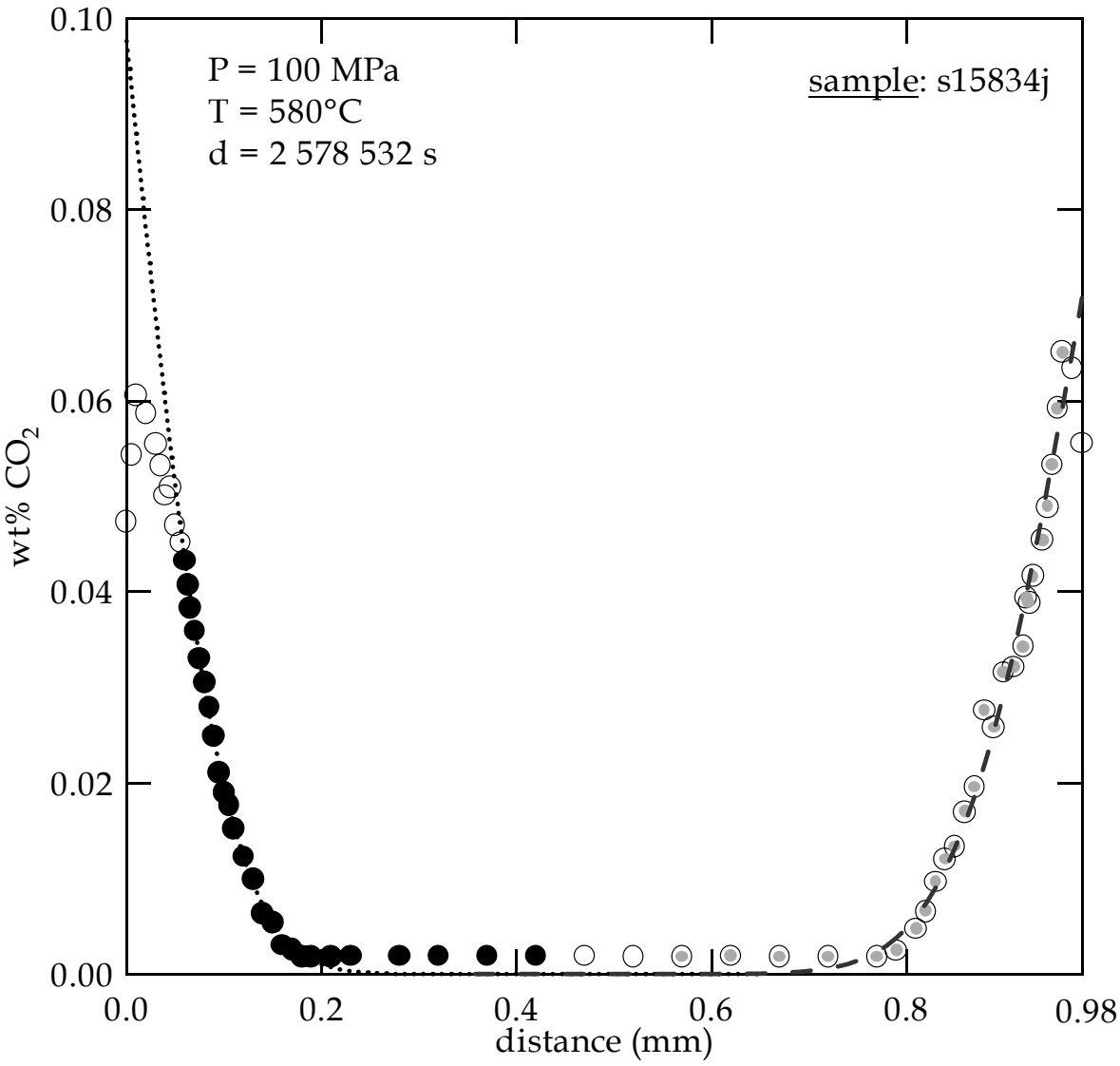

(1-a)

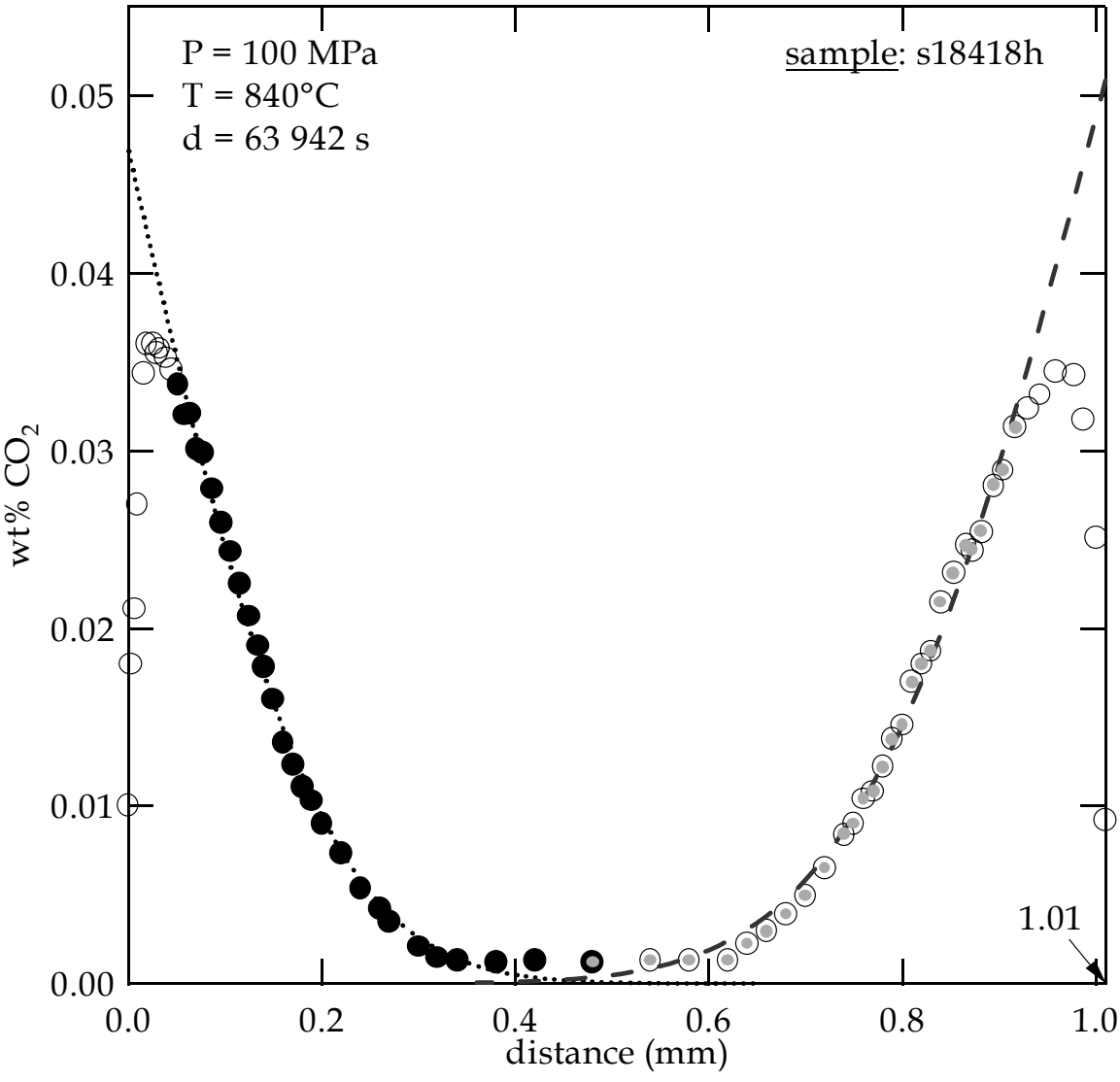
P = 100 MPa
T = 840°C
d = 63 942 s
sample: s18418h
0.05
0.04
0.03
0.02
0.01
0.00
wt% CO_2
0.0
0.2
0.4
0.6
0.8
1.0
distance (mm)
1.01

(1-b)

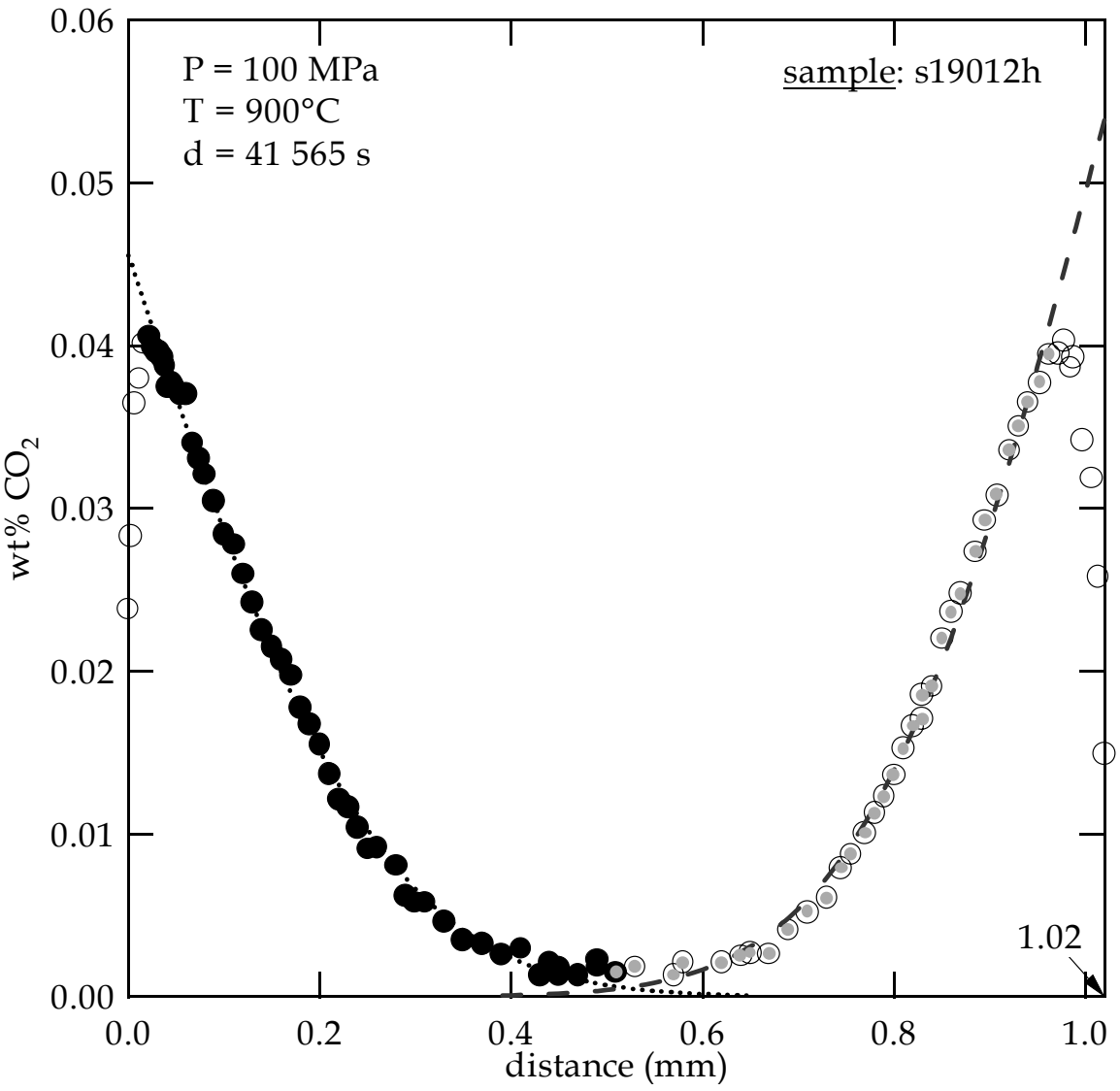
P = 100 MPa
T = 900°C
d = 41 565 s
sample: s19012h
wt% CO_2
distance (mm)
1.02
0.00
0.01
0.02
0.03
0.04
0.05
0.06
0.0
0.2
0.4
0.6
0.8
1.0

(1-c)

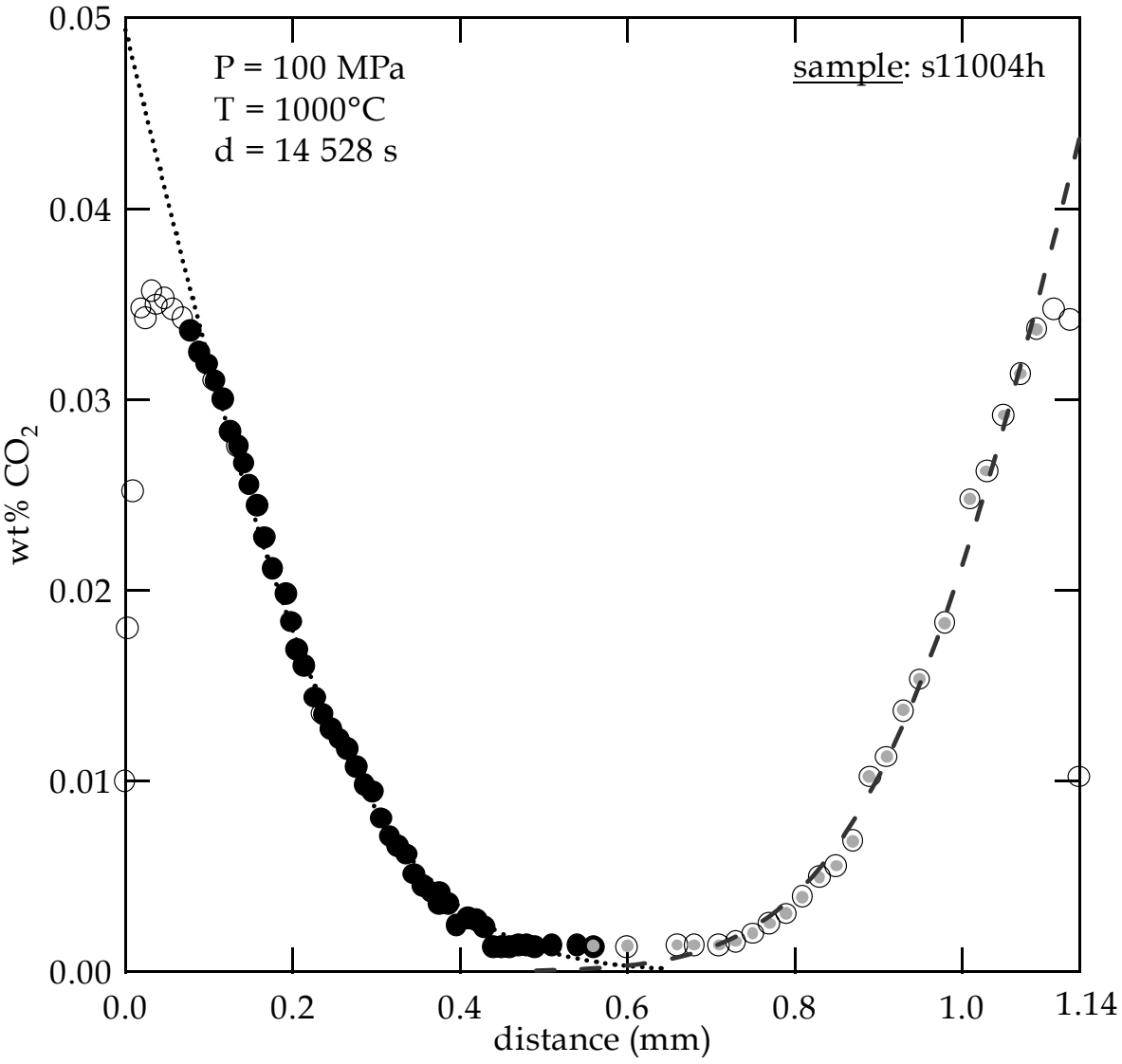
P = 100 MPa
T = 1000°C
d = 14 528 s
sample: s11004h
wt% CO_2
distance (mm)
0.05
0.04
0.03
0.02
0.01
0.00
0.0
0.2
0.4
0.6
0.8
1.0
1.14

(1-d)

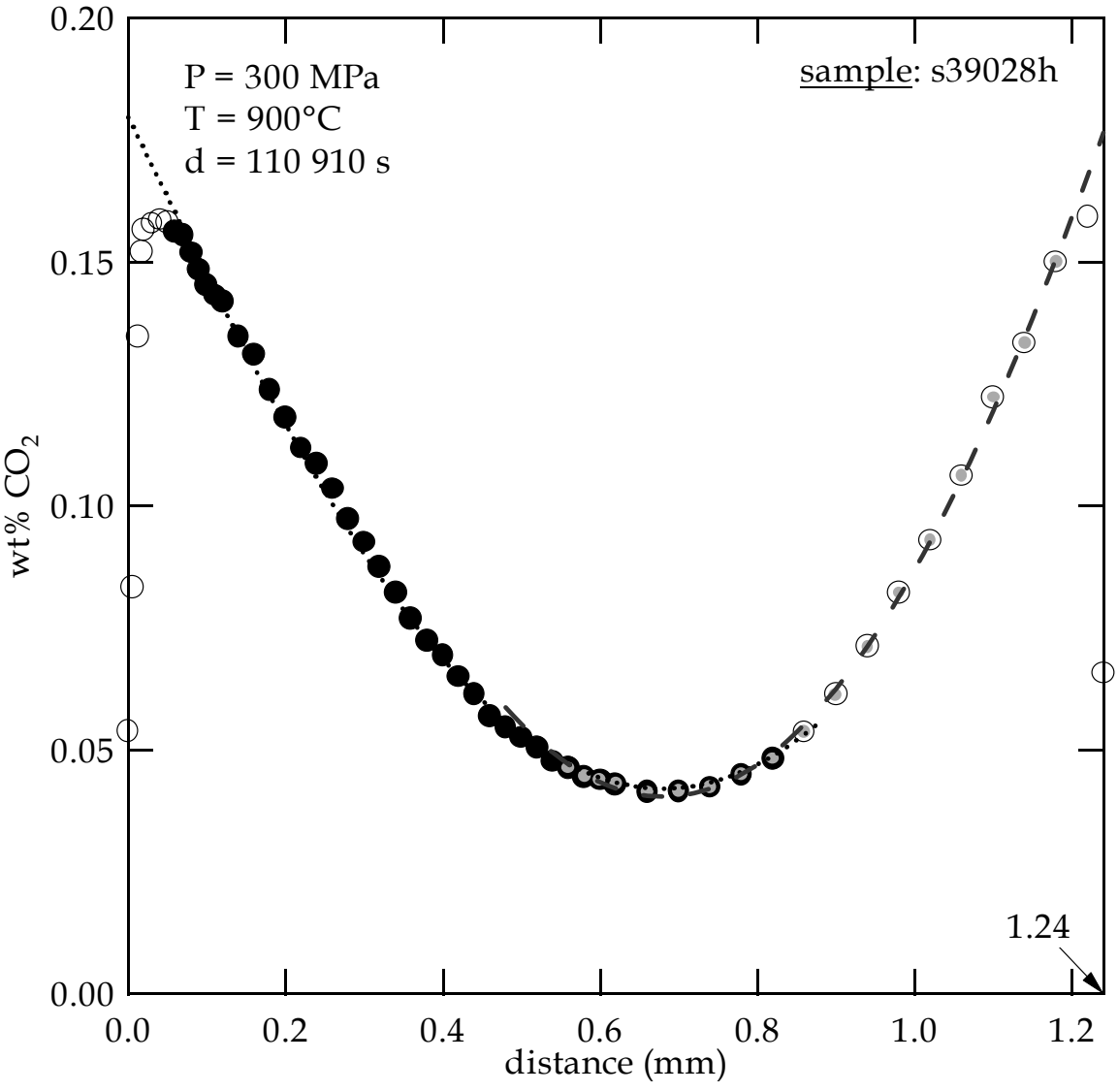
P = 300 MPa
T = 900°C
d = 110 910 s
sample: s39028h
wt% CO_2
distance (mm)
0.20
0.15
0.10
0.05
0.00
0.0
0.2
0.4
0.6
0.8
1.0
1.2
1.24

(1-e)

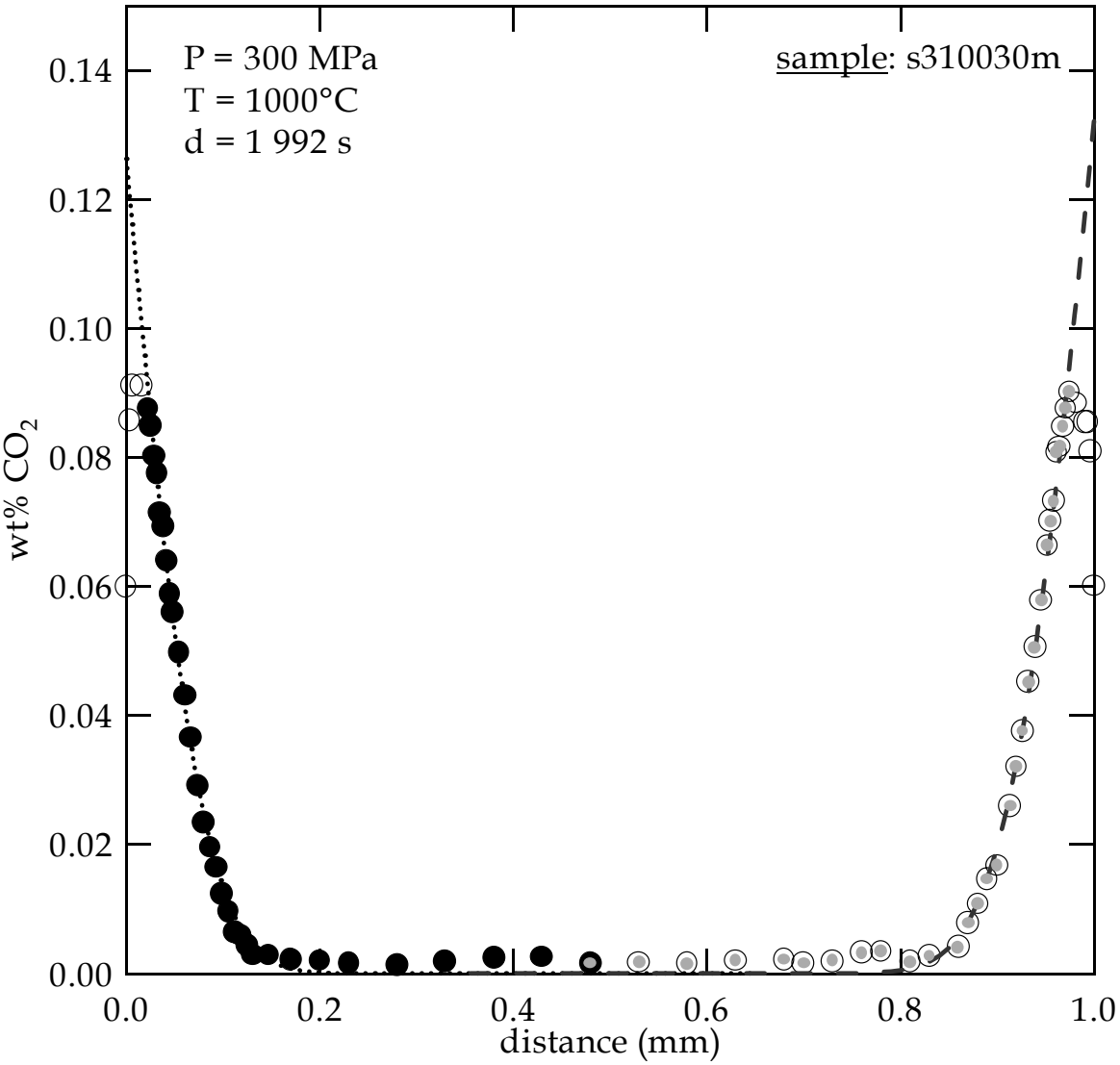
P = 300 MPa
T = 1000°C
d = 1 992 s
sample: s310030m
wt% CO2
distance (mm)
0.00
0.02
0.04
0.06
0.08
0.10
0.12
0.14
0.0
0.2
0.4
0.6
0.8
1.0

(1-f)

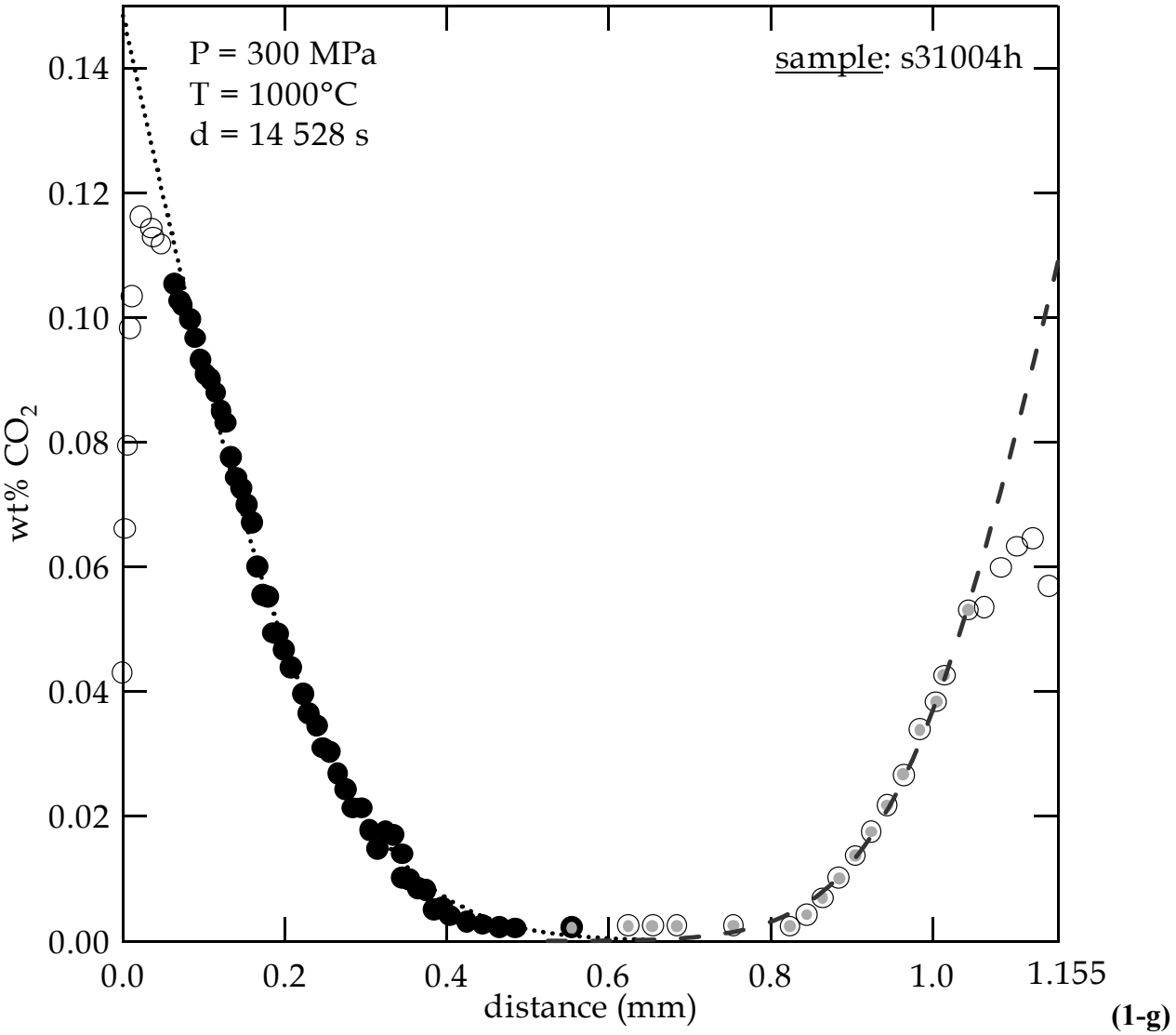
P = 300 MPa
T = 1000°C
d = 14 528 s
sample: s31004h
wt% CO2
0.14
0.12
0.10
0.08
0.06
0.04
0.02
0.00
0.0
0.2
0.4
0.6
0.8
1.0
1.155
distance (mm)

(1-g)

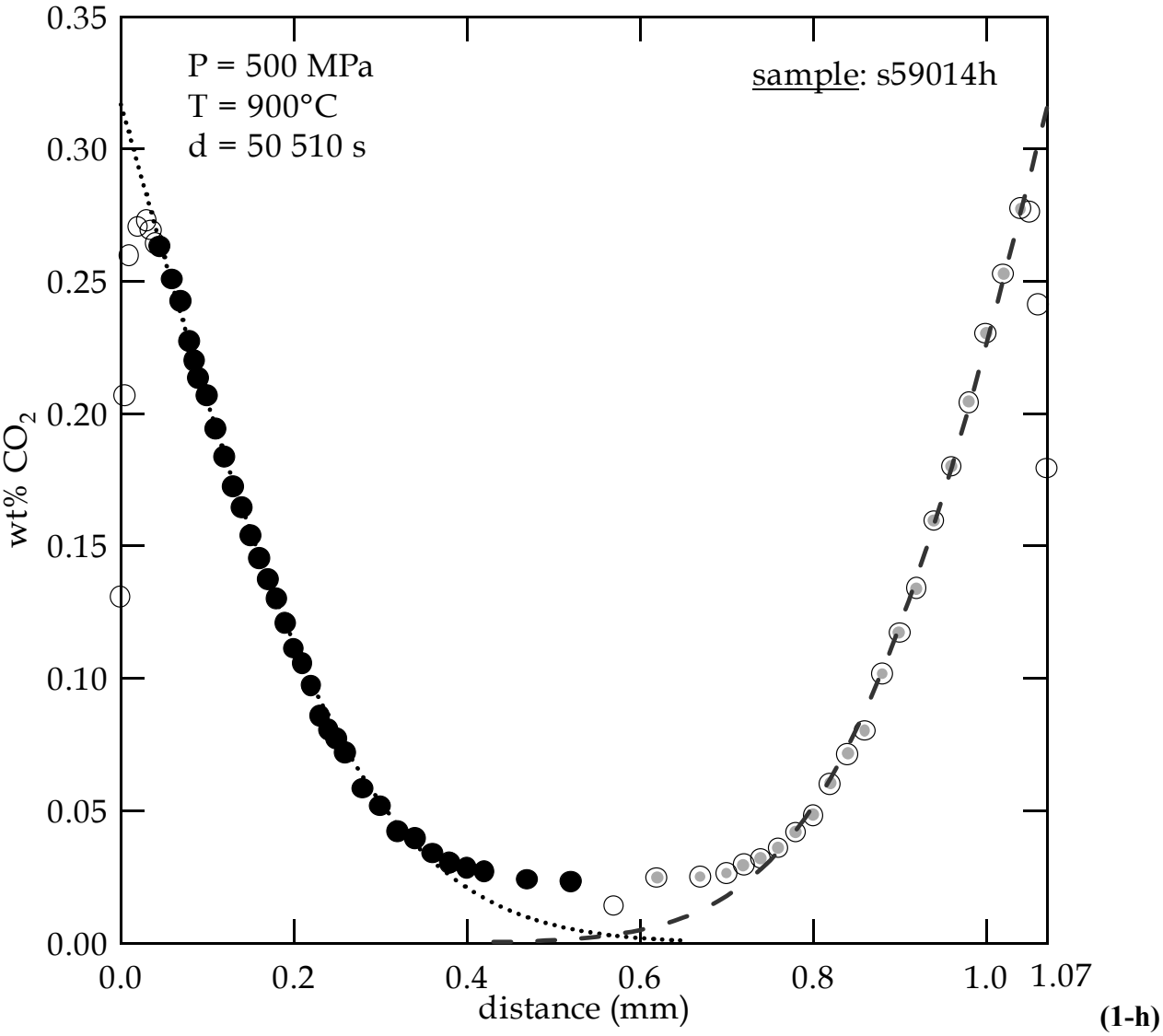
P = 500 MPa
T = 900°C
d = 50 510 s
sample: s59014h
wt% CO_2
distance (mm)
0.35
0.30
0.25
0.20
0.15
0.10
0.05
0.00
0.0
0.2
0.4
0.6
0.8
1.0
1.07

(1-h)

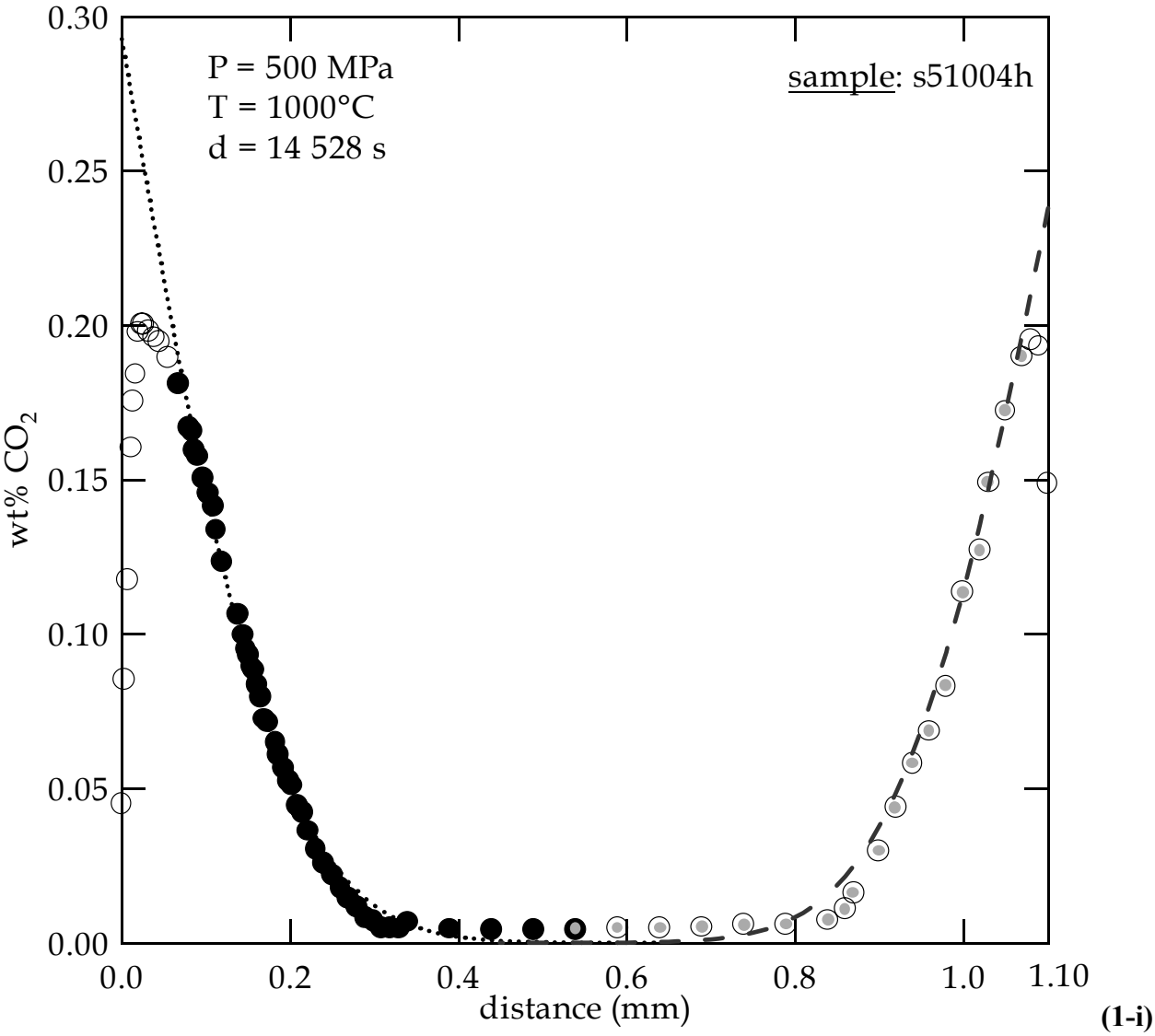
P = 500 MPa
T = 1000°C
d = 14 528 s
sample: s51004h
wt% CO_2
distance (mm)
0.00
0.05
0.10
0.15
0.20
0.25
0.30
0.0
0.2
0.4
0.6
0.8
1.0
1.10

(1-i)

Fig. 2-(a-d): Concentration-distance profiles for CO_2 in hydrous CO_2-bearing rhyolitic glasses after CO_2 desorption experiments. One or two profiles were fitted with eqn. (15) depending on the quality of the profiles. Points chosen for the fit are blacken. Surfaces of the sample are shown by two vertical dotted lines.

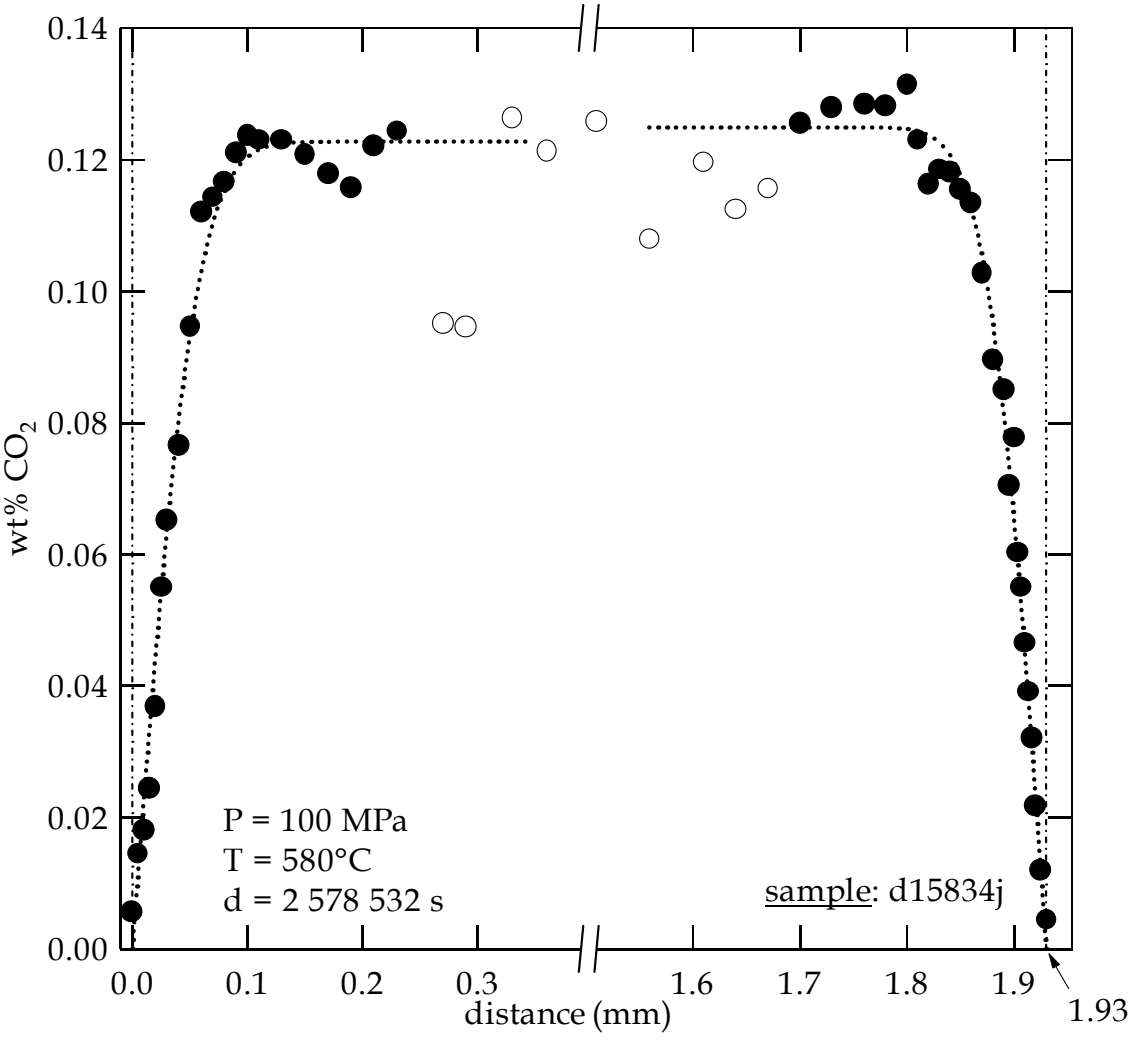

(2-a)

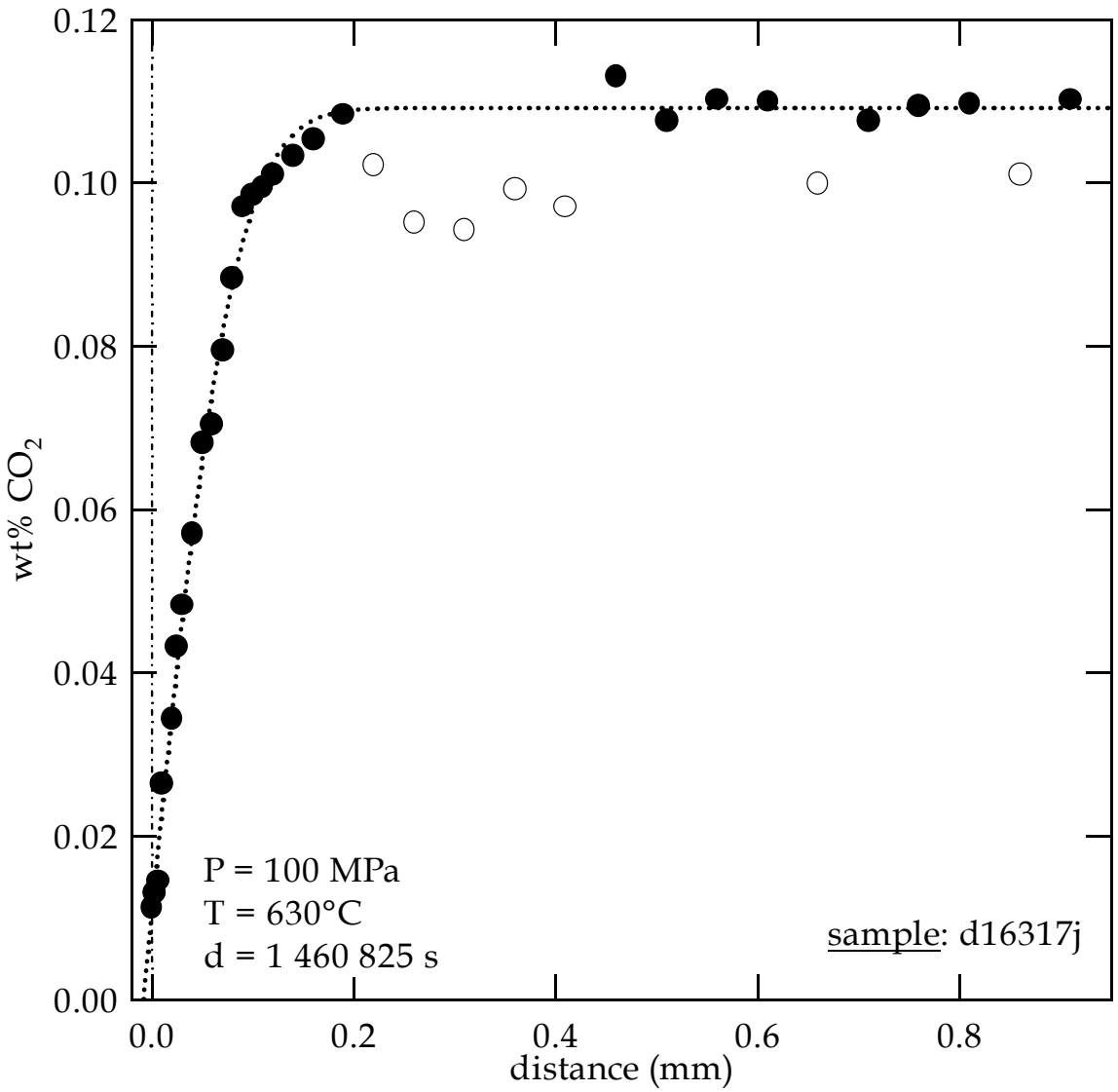
0.12
0.10
0.08
0.06
0.04
0.02
0.00
wt% CO_2
0.0
0.2
0.4
0.6
0.8
distance (mm)
P = 100 MPa
T = 630°C
d = 1 460 825 s
sample: d16317j

(2-b)

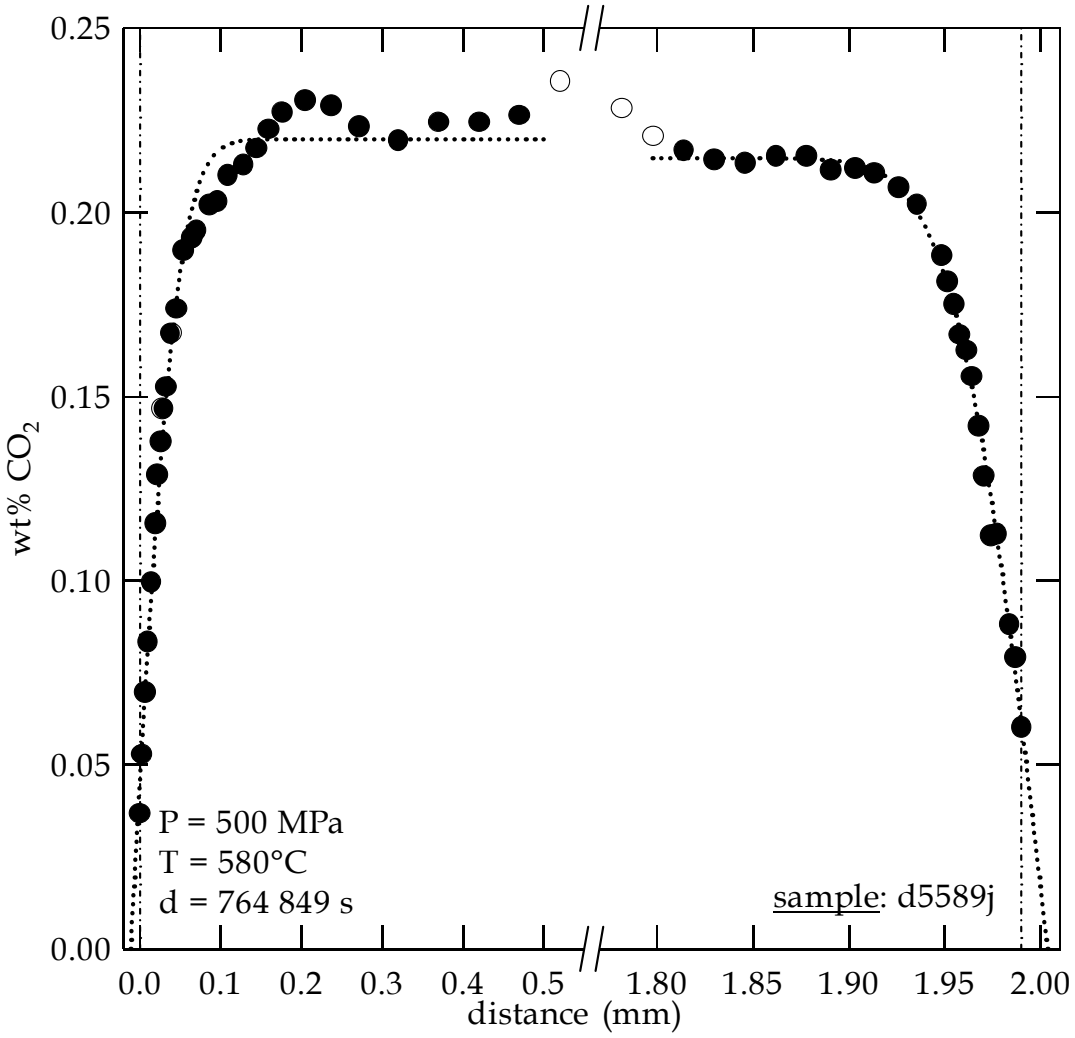
0.25
0.20
0.15
0.10
0.05
0.00
wt% CO_2
P = 500 MPa
T = 580°C
d = 764 849 s
sample: d5589j
0.0
0.1
0.2
0.3
0.4
0.5
1.80
1.85
1.90
1.95
2.00
distance (mm)

(2-c)

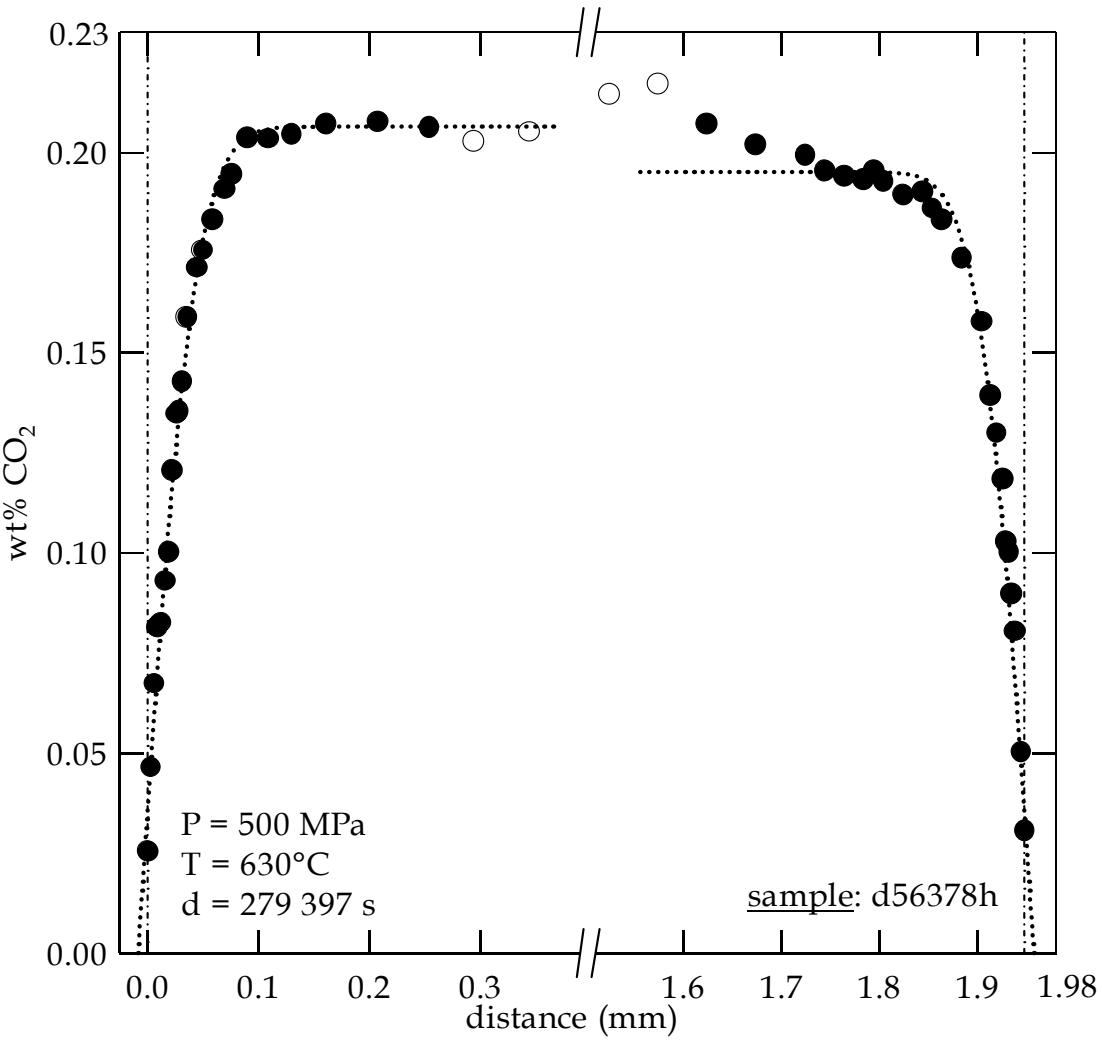
0.23
0.20
0.15
0.10
0.05
0.00
wt% CO_2
P = 500 MPa
T = 630°C
d = 279 397 s
sample: d56378h
0.0
0.1
0.2
0.3
1.6
1.7
1.8
1.9
1.98
distance (mm)

(2-d)

Fig. 3-(a-e): Concentration-distance profiles of CO_2 in natural rhyolitic glasses after CO_2 sorption. One or two profiles (depending on the quality of the profiles) were fitted with eqn. (17) or eqn. (18), depending whether the profiles from both sides do overlap or not. Points chosen for the fits are shown in black for the first fit and in grey for the second.

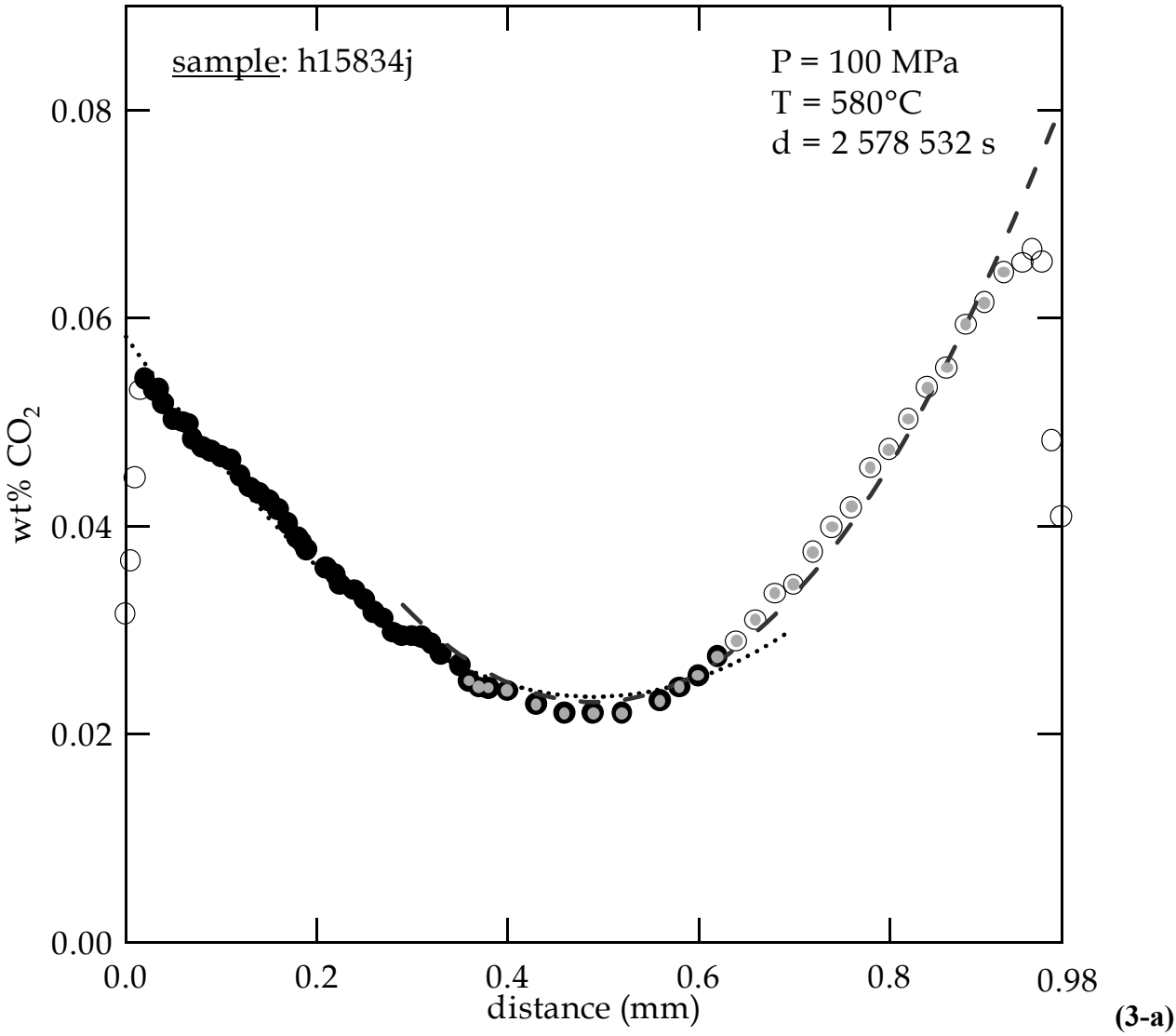

(3-a)

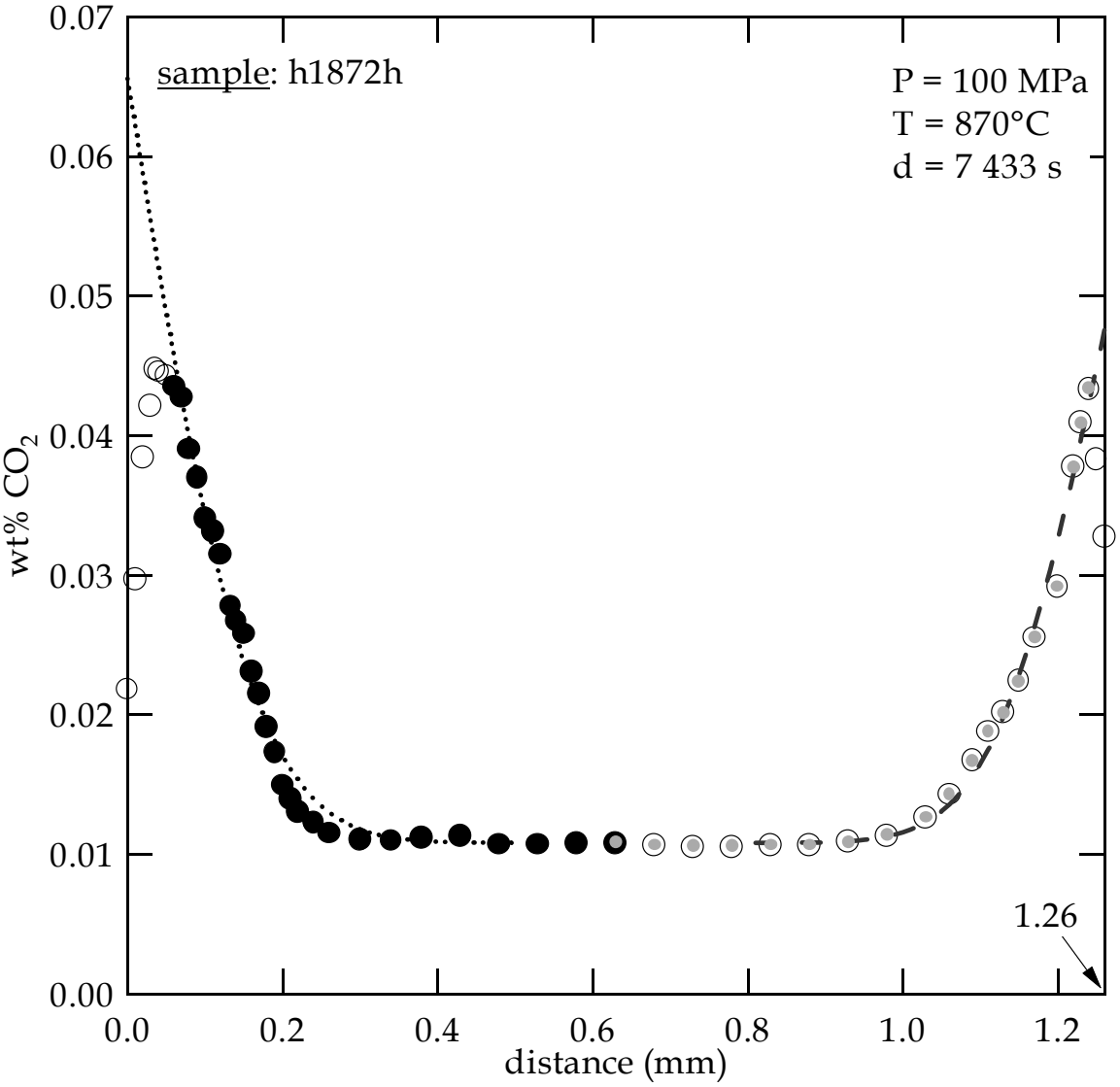
sample: h1872h
P = 100 MPa
T = 870°C
d = 7 433 s
wt% CO_2
distance (mm)
0.00
0.01
0.02
0.03
0.04
0.05
0.06
0.07
0.0
0.2
0.4
0.6
0.8
1.0
1.2
1.26

(3-b)

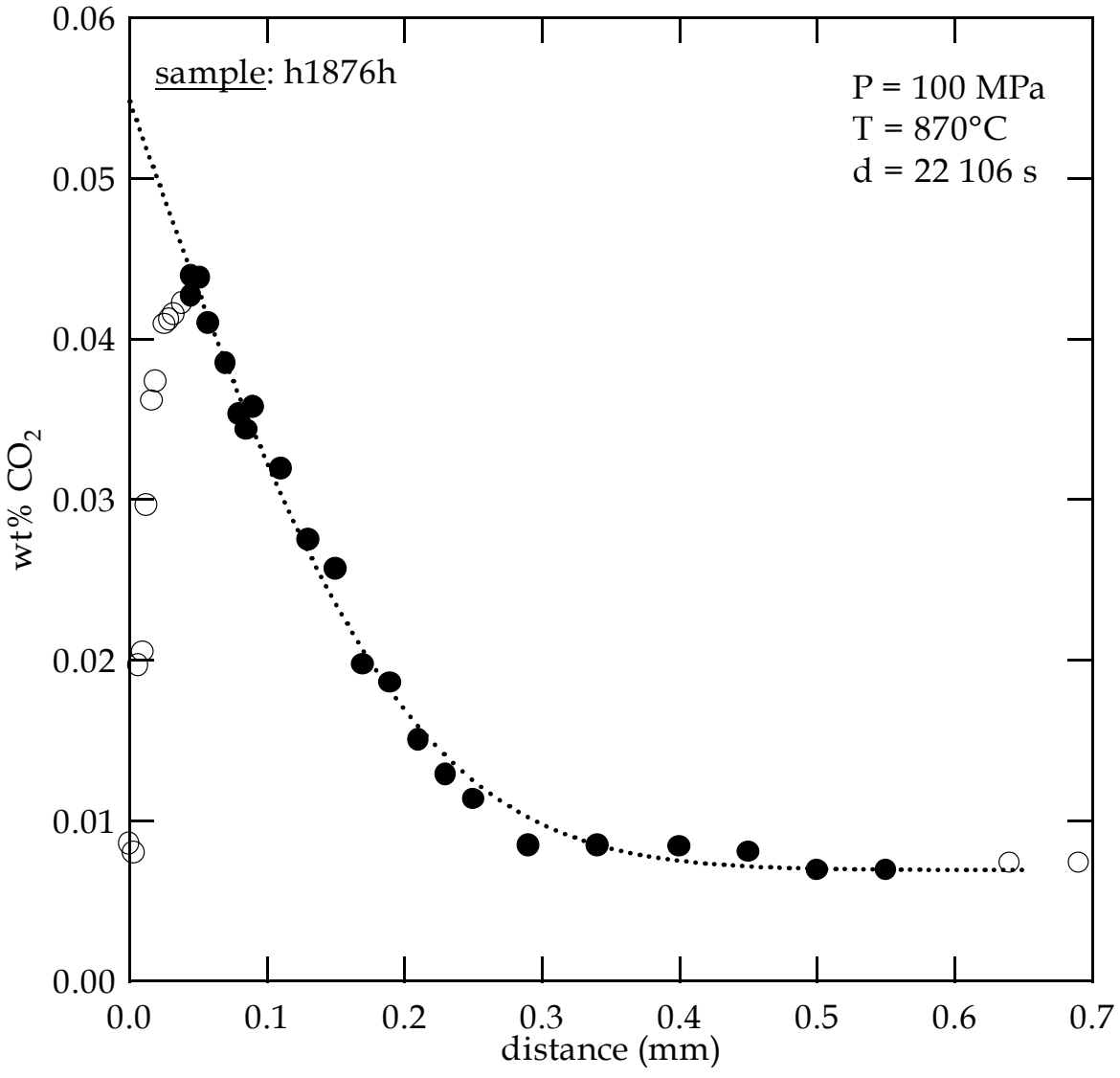
sample: h1876h
P = 100 MPa
T = 870°C
d = 22 106 s
wt% CO_2
distance (mm)
0.00
0.01
0.02
0.03
0.04
0.05
0.06
0.0
0.1
0.2
0.3
0.4
0.5
0.6
0.7

(3-c)

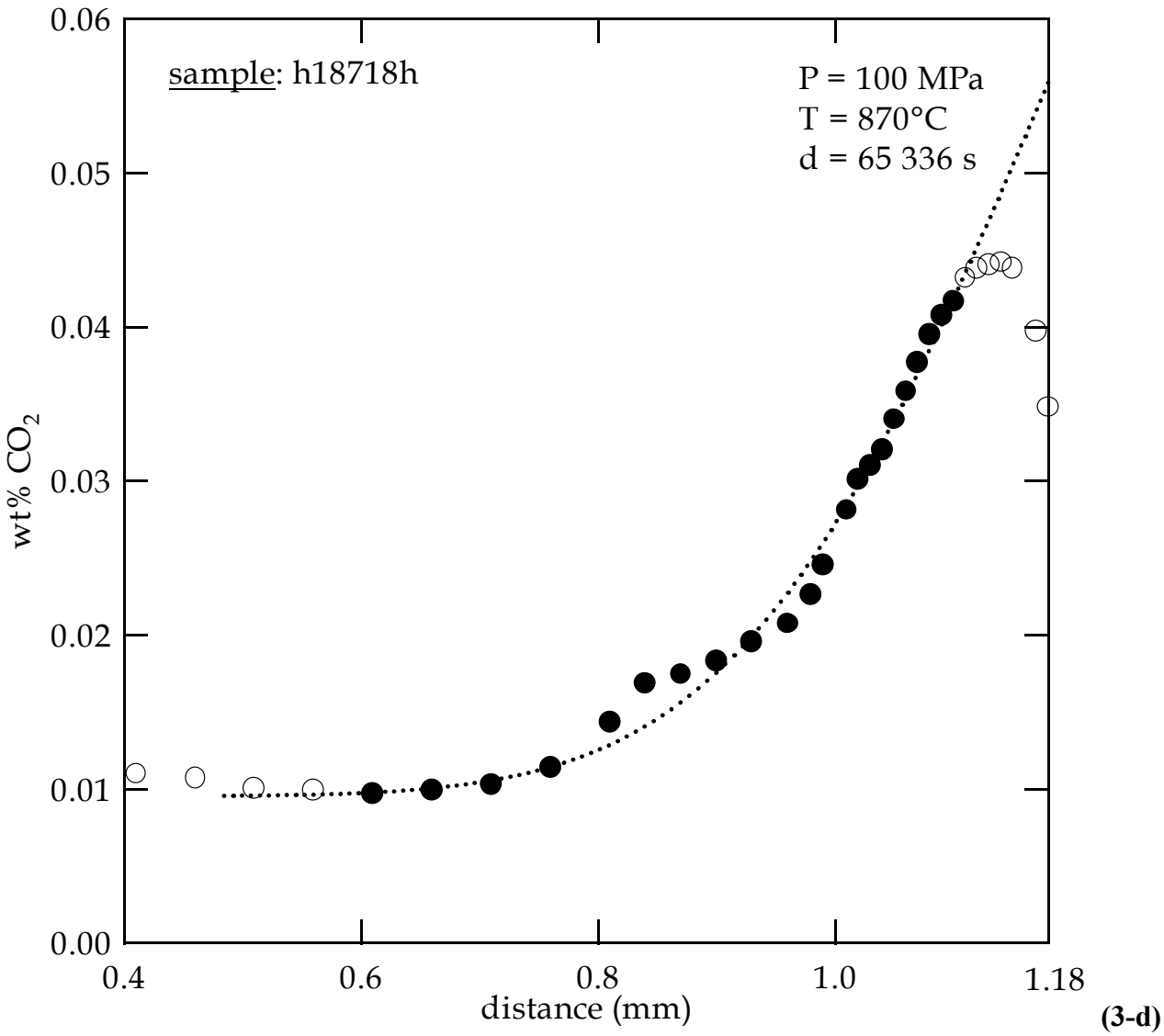
sample: h18718h
P = 100 MPa
T = 870°C
d = 65 336 s
wt% CO_2
distance (mm)
0.00
0.01
0.02
0.03
0.04
0.05
0.06
0.4
0.6
0.8
1.0
1.18

(3-d)

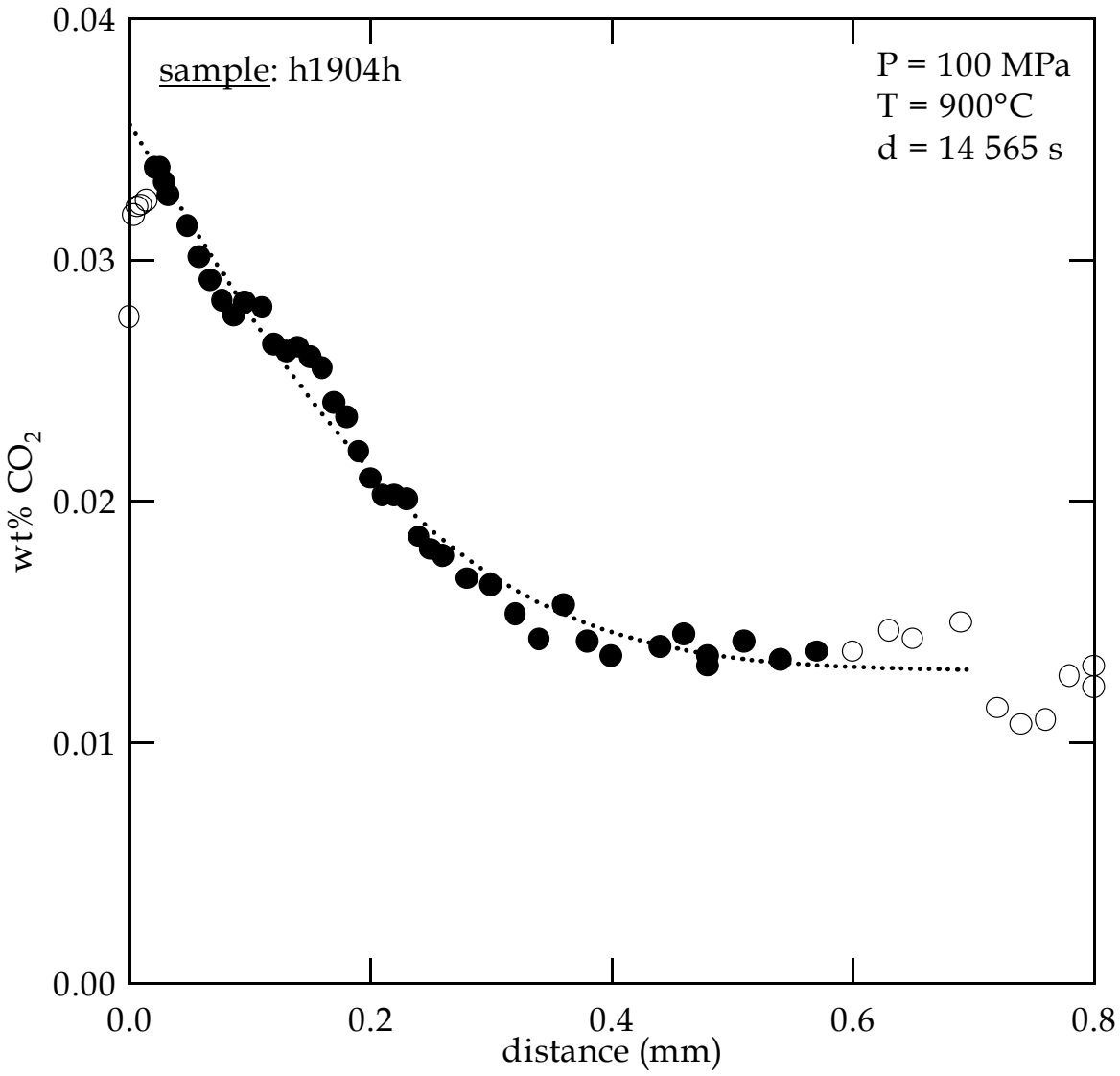
sample: h1904h
P = 100 MPa
T = 900°C
d = 14 565 s
wt% CO_2
0.04
0.03
0.02
0.01
0.00
0.0
0.2
0.4
0.6
0.8
distance (mm)

(3-e)

References

Bagdassarov, N.S., Dingwell, D.B., 1993. Frequency-dependent rheology of vesicular rhyolite. J. Geophys. Res. 98, 6477-6487.

Bartholomew, R.F., Butler, B.L., Hoover, H.L. Wu, C.K., 1980. Infrared spectra of a water-containing glass. J. Am. Ceram. Soc. 63, 481-485.

Becker, A., Holtz F., Johannes W., 1998. Liquidus temperatures and phase compositions in the system Qz-Ab-Or at 5 kbar and very low water activities. Contrib. Mineral. Petrol. 130, 213-224.

Behrens, H., 1995. Determination of water solubilities in high-viscosity melts: an experimental study of $NaAlSi_3O_8$ and $KAlSi_3O_8$ melts. Eur. J. Mineral. 7, 905-920.

Behrens, H., Jantos, N., 2001. The effect of anhydrous composition on water solubility in granitic melts. Am. Mineral. 86, 14-20.

Behrens, H., Schmidt, M.O., 1998. Infrared spectroscopy of hydrous silicic glasses at temperatures up to 600°C and implications for the incorporation and dynamics of water in glasses. N. Jb. Mineral. Abh. 172, 203-226.

Behrens, H., Zhang, Y., 2001. Ar diffusion in hydrous silicic melts: implications for volatile diffusion mechanisms and fractionation. Earth Planet. Sci. Lett. 192, 363-376.

Behrens, H., Tamic, N., Zhang, Y., Holtz, F., 2000a. Diffusion of volatiles in rhyolitic melts: comparison of CO_2, Ar and molecular H_2O. Eur. J. Mineral. Beih. 12, 10.

Behrens, H., Meyer, M., Holtz, F., Benne, D., Nowak, M., 2000b. The effect of alkali ionic radius, temperature, and pressure on the solubility of water in $MAlSi_3O_8$ melts (M=Li, Na, K, Rb). Chem. Geol. 174, 275-289.

Behrens, H., Romano, C., Nowak, M., Holtz, F., Dingwell, D.B., 1996. Near-infrared spectroscopic determination of water species in glasses of the system $MAlSi_3O_8$ (M = Li, Na, K): an interlaboratory study. Chem. Geol. 128, 41-64.

Blank, J.G., 1993. An experimental investigation of the behaviour of carbon dioxide in rhyolitic melt. PhD dissertation, California institute of technology, Pasadena, CA.

Blank, J.G., Brooker, R.A., 1994. Experimental studies of carbon dioxide in silicate melts: solubility, speciation and stable isotope behavior. In: Carroll, M.R., Holloway, J.R. (Eds.),

Volatiles in magmas. Reviews in Mineralogy 30, Mineralogical Society of America, Washington, D.C., pp. 157-186.

Blank, J., Stolper, E.M., Zhang, Y., 1991. Diffusion of CO_2 in rhyolitic melt, Trans. Am. Geophys. Union 72, 312.

Blank, J.G., Stolper, E.M., and Carroll, M.R., 1993. Solubility of carbon dioxide and water in rhyolitic melt at 850°C and 750 bars. Earth Planet. Sci. Lett. 119, 27-36.

Brey, G.,1976. CO_2 solubility and solubility mechanisms in silicate melts at high pressures. Contrib. Mineral. Petrol. 57, 215-221.

Burnham, C.W., 1979. The importance of volatile constituents. In: The evolution of the igneous rocks, H.S. Yoder (ed). Princeton University Press, Princeton, New Jersey, pp. 439-482.

Carroll, M.R., Webster, J.D.,1994. Solubilitites of sulfur, noble gases, nitrogen, chlorine and fluorine in magmas. In: Carroll, M.R., Holloway, J.R. (Eds.), Volatiles in magmas. Reviews in Mineralogy 30, Mineralogical Society of America, Washington, D.C., pp. 231-279.

Crank, J., 1975. The mathemathics of diffusion, 2nd edition. Clarendon press, Oxford, 414 p.

Dingwell, D.B., Hess, K.-U., Romano, C., 1998. Viscosity data for hydrous peraluminous granitic melts: Comparison with a metaluminous model. Am. Mineral. 83, 236-239.

Dixon, J.E., Stolper, E.M., Delaney, J.R., 1988. Infrared spectroscopic measurements of CO_2 and H_2O glasses in the Ruan de Fuca Ridge basaltic glasses. Earth Planet. Sci. Lett. 90, 87-104.

Ernsberger, F.M., 1977. Molecular water in glass. J. Am. Ceram. Soc. 60, 91-92.

Fine, G., Stolper, E., 1985. The speciation of carbon dioxide in sodium aluminosilicate glasses. Contrib. Min. Petrol. 91, 105-121.

Fine, G, Stolper, E., 1986. Carbon doxide in basaltic glasses: concentrations and speciation. Earth Planet. Sci. Lett. 76, 263-278.

Fogel, R.A., Rutherford, M.J. (1990) The solubility of carbon dioxide in rhyolitic melts: a quantitative FTIR study. Am. Mineral. 75, 1311-1326.

Harrison, A.J., 1947.Water content and infrared transmission of simple glasses. Am. Ceram. Soc. J. 30, 362-366.

Hess, K.-U., Dingwell, D.B., Webb, S.L., 1995. The influence of excess alkalies on the viscosity of a haplogranitic melt. Am. Mineral. 80, 297-304.

Holloway, J.R., Blank, J.G., 1994. Application of experimental results to C-H-O species in natural melts. In: Carroll, M.R., Holloway, J.R. (Eds.), Volatiles in magmas. Reviews in Mineralogy 30, Mineralogical Society of America, Washington, D.C., pp. 187-230.

Holtz F., Behrens H., Dingwell D.B., Johannes W., 1995. H_2O solubility in haplogranitic melts: compositional, pressure and temperature dependence. Am. Mineral. 80, 94-108.

Holtz F., Behrens H., Dingwell D.B., Taylor, R.P., 1992. Water solubility in melts of haplogranitic composition at 2 kbar. Chem. Geol. 96, 289-302.

Holtz, F., Scaillet, B., Behrens, H., Schulze, F., Pichavant, M., 1996. Water contents of felsic melts: constraints for the viscosity of granitic magmas. Trans. Roy. Soc. Edingburgh Earth Sci. 87, 57-64.

Hurwitz, S., Navon, O., 1994. Bubble nucleation in rhyolitic melts: experiments at high pressure, temperature, and water content, Earth Planet. Sci. Lett. 122, 267-280.

Ihinger, P.D.,1991.An experimental study of the interaction of water with granitic melt. Ph D thesis, California Institute of Technology.

Ihinger, P.D., Hervig, R.L., McMillan, P.F., 1994. Analytical methods for volatiles in glasses. In: Carroll, M.R., Holloway, J.R. (Eds.), Volatiles in magmas. Reviews in Mineralogy 30, Mineralogical Society of America, Washington, D.C., pp. 67-121.

Kadik, A.A., Lukanin, O.A., Lebedev, Y.B., and Korovushkina, E.Y., 1972. Solubility of H_2O and CO_2 in granite and basalt melts at high pressures. Geochem. Int. 9, 1041-1050.

Kohn, S.C., 2000. The dissolution mechanisms of water in silicate melts: a synthesis of recent data. Mineral. Mag. 64, 389-408.

Lejeune, A.M., Richet, P., 1995. Rheology of crystal-bearing silicate melts : An experimental study at high vixcosities. J. Geophys. Res. 100, 4215-4229.

Lejeune, A.M., Bottinga, Y., Trull, T.W., Richet, P., 1999. Rheology of bubble-bearing magmas. Earth Planet. Sci. Lett. 166, 71-84.

Liu, Y., Zhang, Y., 2000. Bubble growth in rhyolitic melt. Earth Planet. Sci. Lett. 181, 251-264.

Lyakhovsky, V., Hurwitz, S., Navon, O., 1996. Bubble growth in rhyolitic melt: experimental and numerical investigation, Bull. Volcanol. 58, 19-32.

McMillan, P., 1994. Water solubility and speciation models. In: Carroll, M.R., Holloway, J.R. (Eds.), Volatiles in magmas. Reviews in Mineralogy 30, Mineralogical Society of America, Washington, D.C., pp. 131-156.

Mourtada-Bonnefoi, C., 1998. Volcanologie physique: Dynamique thermochimique des chambres magmatiques et vésiculation des magmas rhyolitiques. Ph D thesis. Université Blaise Pascal, Clermont Ferrand.

Mysen, B.O., 1976. The role of volatiles in silicate melts: solubility of carbon dioxide and water in felspar, pyroxene, and feldspathoid melts to 30 kb and 1625°C. Am. J. Sci. 276, 969-996.

Mysen, B.O., Eggler, D.H., Seitz, M.G., Holloway, J.R., 1976. Ca rbon dioxide in silicate melts and crystals. Part 1 solubility measurements. Am. J. Sci. 276, 455-479.

Navon, O., Chekhmir, A., Lyakhovsky, V., 1998. Bubble growth in highly viscous melts: theory, experiments, and autoexplosivity of dome lavas. Earth Planet. Sci. Lett. 160, 763-776.

Newman, S., Stolper, E.M., Epstein, S., 1986. Measurement of water in rhyolitic glasses: calibration of an infrared spectroscopic technique. Am. Mineral. 71, 1527-1541.

Newman, S., Epstein, S., Stolper, E.M., 1988. Water, carbon dioxide, and hydrogen isotopes in glasses from the ca 1340 AD eruption of the Mono Craters, California: Constraints on degassing phenomena and initial volatile content. J. Volcan. Geotherm. Res. 35, 75-96.

Nowak, M., Behrens, H., 1995. The speciation of water in haplogranitic glasses and melts determined by in situ near-infrared spectroscopy. Geochim. Cosmochim. Acta 59, 3445-3450

Nowak, M., Behrens, H., 1997. An experimental investigation on diffusion of water in haplogranitic melts. Contrib. Mineral. Petrol. 126, 365-376.

Paillat, O., Elphick, S.C. and Brown W.L., 1992. The solubility of water in $NaAlSi_3O_8$ melts: a re-examination of Ab-H_2O phase relationships and critical behaviour at high pressure. Contrib. Mineral. Petrol. 112, 490-500.

Pan, V., Holloway, J.R., Hervig, R.L., 1991. The pressure and temperature dependence of carbon dioxide solubility in tholeiitic basalt melts. Geochim. Cosmochim. Acta, 55, 1587-1595.

Papale, P., 1999. Modeling of the solubility of a two-component H_2O + CO_2 fluid in silicate liquids. Am. Mineral. 84, 477-492.

Papale, P., Polacci, M., 1999. Role of carbon dioxide in the dynamics of magma ascent in explosive eruptions. Bull. Volcanol. 60, 583-594.

Pawley, A.R., Holloway, J.R., McMillan, P.F., 1992. The effect of oxygen fugacity on the solubility of carbon-oxygen fluids in basaltic melt. Earth Planet. Sci. Lett. 110, 213-225.

Persikov, E.S., 1991. The viscosity of magmatic liquids: Experiment, generalized patterns: A model for calculation and prediction: Applications. In: Advances in Physical Geochemistry 9, pp. 1-40.

Proussevitch, A.A., Sahagian, D.L., 1998. Dynamics and energetics of bubble growth in magmas: analytical formulation and numerical modeling. J. Geophys. Res. 103, 18223-18251.

Richet P., Polian A., 1998. Water as a dense, icelike component of silicate glasses. Science 281, 396-398.

Richet P., Lejeune A.M., Holtz F., Roux J., 1996. Water and the viscosity of andesite melts. Chem. Geol. 128, 185-197.

Schmidt, B.C., Behrens, H., Tamic, N., Holtz, F., Pichavant, M., 1998. Water solubility in haplogranitic melts coexisting with H_2O-H_2 and H_2O-CO_2 fluids. 8th V.M. Goldschmidt Conf. (abstract), Mineral. Mag. 62A, 1343-1344.

Schmidt, B.C., Holtz, F., Pichavant, M., 1999. Water solubility in haplogranitic melts coexisting with H_2O-H_2 fluids. Contrib. Mineral. Petrol. 136, 213-224.

Scholze, H., 1960. Zur Frage der Unterscheidung zwischen H_2O-Molekeln und OH-gruppen in Gläsern und Mineralen. Naturwissenschaften 47, 226-227.

Scholze, H., 1966. Gases and water in glass: Parts I, II, III. The Glass Industry 47: 546-551; 622-628; 670-674.

Schulze, F., Behrens, H., Holtz, F., Roux, J., Johannes, W., 1996. The influence of water on the viscosity of a haplogranitic melt. Am. Mineral. 81, 1155-1165.

Silver, L.A., Stolper, E.M., 1989. Water in albitic glasses. J. Petrol. 30: 667-709.

Silver, L.A., Ihinger P.D., Stolper E., 1990. The influence of bulk composition on the speciation of water in silicate glasses. Contrib. Mineral. Petrol. 104, 142-162.

Sowerby, J. R., Keppler, H., 1999. Water speciation in rhyolitic melt determined by in-situ infrared spectroscopy. Am. Mineral. 84, 1843-1849.

Sparks, R.S.J., 1978.The dynamics of bubble formation and growth in magma: a review and analysis, J. Volc. Geoth. Res. 3, 1-37.

Spera, F.J., Bergman, S.C., 1980. Carbon dioxide in igneous petrogenesis: I. Aspects of the dissolution of CO_2 in silicate liquids. Contrib. Mineral. Petrol. 74, 55-66.

Stevenson, R.J., Dingwell, D.B., Webb, S.L., Bagdassarov, N.S., 1995. The equivalence of enthalpy and shear stress relaxation in rhyolitic obsidians and quantification of the liquid-glass transition in volcanic processes. J. Volcan. Geotherm. Res. 68, 297-306.

Stolper, E., 1982. Water in silicate glasses: an infrared spectroscopic study. Contrib. Mineral. Petrol. 81, 1-17.

Stolper, E.M., 1989. Temperature dependence of the speciation of water in rhyolitic melts and glasses. Am. Mineral. 74, 1247-1257.

Stolper, E.M., Newman, S., 1994. The role of water in the petrogenesis of Mariana trough magmas. Earth Planet. Sci. Lett. 121, 293-325.

Stolper, E.M., Fine, G.J., Johnson, T., Newman, S., 1987. The solubility of carbon dioxide in albitic melt. Am. Mineral. 72, 1071-1085.

Taylor, W., 1990. The dissolution mechanism of CO_2 in aluminosilicate melts – infrared spectroscopic constraints on the cationic environment of dissolved $[CO_3]^{2-}$. Eur. J. Mineral. 2, 547-563.

Taylor, J.R., Wall, V.J., Pownceby M.I., 1992. The calibration and application of accurate redox sensors. Am. Mineral. 77, 284-295.

Toramaru, A., 1995. Numerical study of nucleation and growth of bubbles in viscous magmas. J. Geophys. Res. 100, 1913-1931.

Tröger, W.E., 1959. Optische Bestimmung der gesteinsbildenden Minerale: Teil 1, Bestimmungstabellen. E. Schweizerbart'sche Verlagsbuchhandlung, Stuttgart.

Watson, E.B., 1991. Diffusion of dissolved CO_2 and Cl in hydrous silicic to intermediate magmas. Geochim. Cosmochim. Acta 55, 1897-1902.

Watson, E. B., 1994. Diffusion in volatile-bearing magmas. In: Carroll, M.R., Holloway, J.R. (Eds.), Volatiles in magmas. Reviews in Mineralogy 30, Mineralogical Society of America, Washington, D.C., pp. 371-411.

Watson, E.B., Sneeringer, M.A., Ross, A., 1982. Diffusion of dissolved carbonate in magmas: experimental results and applications. Earth Planet. Sci. Lett. 61, 346-358.

Wilke, M. and Behrens, H., 1999. The dependence of partitioning of Fe and Eu between plagioclase and hydrous tonalitic melts on oxygen fugacity. Contrib. Mineral. Petrol. 137, 102-114.

Withers, A.C., Behrens, H., 1999. Temperature induced changes in the NIR spectra of hydrous albitic and rhyolitic glasses: implications for hydrous species reaction. Phys. Chem. Mineral. 27, 119-132.

Wu, C.K., 1980. Nature of incorporated water in hydrated silicate glasses. J. Am. Ceram. Soc. 63, 453-457.

Wyllie, P.J., Tuttle, O.F., 1959. Effect of carbon dioxide on the melting of granite and feldspars. Am. J. Sci. 257, 548-655.

Yamashita, S., 1999. Experimental study of the effect of temperature on water solubility in natural rhyolitic melt to 100 MPa. J. Petrol. 40, 1497-1507.

Zhang, Y., 1999. H_2O in rhyolitic glasses and melts: Measurement, speciation, solubility, and diffusion. Rev. Geophys. 37, 493-516.

Zhang, Y., Behrens, H., 2000. H_2O diffusion in rhyolitic melts and glasses. Chem. Geol. 169, 243-262.

Zhang, Y., Belcher, R., Ihinger, P.D., Wang, L., Zhengjiu, X., Newman, S., 1997. New calibration of infrared measurements of dissolved water in rhyolitic glasses. Geochim. Cosmochim. Acta 61, 3089-3100.

Lebenslauf

Persönliche Daten

Name:	Nathalie Tamic
Anschrift:	8, rue Thibault Chemin; 45130 Meung/Loire; Frankreich
e-mail:	n.tamic@bigfoot.com
Geburtsdatum:	16.05.1972
Staatsangehörigkeit:	französich
Familienstand:	seit 08/1996 verheiratet mit Riwan Tamic
Kinder:	Enora Tamic, geb. 16.09.2000; Geburt meines zweites Kindes voraussichtlich im Juli 2002

Schulbildung

09/78 – 06/82	Ecole primaire Clémenceau A, Le Perreux/Marne (94), Frankreich
09/82 – 06/84	Collège P. Brossolette, Le Perreux/Marne (94), Frankreich
09/84 – 06/89	Collège-lycée Branly, Nogent/Marne (94), Frankreich
09/89 – 06/91	Lycée Kersa, Ploubazlanec (22), Frankreich, Schulabschluß Abitur

Studium

09/91 – 06/93	DEUG A, option Physique, Chimie, Sciences de la Terre, université de Rennes 1 (35), Frankreich
09/93 – 06/95	Licence-Maîtrise de géologie fondamentale et appliquée, université de Rennes 1 (35), Frankreich
06/95 – 06/96	DEA matériaux minéraux, université d'Orléans (45), Frankreich, Abschluß Diplom, Thema der Diplomarbeit: Experimental reproduction of magmatic fabrics by in situ deformation.
03/97 – 04/2000	Wissenschaftliche Mitarbeiterin am Institut für Mineralogie, Hannover. Betreuung der coulometrischen CO_2-Titration sowie verschiedener Hochdruckanlagen.
seit 05/2000	Anfertigung der Dissertation mit dem Thema "Löslichkeit von H_2O und CO_2 und CO_2 Diffusion in rhyolitischen Schmelzen: eine experimentelle untersuchung.", und Vollzeit Mutter.

Sonstige Tätigkeiten

09/95 – 02/97	Kinderbetreuung und Hausaufgaben Nachhilfe, Collège Maîtrise-Notre-Dame, Beaugency (45), Frankreich